Spring 2022

MINERALOGY AND FLUID INCLUSION STUDY OF THE MARGET ANN MINE OF THE BUTTE MINING DISTRICT, SILVER BOW COUNTY, MONTANA

Tiffany Ostenburg

MINERALOGY AND FLUID INCLUSION STUDY OF THE MARGET ANN MINE OF THE BUTTE MINING DISTRICT, SILVER BOW COUNTY, MONTANA

by

Tiffany Ostenburg

A thesis submitted in partial fulfillment of the
requirements for the degree of

Master of Science in Geoscience
Geology Option

Montana Tech
2022

Abstract

Butte, Montana, is a famous example of a zoned, polymetallic, porphyry-lode deposit. Whereas over a century of previous work has focused on the porphyry-style mineralization and centrally located, copper-rich lode deposits, relatively little has been written on the outer, silver-rich veins. The Marget Ann mine, in the northern portion of the district, was chosen for this study because of ease of access to the mine dumps as well as archived samples of high-grade vein mineralization. In addition, the Marget Ann mine is somewhat unique in Butte because gold has been found there and previously recorded in the veins. The main methods used in this study include optical mineralogy, scanning electron microscopy, and examination of fluid inclusions in quartz.

The 76 Ma Butte Granite is the host to mineralization at Marget Ann. Primary ore minerals in the veins include pyrite, sphalerite, galena, chalcopyrite, Ag-bearing tetrahedrite, pearceite-polybasite, acanthite/argentite, jalpaite, electrum, and uytenbogaardtite. Gangue minerals include quartz, rhodonite, rhodochrosite, calcite, dolomite, adularia, and sericite. Supergene minerals include secondary acanthite, native silver, covellite, and unidentified Mn- and Fe-oxides. High-grade ore shoots containing electrum and fine-grained Ag-Au-Cu sulfides occur with rhodonite + rhodochrosite + adularia, and may have formed by boiling. In contrast, most of the base-metal sulfides and coarse, comb-textured quartz likely formed by simple cooling or fluid mixing. Overall, the mineral assemblage is indicative of an “intermediate sulfidation” style of vein deposit.

Most of the fluid inclusions in quartz are simple two-phase, water-rich inclusions, and many are quite large (> 50 μm diameter). Homogenization temperatures range from 160 to 300°C (average of 251°C) with a salinity range of 0.5 to 7 wt% $NaCl_{eq}$ (average of 2.2 wt%). No direct evidence for CO_2 was shown in any of the inclusions, other than the occasional presence of anisotropic daughter minerals believed to be dawsonite. The overall spread in the data suggests mixing of a high temperature, higher salinity fluid (possibly a magmatic fluid) with a lower salinity fluid (heated meteoric water) during growth of quartz. The Marget Ann veins have a lower average homogenization temperature and salinity compared to the famous copper-rich Main Stage veins of Butte, which might indicate a greater involvement of meteoric waters on the outer edge of the district. This could also help to explain the higher gold content of the veins.

Keywords: Porphyry-lode deposit, jalpaite, pearceite, electrum, mineralogy, fluid mixing

Dedication

I want to first dedicate this to my husband Eric Ostenburg and our two wonderful boys; they are my biggest cheerleaders and are the reason I want to keep pursuing my goals. Secondly, I would like to dedicate this to my father, Todd Fayram. My father would take me rock collecting with my uncle Jon, allowing me to tag along on workdays, and has also been a rock when I felt like I could get through college. Also, to my mother for helping me with my two boys while my husband and I had to work and go to school. To all my extended family that has always been there in the background supporting our family. Without the help, love, and continued confidence I would not have made it through my bachelors, let alone my masters. Thank you!

Acknowledgements

I would like to acknowledge Dr. Chris Gammons for leading the research on the Marget Ann and for pushing me to try harder and to stay on track. I would like to thank Kaleb Scarberry for being a part of my committee and for being a mentor and supporting me when I needed to juggle work and school. Gary Wyss for his help on the Scanning Electron Microscope (SEM) to identify minerals. I would like to acknowledge David Harvey and Robert Hogan from Butte Blackjack Silver LLC for allowing the use of their archive of information and core collection. I would also like to thank the Uuno Sahinen Memorial Fund and match from the Montana Bureau of Mines and Geology for their generous scholarship award. I was also awarded the Gary L. Grauberger scholarship and a substantial scholarship from the American Federation of Mineralogical Societies, Thank you!

Table of Contents

List of Tables

List of Figures

Thesis Statement

Gold found at the Marget Ann Mine makes this mine unique to Butte. Modern methods have been employed to explain the minerology using transmitted and reflected microscopy, use of a scanning electron microscope, X-ray diffraction, and fluid inclusions. The fluid inclusion study will include temperature of formation of the deposit and the salinity of ore fluids. This study will then compare the Marget Ann mine to that of the rest of the Butte District, pertaining more specifically to the Main Stage veins of the Butte porphyry-lode deposit.

1. Introduction

1.1. Marget Ann Mine

1.1.1. Location

The Marget Ann Mine is in Section 1, Township 3 North, and Range 8 West. The latitude and longitude taken from Google Earth is 46.037113°, -112.542371°. This location is visible from many of the roads in the area and sits slightly northwest of the Alice Mine Pit overlook. The Marget Ann Mine is in the Butte District, but also known as the Summit Valley district (Elliot, Loen, Wise, & Blaskowski, 1992). The mine is in Walkerville, Montana (MT), just north of Butte in Figure 1.

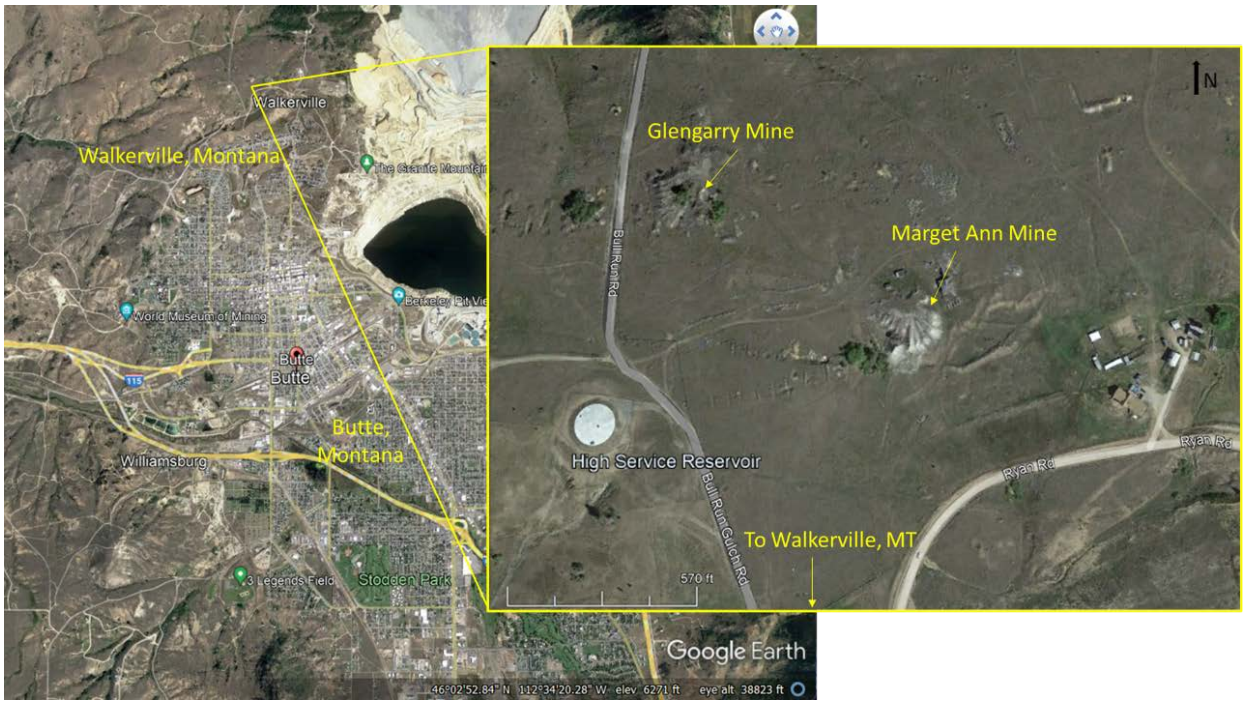

Figure 1. Location of the Marget Ann mine using Google Earth imaging. Zoomed in photo shows Marget Ann Mine in the middle and the Glengarry Mine to the west.

1.1.2. History

The Marget Ann was discovered by two men back in 1878 by the names of Dennis Driscoll and John O'Donnell (O'Donnel) (Sahinen, 1953). The claim block was worked until 1882 before it became dormant for 68 years. The mine was then opened again in 1950 by the Mitchell Mining Company (Sahinen, 1953). The Mitchell Mining Company only worked the mine until 1954, when the Marget Ann was closed. The Marget Ann Mine has had no active mining since. One mining company in the 1980's by the name of New Butte Mining Company showed interest, and completed a number of exploration drill holes in the northern part of the Butte district. Currently, Blackjack Silver is trying to define an unmined Zn-Ag resource in the upper levels of the historic underground mines, which includes the Marget Ann property. Many of the claim blocks near the Marget Ann mine are held by Arco Environmental Remediation LLC as seen in Figure 2. Other previous owners according to the property files held at the Montana Bureau of Mines and Geology (MBMG) include leasing by the Lee Enterprises, Inc., and Frank Benich in June of 1983.

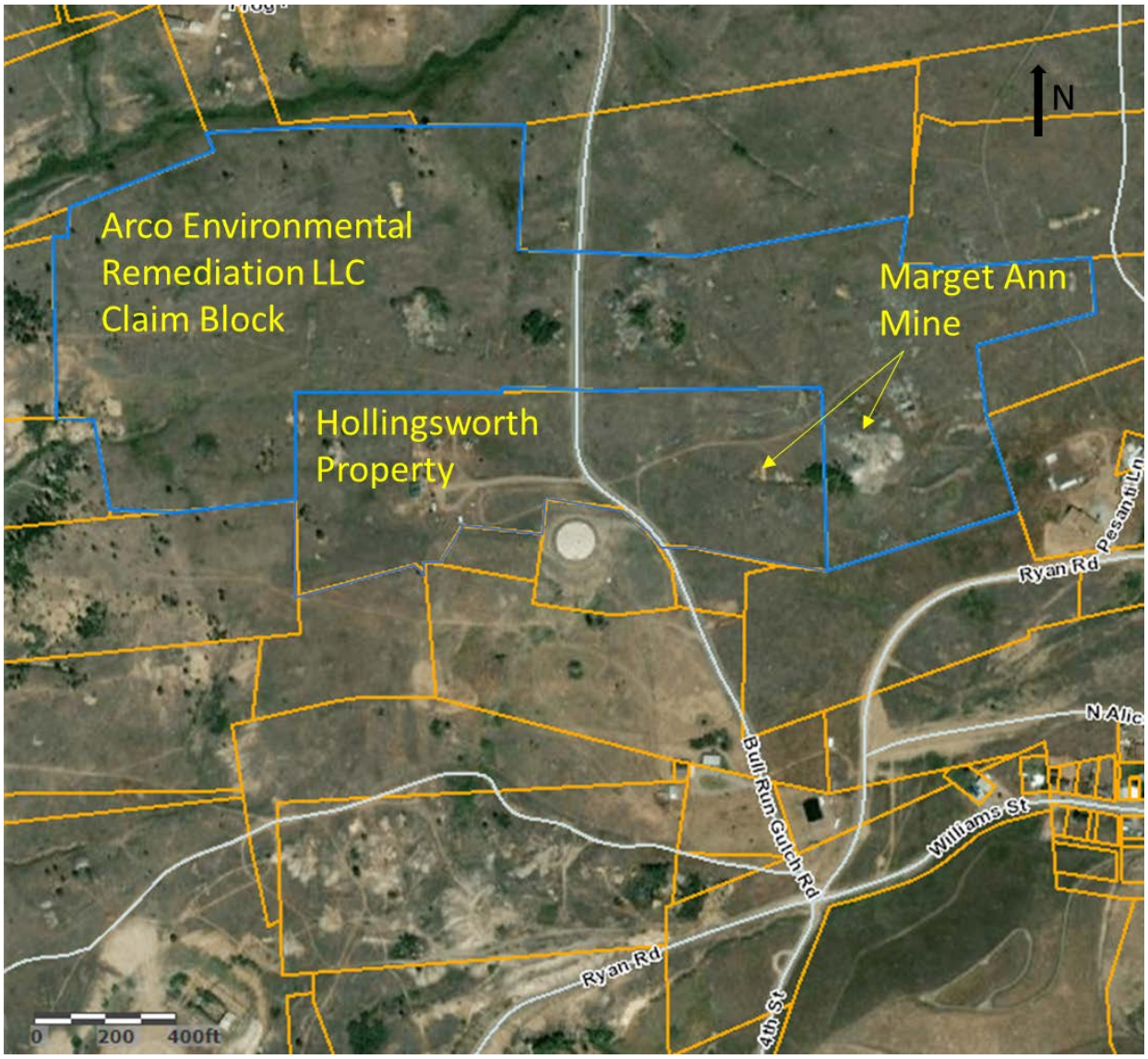

Figure 2. Arco Environmental Remediation LLC Claim block and the Hollingsworth property that encases the Marget Ann Mine.

1.1.3. Property Characteristics

The Marget Ann sits on four historical claim blocks as seen in Figure 3. These blocks are now included in the new property groups that can be viewed using geographical information systems (GIS) like Montana Cadastral. These blocks are the Glengarry,

the Silver Lick, the Marget Ann, and the Rescue. On the Marget Ann claim block, old structures still sit on the property and are visible from surrounding roads (Figure 4).

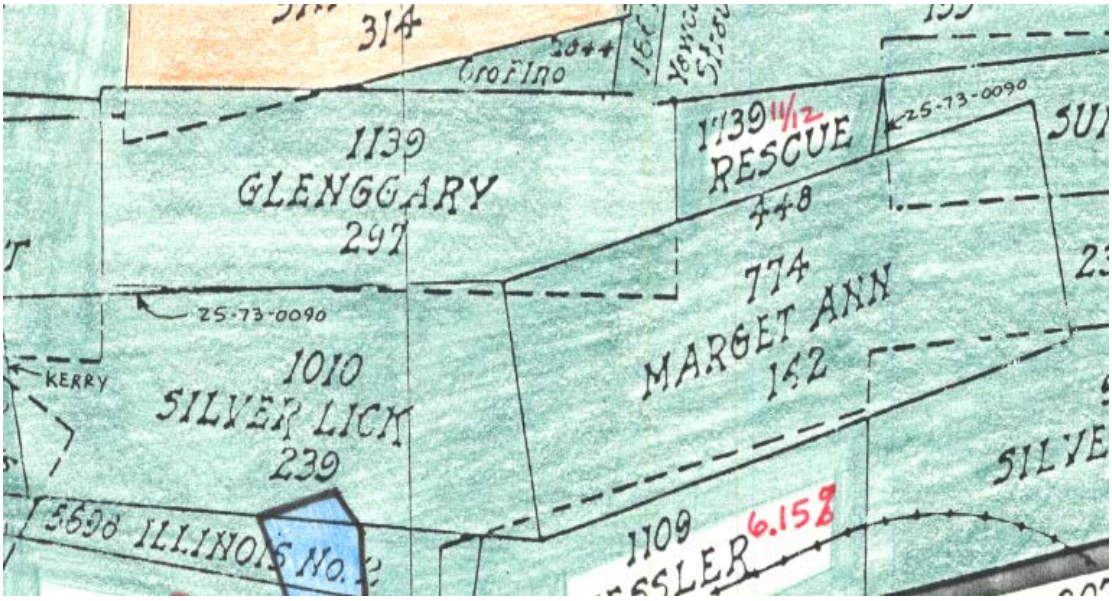

Figure 3. Historical claim blocks drawn by J. Goebel on January 14th, 1988, Image of 4 claim blocks that include the Marget Ann, The Rescue, Silver Lick, and the Glengarry.

Figure 4. Photos taken on site in 2020 of the various sturctures on the Marget Ann property.

There is also a large dump pile, the outlines of an old tailings pile that has since been cleaned up, and many trenches which can be seen using Google Earth (Figure 1). The trenches follow outcrops of two of the major veins which run roughly east-west.

1.2. Geological Setting

1.2.1. Regional and District Geology

The mineral deposits of Butte are hosted by the Butte Granite (formerly known as the Butte Quartz Monzonite). This pluton, dated to 74-76 Ma (Lund et al., 2002), stretches from Butte to near Helena, MT, and is part of the larger Boulder Batholith (Figure 5). The Boulder Batholith was emplaced in the late Cretaceous (80.4 to 74.5 Ma) (Lund et al., 2002), and is roughly the same age or younger than the associated Elkhorn Mountains Volcanics (shown in light blue color in Figure 5). Major minerals in the Butte Granite include hornblende, biotite, plagioclase, alkali feldspar, and quartz, with accessory apatite, magnetite, ilmenite, titanite, and zircon (Reed & Dilles, in press). The Butte Granite includes aplite and pegmatite variants that are roughly the same age. Although the Butte Granite is the main host rock in the district, most of the porphyry-lode mineralization is thought to be associated with a younger set of felsic porphyry dikes, dated at 65 Ma (Lund, McAleer, Aleinikoff, Cosca, & Kunk, 2018). These porphyritic intrusions crop out sparsely in the district but have been intersected by drill core and underground workings. Cutting and overlying the eroded surface of the Butte Granite and porphyry dikes are younger rhyolite intrusions and ignimbrites of the Lowland Creek volcanics (52-48 Ma, (Dudás, Ispolatov, Harlan, & Snee, 2010)). These rocks crop out on Big Butte, north of Montana Tech campus, and are unmineralized in the Butte district. Beginning in the Tertiary and continuing to the present day, faulting has disrupted the landscape, leading to more erosion and supergene enrichment of primary mineralization of Butte by descending groundwaters. The Continental Fault, which separates the inactive Berkeley Pit and the active Continental Pit, has an estimated one-kilometer (km) of normal (west side down) offset.

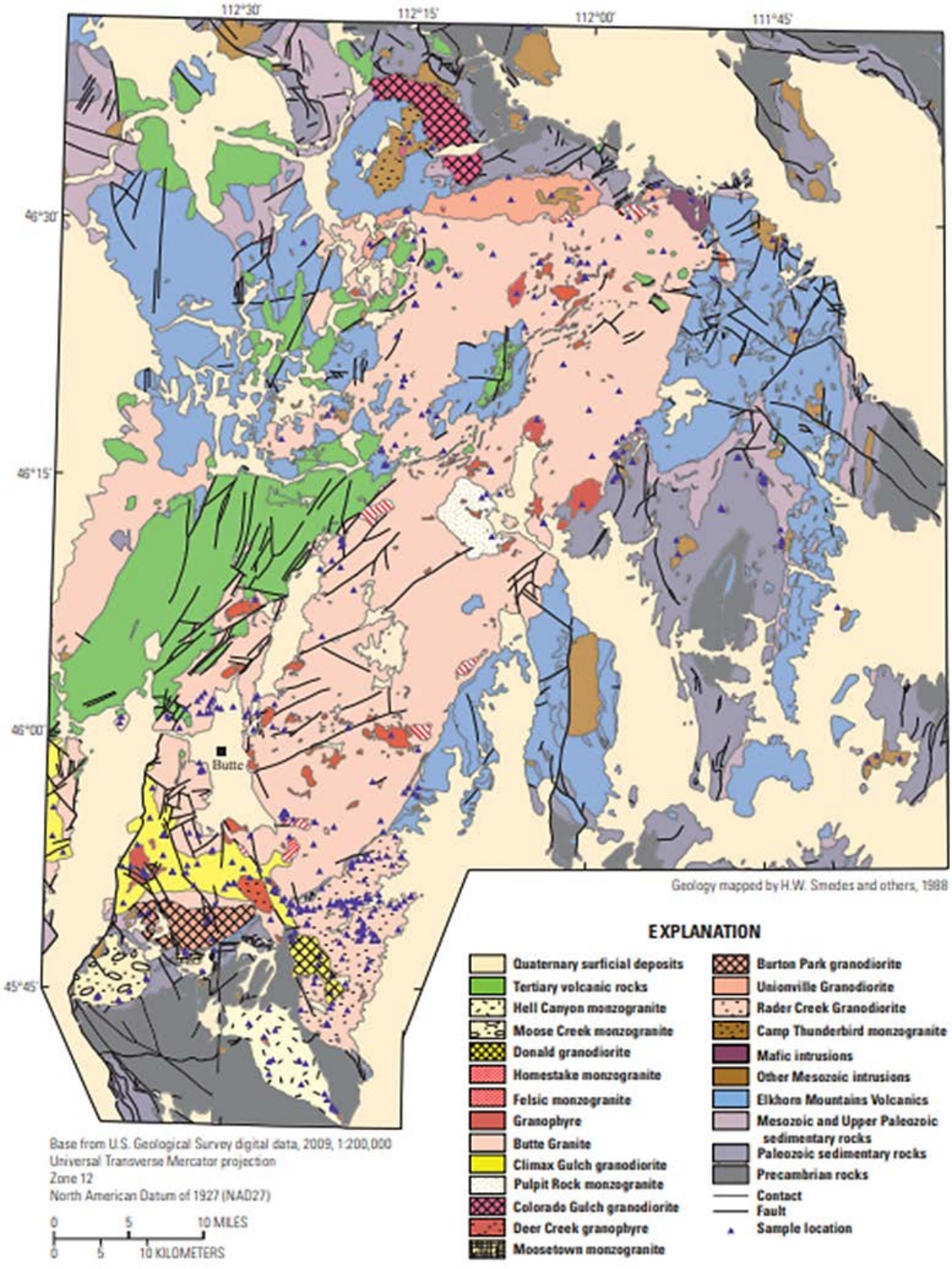

Figure 5: Geologic map of the Boulder Batholith and surrounding area (du Bray, Aleinikoff, & Lund, 2012). Butte is near the left bottom.

To economic geologists, the Butte district is a classic example of a Cordilleran-type, porphyry-lode deposit (Rusk et al., 2008b; Reed & Dilles, 2008b). The “porphyry” part of the mineral system consists of low-grade, disseminated chalcopyrite + molybdenite in veinlets cutting the Butte Granite. It is present at depth beneath the Berkeley Pit and is currently being mined in the Continental Pit by Montana Resources, LLC (Czehura, 2006; Reed & Dilles, in press). The “lode” part of the system consists of a vast network of steeply dipping hydrothermal veins, some up to 10 meters (m) in thickness and up to 1 km in length along strike and dip. These are referred to as Main Stage Veins in the literature (Meyer, Shea, Goddard, & and staff, 1968), and are zoned, with a Central Zone rich in copper sulfides (bornite, chalcocite, covellite, enargite), a Cu + Zn rich Intermediate Zone, and Ag-Pb-Zn-Mn rich Peripheral Zone rich in galena, sphalerite, rhodochrosite, and Ag-minerals (Figure 6). The veins of the Marget Ann mine, which are the topic of this thesis, belong to the Peripheral Zone of the Main Stage system. This zone includes other mines such as the Alice, Orphan Girl, and Bluebird mines. Overall, Marget Ann is one of the furthest north and highest elevation mines in the district.

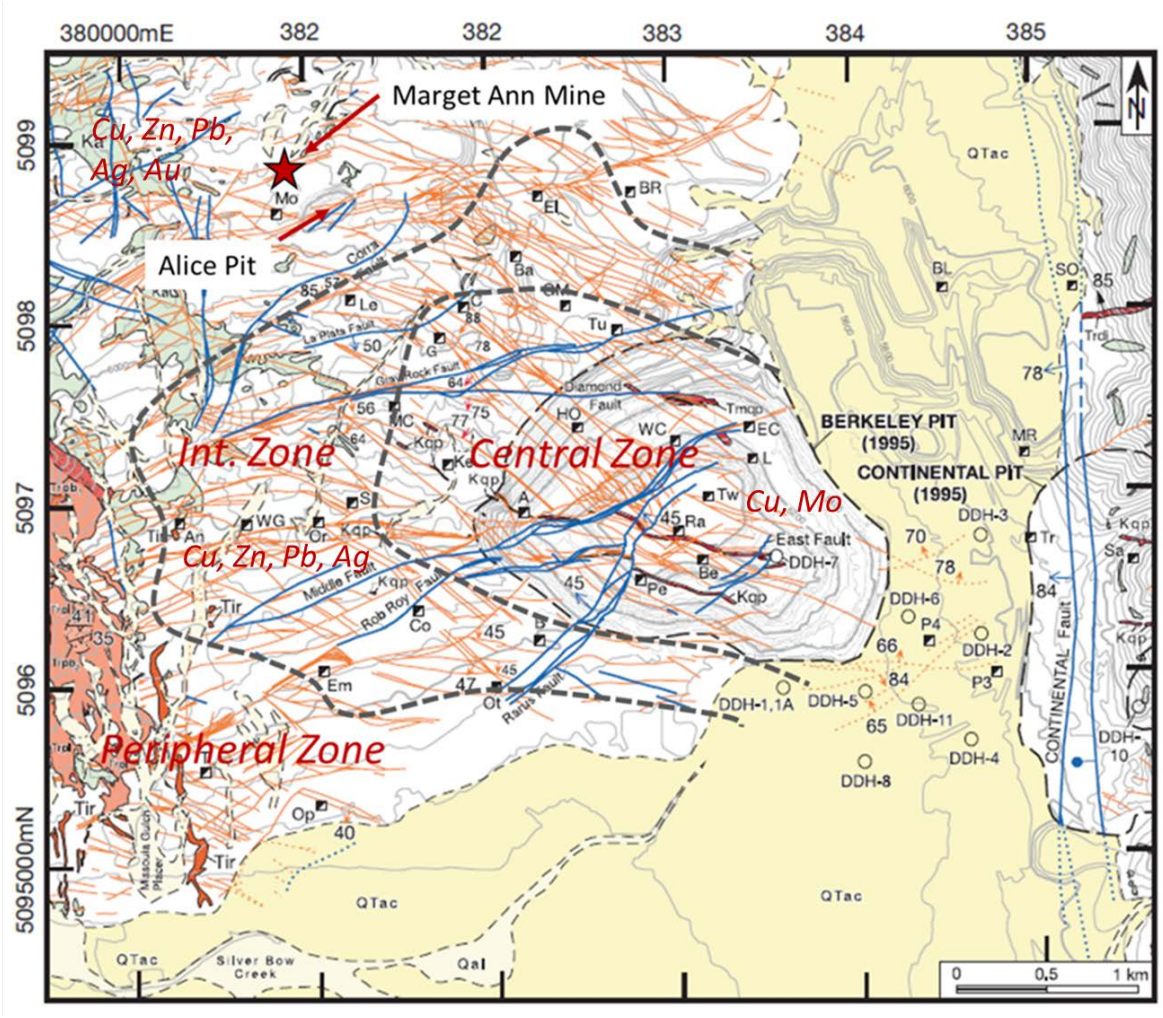

Figure 6: Fracture network and zoning of the Butte porphyry (after Houston & Dilles, 2013) with zoning and other mine locations added. The blue lines are the major faults, the light red are the Main Stage veins. The small boxes correspond to individual mines. From top to bottom, left to right: Mo = Moulton, El = Elmorlu, Br = Black Rock, Ba = Badger, Bl = Butte & London, SO = Six O' Clock, Le = Lexington, C = Corra, GM = Granite Mountain, G = Gray Rock, Tu -= Tuolumne, MC = Mountain Con, HO = High Ore, WC = West Colusa, EC = East Colusa, MR = Main Range, Ke = Kelly, L = Leonard, S = Steward, A = Anaconda, Tw = Tramway, Ra = Rarus, Tr = Tropic, Sa = Sarsfield, An = Anselmo, WG = West Gagnon, Or = Original, Be = Berkeley, Pe = Pennsylvania, Co = Colorado, B = Belmont, P4 = Pittsmont no. 4, P3 = Pittsmont no. 3., Em = Emma, Ot = Otisco, T= Travona, and Op = Ophir.

1.2.2. Local Geology

Early investigations of the geology and mineralogy of the Marget Ann mine include the B.S. thesis of Sahinen (1953) and the M.S. thesis of Win (1955). Both of these theses were done at Montana Tech, during the period that the underground mine was operating. The Marget Ann shaft is over 550' deep, and intersected 3 large veins, the North Vein, the South Vein, and the Middle Vein (Figure 7A). The major veins in the Marget Ann mine strike ENE-WSW, and therefore belong to the Anaconda set of the Main Stage Veins of the Butte district (Meyer, Shea, Goddard, & and staff, 1968). However, the Marget Ann veins are unique because they do not follow the normal pattern of dipping to the south. The veins in the Marget Ann dip to the north (Figure 7B). At the surface, the veins are highly oxidized with abundant Fe-oxide and black Mn-oxide staining (Figure 7B). The depth of oxidation within the mine is estimated to be between 50 ft. and 110 ft. (Win,1955).

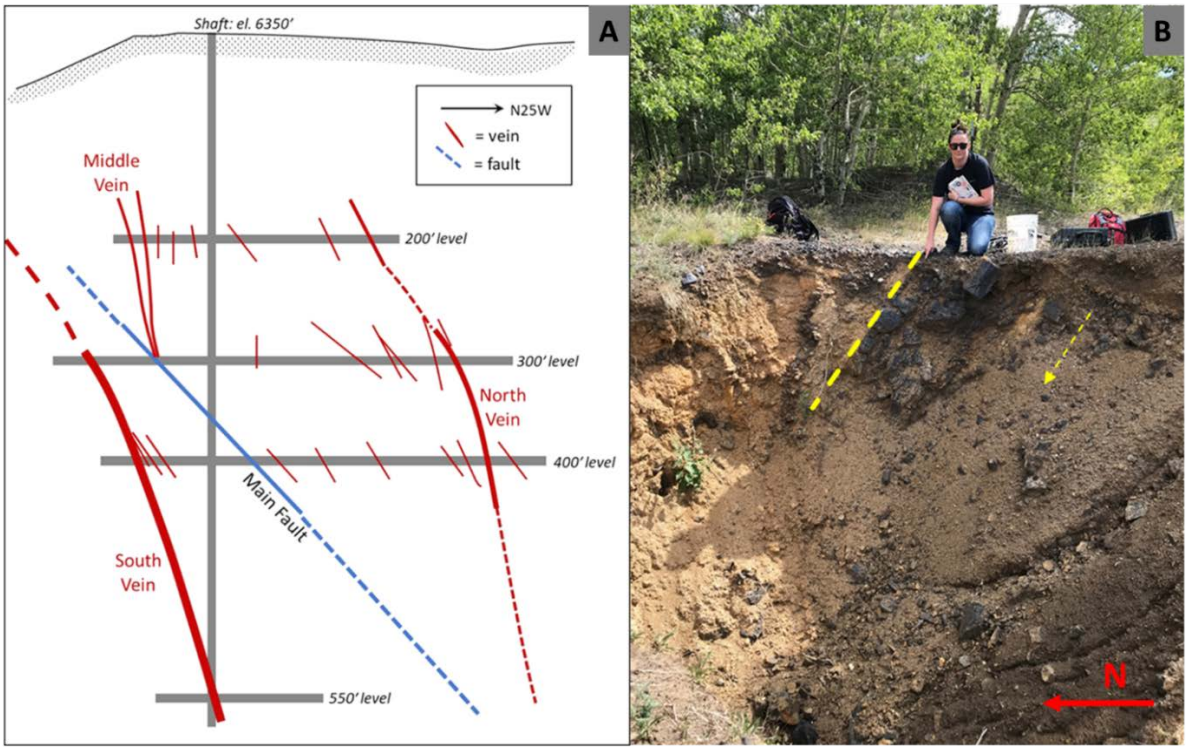

Figure 7: A) Cross-section view (looking west) of the Marget Ann mine workings (from Win, 1955). B) The Middle Vein as it crops out in a small pit near the surface (looking east).

Figure 8 (below) is a composite plan view of the mine workings, redrawn from information compiled by Noranda Exploration (1974). This map shows the distribution of veins in the subsurface at different levels (200, 300, 400, and 550 feet), also the three mining claims (Glengarry, Rescue, and Marget Ann). A north-dipping fault, referred to by Win (1955) as the Main Fault, cuts through the mine workings with a NE strike, dipping about 45 degrees to the northwest. Although this fault cuts the veins, the exact sense of offset along the fault is not known (Win, 1955).

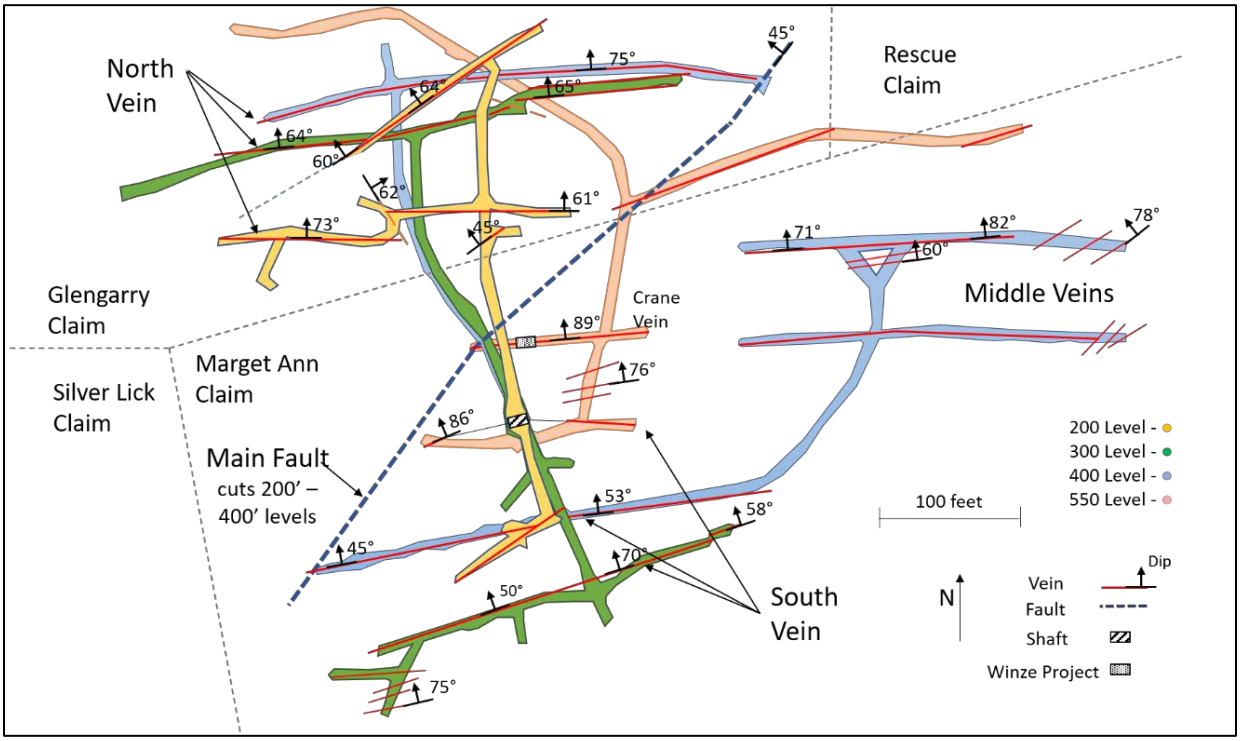

Figure 8: Plan view composite redrawn and recolored of the Marget Ann mine within the extents of Glengarry, Silver Lick, Marget Ann, and Rescue claim blocks (Noranda Exploration, Inc. & Others, 1974).

2. Methods

Methods used in this thesis include field work and sampling at the Marget Ann Mine; sampling from the Anaconda Research Collection (ARC); use of core logs and samples from the Blackjack Mining Company's core collection; sample preparation for lab work; ore microscopy; scanning electron microscopy; X-ray diffraction; and fluid inclusion micro-thermometry. Unlike the studies of Sahinen (1953) and Win (1955), the current thesis could not access the underground workings.

2.1. Location Sampling/Fieldwork

Field work done on site includes taking photos of the existing structures, surrounding area, and the dump piles, taking strike and dip measurements, and included collecting various samples of rocks from the dump piles (Figure 9). Samples that looked to have a lot of sulfides (metallic spots), rhodonite (dark pink), rhodochrosite (like milky pink), and clear to slightly milky quartz were preferred (Figure 10). Some veins crop out at the surface within the mine compound, and strikes and dips were recorded for the Middle and South veins (Table 1).

Table 1: Strikes and Dips of the Middle and South Veins

Vein	Strike	Dip
M1	235	87 N
M2	235	87 N
M3	240	66 N
S1	245	66 N
S2	210	NA
S3	215	NA
S4	265	NA
S5	NA	NA
S6	215	NA
S7	235	NA
S8	225	NA

Figure 9. Image of chalcopyrite or pyrite in a rock at the base of a dump pile located at the Marget Ann.

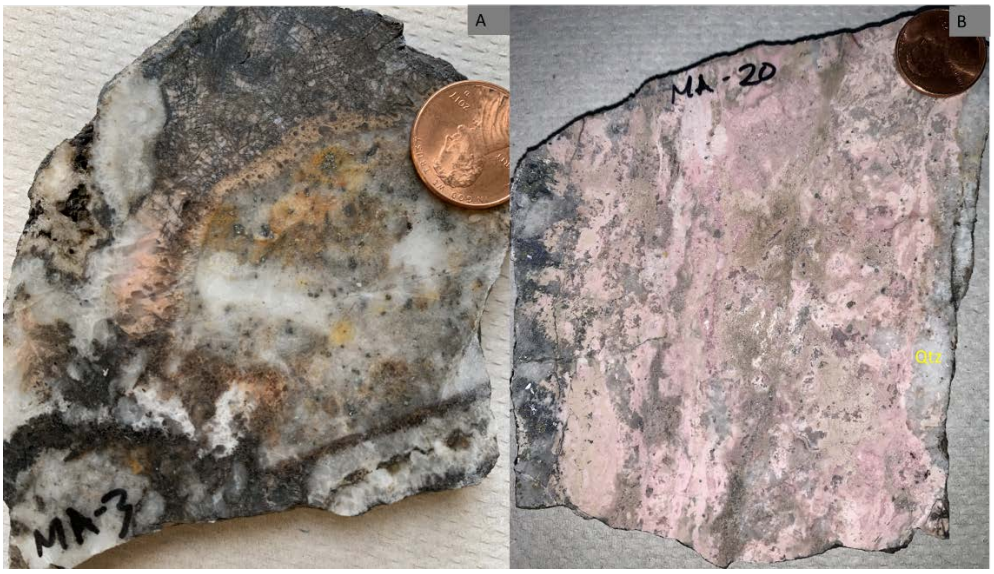

Figure 10. A) Weathered rock with quartz, rhodochrosite, sulfides, and manganese-oxide staining along the edges. B) Sample containing the pink coloring of rhodochrosite, rhodonite, and sulfides.

2.2. Collection of Archived Samples

Samples being used that do not come from the Marget Ann Mine dump piles or surrounding area have come from the Anaconda Research Collection (ARC) and Blackjack's core collection at the Badger Hoist building that is located near the Granite Mountain Memorial in Butte, Mt. as seen in Figure 11. Most of the core was in good shape, but some of it was deteriorating into granules. Only competent samples were used. For the ARC samples, a small piece of each archived specimen was sawn and made into polished epoxy plugs, and the remainder of the sample returned to the collection. The Blackjack samples came from various core boxes. The core samples also had core logs that correspond with the boxes and were transposed from the originals by Blackjack Silver Company.

Figure 11. A) Core boxes from the Blackjack Silver collection located in the Badger Hoist building. The samples were originally collected by the New Butte mining company. B) Core box DMA 88-10, box 20, depth interval between 177 ft. and 186 ft. C) Example of core sample used to make plugs for micrographs and SEM-EDS. D) Mostly competent core with some visible small veining.

2.3. Sample Preparation

All samples that have been turned into polished epoxy plugs have an identifying name, a date the sample was made, the location the sample was taken from, and what type of analysis was done (Table 2).

Table 2: List of Samples and the Type of Analysis.

Analyzed Samples List			
Name	Date	Sample Location	Analysis
AMC #3720a	10/18/2013	350’ Level	Microscopy
AMC #4316a	10/18/2013	North Vein, 500' Level	Microscopy
AMC #4316b	10/18/2013	North Vein, 500' Level	Microscopy
AMC #3867	5/26/2015	North Vein, 400' Level	SEM
AMC #5060	5/26/2015	500' Level	SEM
AMC #4316	5/26/2015	North Vein, 500' Level	SEM
MA-6	5/17/2016	Dumps	SEM
MA-8	5/17/2016	Dumps	SEM
MA 13A	5/17/2016	Dumps	SEM
MA-7A	5/17/2016	Dumps	Microscopy
MA 10	5/17/2016	Dumps	Microscopy
MA 1	5/17/2016	Dumps	Microscopy
MA 4	5/17/2016	Dumps	Microscopy
MA 7B	5/17/2016	Dumps	Microscopy
MA 2	5/17/2016	Dumps	Microscopy
MA 5	5/17/2016	Dumps	Microscopy
MA 31	8/26/2020	Dumps	Fluid Inclusion
MA 14B	8/26/2020	Dumps	Fluid Inclusion
MA 14C	8/26/2020	Dumps	SEM
MA 30A	8/26/2020	Dumps	SEM
MA 15	8/26/2020	Dumps	SEM
MA 19	8/26/2020	Dumps	SEM
MA 14A	8/26/2020	Dumps	Fluid Inclusion
MA 26A	8/26/2020	Dumps	Fluid Inclusion
MA 13	8/26/2020	Dumps	SEM
MA 23	8/26/2020	Dumps	SEM
MA 26B	8/26/2020	Dumps	SEM
MA 30B	8/26/2020	Dumps	SEM
DMA 88-10-A	2/26/2021	Drill core: 181’	SEM
DMA 88-10-B	2/26/2021	Drill core: 181'	Microscopy
DMA 88-10-A	2/26/2021	Drill core: 220'	Microscopy
DMA 88-10-B	2/26/2021	Drill core: 220'	Microscopy
DMA 88-10-A	2/26/2021	Drill core: 571'	Microscopy
DMA 88-10-B	2/26/2021	Drill core: 571'	Microscopy
DMA 88-11-A	2/26/2021	Drill core: 261'	Microscopy
DMA 88-11-B	2/26/2021	Drill core: 265'	Fluid Inclusion

2.3.1. Epoxy Plugs

Rock samples were first cut into thin (about ½ inch) slabs using either an oil saw or a water saw. The samples were then trimmed to fit inside a 1-inch diameter mold and mounted with clear epoxy (Figure 12). The epoxy mounts were then polished using a Buehler automated polisher with 75 microns (µm), 35 µm, 15 µm, and 8 µm Buehler DGD polishing disks, followed by 6 µm and 1 µm diamond paste, and finally with 0.25-micron alumina powder. The finished samples were placed in an ultrasonic cleaner for several minutes to dislodge polishing powder and rinsed thoroughly with tap water.

Figure 12. Example of completed resin plugs.

2.3.2. Fluid Inclusion Samples

Fluid inclusion samples were first made into polished plugs as described in the previous section. Each plug was then super-glued to a frosted (sanded) petrographic slide. The sample was then sliced with a Buehler Isomet low speed saw to about 100-micron (μm) thickness. The freshly cut side of the slide was then polished again with the Buehler set up (as above) and placed in an acetone bath to remove the epoxy and superglue. After 1-2 days in the acetone, the doubly polished "thick" section was carefully cleaned with warm soapy water to remove residual acetone. Next, the section was examined with a reflected-light microscope to search for fluid inclusions and to make notes about their size, shape, and phase relationships. Finally, the section was cut into several smaller "chips", each about 1 centimeter (cm) in diameter or less, for use on the fluid inclusion heating-freezing stage. (Figure 13)

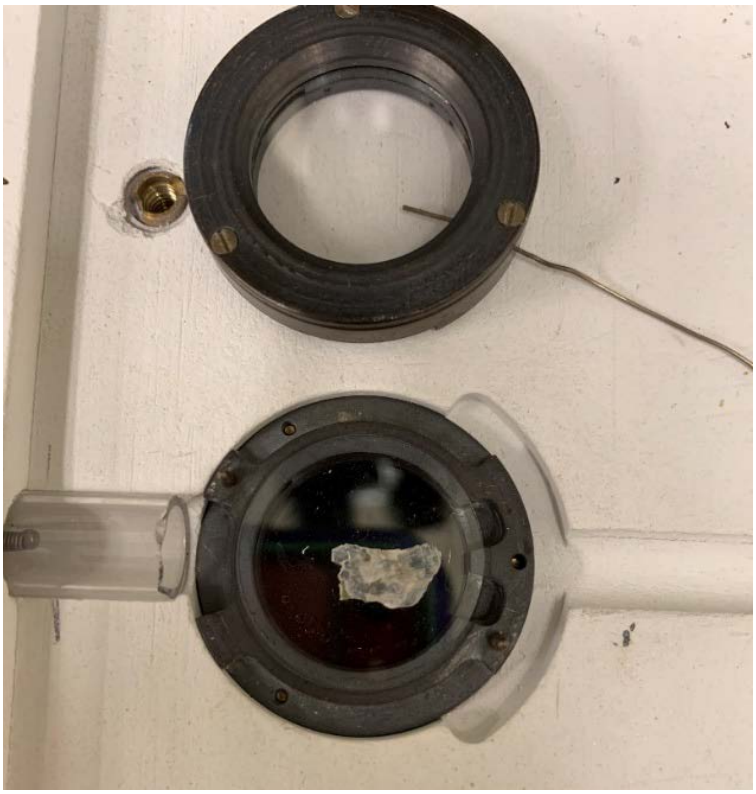

Figure 13. Example of the fluid inclusion chip after it has been trimmed and broken into sample pieces.

2.4. Analytical Methods

2.4.1. Microscopy

Polished plugs containing sulfide minerals were viewed under a Leica petrographic microscope using reflected light, which is set up to collect digital images using Leica Application Suite v4.12 (LAS) (Figure 14). Fluid inclusion samples were examined on the same microscope using transmitted light.

Figure 14. Precise measurement stage on a petrographic microscope.

2.4.2. Scanning Electron Microscope

Several polished plugs from the Marget Ann mine were examined by scanning electron microscopy (SEM) using equipment in the Center for Advanced Mineral Processing (CAMP) laboratory at Montana Tech (Figure 15). The SEM is a Tescan Mira 3 GMU. The Tescan has a field emission gun that is the electron source. The Tescan has a large specimen chamber, which is what the GMU specifies. The samples were first coated with a thin film of carbon, and then mounted in the sample tray (Figure 16). The samples were examined in several modes, including imaged backscatter electron (BSE) and elemental analysis using energy dispersive spectroscopy (EDS). The BSE detector is a scintillator type with a YAG (yttrium aluminum garnet) crystal. Under BSE, different minerals appear as different shades of gray, with minerals with high average atomic mass (e.g., galena) appearing bright, and low atomic mass (e.g., quartz) as dark regions/areas. The EDS is an EDAX Octane Elect Plus detector with a silicon drift detector (SDD) and a silicon nitride (S_3N_4) window ($30mm^2$) for light element sensitivity and low kV performance. Once the sample was imaged, individual minerals were analyzed for their chemical composition using the EDS spot mode.

Figure 15: Scanning electron microscope (SEM).

Figure 16: Loaded SEM tray with plugs that have carbon coating.

2.4.3. Fluid Inclusion Analysis

Fluid inclusion runs were performed using a United States Geological Survey (USGS) heating-freezing stage purchased from Fluid, Inc. One small, doubly polished chip is placed in the sample chamber and a thermocouple holds it in place. The sample is then heated or cooled by passing gas across the sample chamber. For freezing runs, N_2(g) is routed to a dewar containing liquid nitrogen. By forcing liquid nitrogen across the stage, inclusions can be frozen to temperatures < -100°C in less than a minute. The samples are then slowly warmed back up by blowing cold N_2(g) across the chamber and using a heating element controlled by a variac. The rate of warming is decreased to about 1°C per minute to allow for accurate recording of the temperature of final melting of ice (T_m). For heating runs, compressed air is connected to the stage and heated using the same variac power supply. Temperature is raised quickly until the vapor bubbles noticeably shrink in size, and then is slowed to about 5°C per minute to record the temperature of final bubble disappearance (temperature of homogenization, or T_h). Many of the measurements were repeated on individual inclusions in this study, and the precision of the measurements is estimated to be roughly ±0.1°C for T_m and ±2°C for T_h. Measurement precision decreases rapidly for fluid inclusions that are smaller than about 5μm in diameter. Fortunately, most of the inclusions examined in this study were > 10 μm, often > 50 μm in diameter. The thermocouple used in Dr. Gammons' set up as seen in Figure 17 is calibrated twice a year with an ice-water bath and pure H_2O synthetic fluid inclusions that homogenize by critical behavior at 374°C.

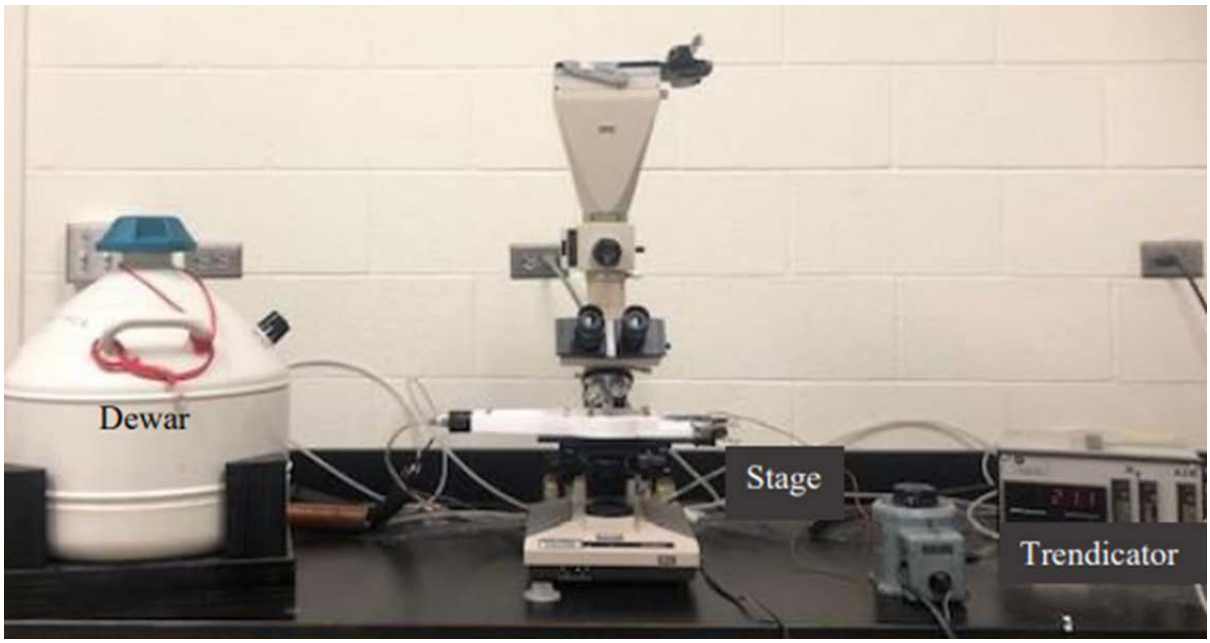

Figure 17: Fluid inclusion lab set up.

3. Results

3.1. Mineral Paragenesis

Table 3 is a list of the hypogene, and supergene minerals found in this study from the Marget Ann Mine, with their approximate abundance based on qualitative estimates. Several of the larger vein samples from the mine dumps showed a roughly 2 cm band of massive sulfide (pyrite, galena, sphalerite, chalcopyrite, tetrahedrite) on the edge of the vein next to altered granite (Figure 18A). The sulfide-rich veins were later reopened and filled with later minerals including quartz, rhodochrosite, rhodonite, dolomite, and Ag-rich minerals like acanthite, pearceite, and jalpaite (Figure 18B, 19). The later vein filling shows a variety of textures, including colloform banding, growth of comb quartz, brecciation with inclusions of wall-rock and banded massive sulfides, and multiple generations of pink Mn-rich gangue (see photos of sawn slabs in the Appendix). Coarse-grained (cm-scale), comb quartz with transparent or translucent growth zones was targeted for fluid inclusion analysis. Some of the massive-textured, pink vein fillings were spotted with dark sulfides (Figure 19) which turned out to be very rich in silver and, in some cases, gold. More details on individual hypogene minerals are given below.

Supergene minerals from Marget Ann include native silver (nearly 100% Ag), acanthite (Ag_2S), covellite, manganese (Mn) oxides, and iron (Fe) oxides. Although acanthite is more common as a hypogene mineral at Marget Ann, it can also form by leaching of silver during weathering and redeposition below the water table, much like chalcocite (Cu_2S) (Gammons et al., 2016). The manganese oxides can be seen in the dump piles and on a vein cut in one of the old open exploration pits (Figure 7). Attempts to identify the black oxide coatings by XRD were unsuccessful, and only gave peaks for quartz. This means that the manganese oxides were poorly

ordered or amorphous. Based on analysis using a Terraspec Halo infrared mineral analyzer, most of the Fe-oxides were identified as goethite.

Table 3: Paragenesis of the Marget Ann Mine. Darker shades are greater mineral abundances. Lighter shades are a lower mineral abundance.

Gangue Minerals	**Formula**	**Hypogene**	**Supergene**
Quartz	SiO_2		
Rhodonite	$(Ca,Mn)Mn_4[Si_5O_{15}]$		
Calcite	$(Ca,Mn)CO_3$		
Rhodochrosite	$(Mn,Ca)CO_3$		
Sericite	$KAl_2(AlSi_3O_{10})(OH)_2$		
Adularia	$KAlSi_3O_8$		
Mn-Oxides	Not specified		
Goethite	FeOOH		
Fluorapatite	$Ca_5(PO_4)_3F$		
Dolomite	$Ca(Mg,Fe,Mn)(CO_3)_2$		
Ore Minerals		**Hypogene**	**Supergene**
Pyrite	FeS_2		
Chalcopyrite	$CuFeS_2$		
Galena	PbS		
Sphalerite	(Zn,Mn,Fe)S		
Electrum	(Au,Ag)		
Native silver	Ag		
Acanthite	Ag_2S		
Jalpaite	Ag_3CuS_2		
Covellite	CuS		
Uytenbogaardtite	Ag_3AuS_2		
Pearceite	$((Ag,Au)_6(As,Sb)_2S_7)(Ag_9CuS_4)$		
Polybasite	$((Ag,Au)_6(Sb,As)_2S_7)(Ag_9CuS_4)$		
Tetrahedrite	$(Cu,Ag)_6(Cu)_4(Zn,Fe)_2Sb_4S_{13}$		
Tennantite	$(Cu,Ag)_6(Cu)_4(Zn,Fe)_2As_4S_{13}$		
Stromeyerite	AgCuS	?	?
Wulfenite	$PbMoO_4$	?	?

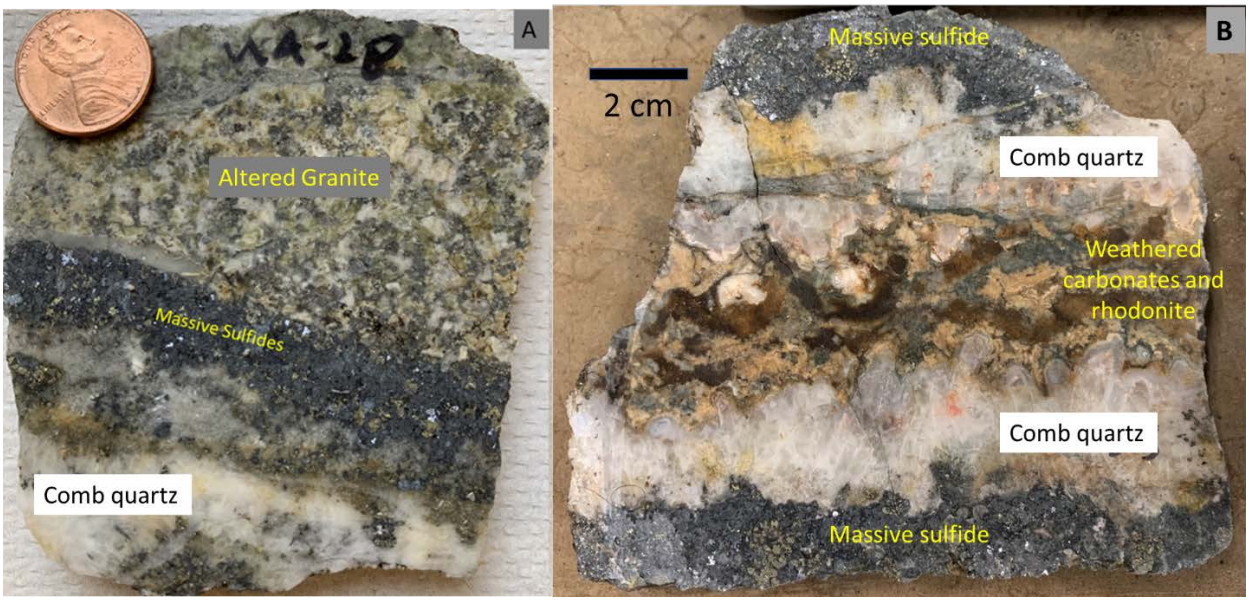

Figure 18: A) Half of a banded vein showing massive sulfide next to altered granite with later comb quartz at the bottom (sample MA-28). B) An intact vein showing rims of massive sulfide, comb quartz, and a central band of weathered carbonates and rhodonite (MA-33).

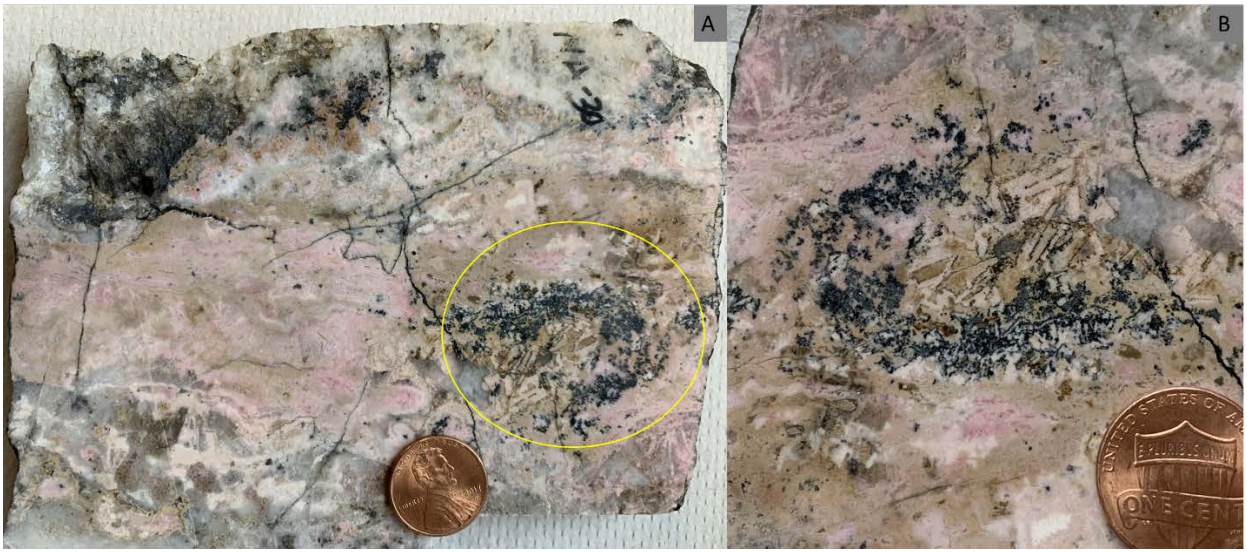

Figure 18: A) Disseminated silver-rich sulfides in a band of Mn-rich gangue (area in yellow circle) from sample MA-30. B) Zoomed in area of sulfides surrounded by quartz, rhodonite (weathering pale brown), and rhodochrosite.

3.1.1. Mineral Chemistry

3.1.1.1. Electrum

Gold in the Marget Ann mine comes in the form of the mineral alloy, electrum (El) (Au,Ag). Electrum was found in several samples from the dump piles, drill core (181 ft. interval), and ARC samples 4316 and 5060 collected by Anaconda geologists in the 1950s from the 500 ft. level drift. The electrum is associated with many silver-bearing sulfide minerals, particularly acanthite (Ac) and pearceite (Prc), as shown in Figures 20 and 21. As shown in Figure 20, electrum tends to be more gold rich towards the center of the grain. The atomic percentage of Au (X_{Au}) in the middle is 0.6 whereas the rims have $X_{Au} = 0.2$. Although zoned electrum grains can sometimes form during weathering, in this case the electrum is completely surrounded by pearceite. Also, the sample (ARC 4316) came from the 500' level of the mine, and is therefore unlikely to have been weathered. Therefore, it is more likely that the change in composition of the electrum was due to a change in the chemistry of the ore-forming fluid, evolving to more Ag-rich over time. Most of the electrum in the Marget Ann samples range from approximately 5µm to 100µm in size. The compositions of 44 grains of electrum found in this study are summarized in Table 4 and Figure 22; the gold and silver compositions form a bell-shaped curve. The average atomic percent of gold is $X_{Au} = 0.44$, equivalent to 58.9 weight% Au, or a fineness of 589 (Table 4).

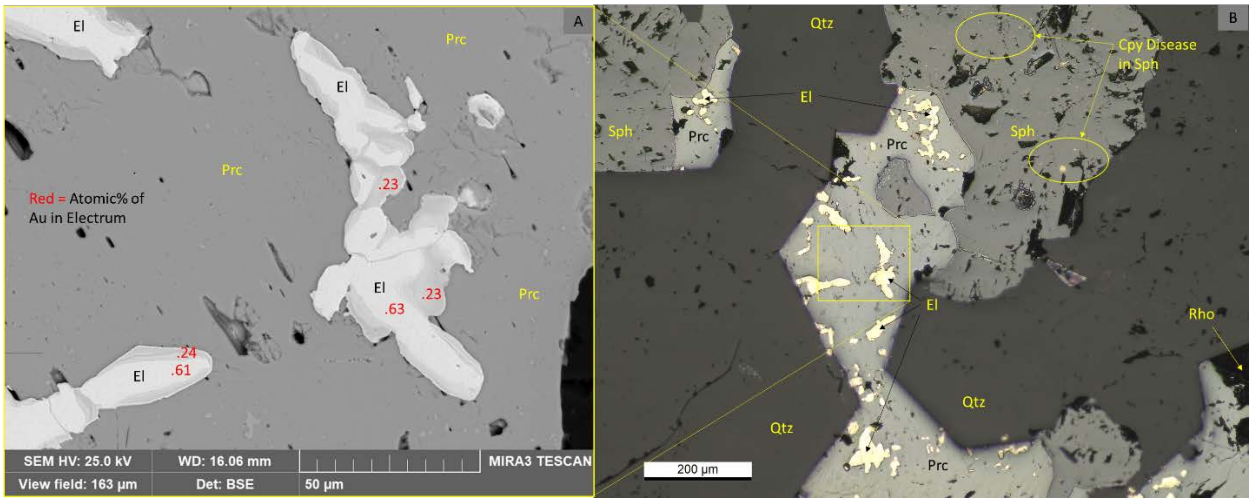

Figure 19. A) SEM-BSE image of electrum (El) from sample AMC4316 with lower gold atomic percentage (X_{Au}) around the darker gray edges, surrounded by pearceite (Prc). B) Reflected light photo of zoomed out area showing the electrum (El) in the pearceite (Prc), next to sphalerite (Sph) with chalcopyrite disease. Gangue minerals include rhodochrosite (Rho) and quartz (Qtz).

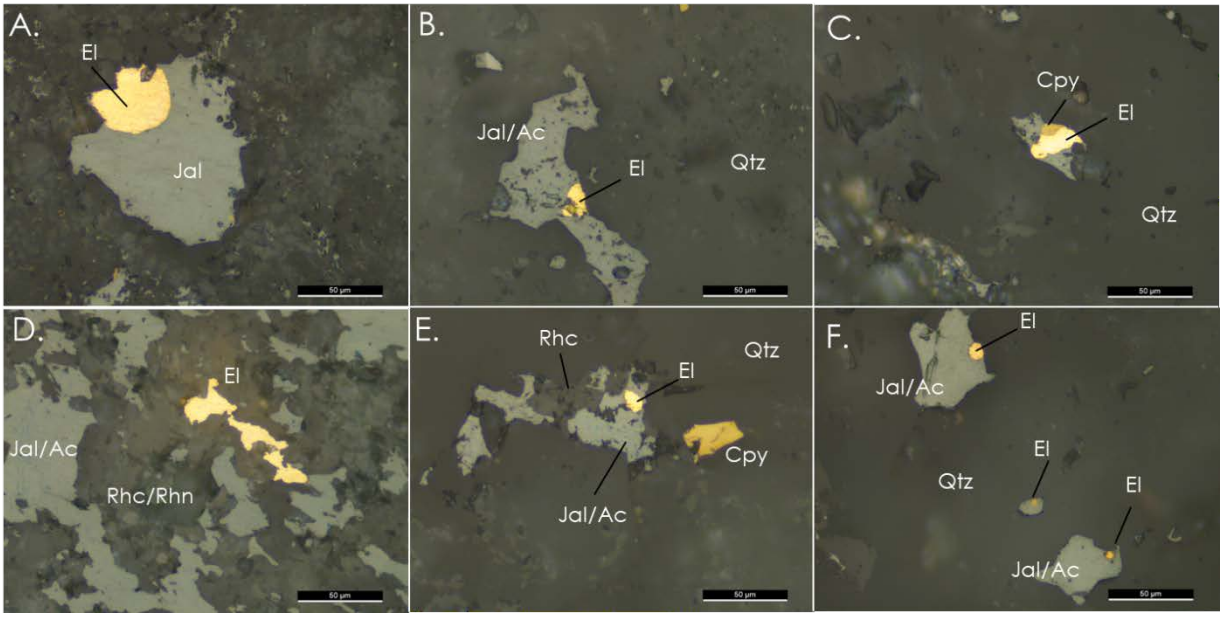

Figure 20: Example reflected light pictures of electrum (El) intergrown with jalpaite (Jal) and acanthite (Ac). The dark gangue is a mixture of quartz (Qtz), rhodochrosite (Rhc) and rhodonite (Rhn). Panels A through E are from sample MA-13, and Panel F is sample MA-30.

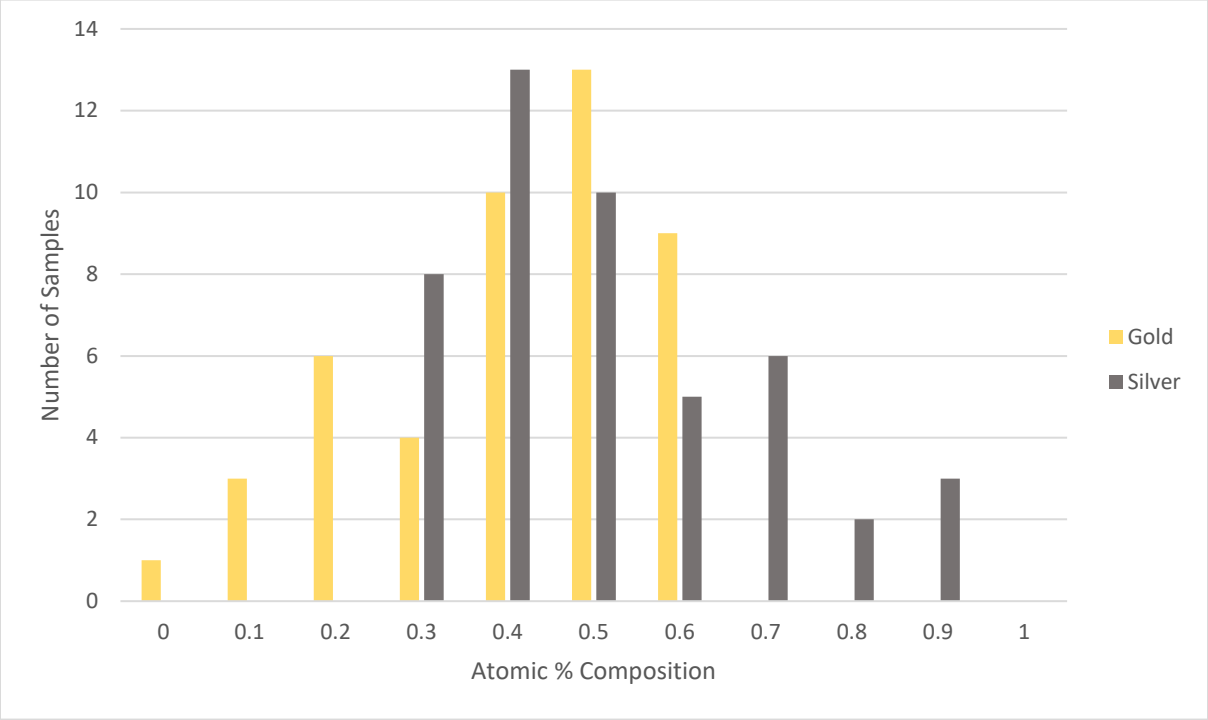

Figure 21: Histogram of electrum compositions.

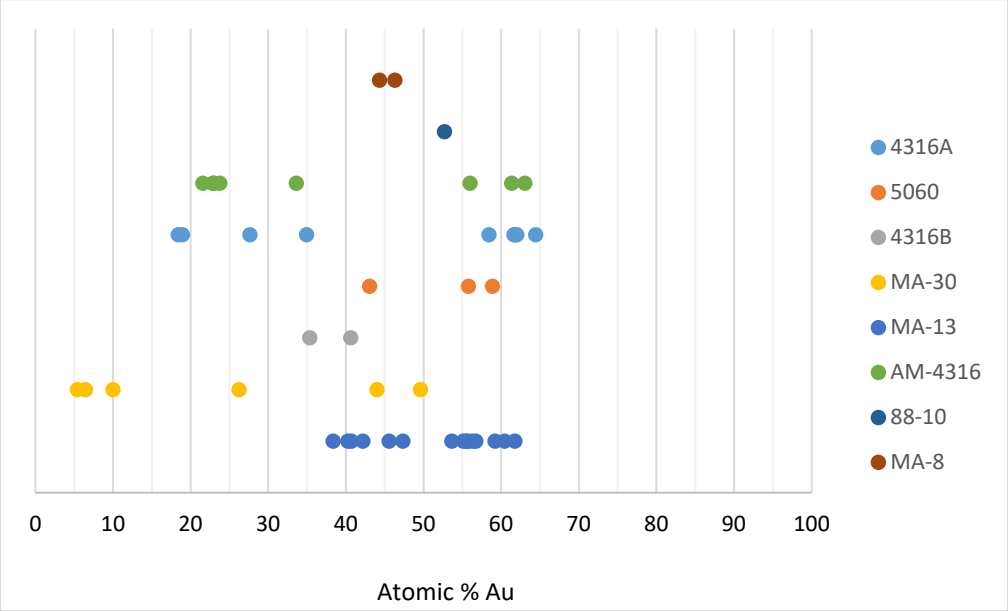

Figure 22: Atomic % of gold in electrum.

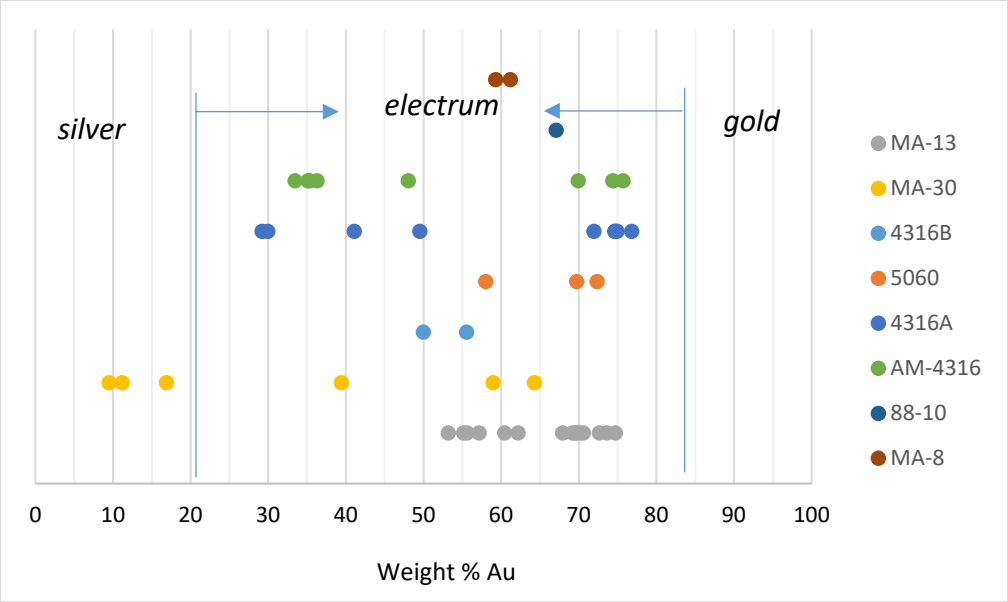

Figure 23: Weight % of gold in electrum.

Table 4: Atomic Percentages and Calculated Formulas from SEM-EDS Analysis of Electrum

	Atomic %			
Mineral	Sample #	Ag	Au	Chemical Formula
Electrum	AMC 4316B	64.7	35.3	**$(Au_{.35}Ag_{.65})$**
Electrum	AMC 4316B	59.4	40.6	**$(Au_{.41}Ag_{.59})$**
Electrum	AMC 4316A	38.3	61.7	**$(Au_{.62}Ag_{.38})$**
Silver	AMC 4316A	81.1	19.0	**$(Au_{.19}Ag_{.81})$**
Electrum	AMC 4316A	41.6	58.4	**$(Au_{.58}Ag_{.42})$**
Electrum	AMC 4316A	37.7	62.3	**$(Au_{.62}Ag_{.38})$**
Electrum	AMC 4316A	38.0	62.0	**$(Au_{.62}Ag_{.38})$**
Electrum	AMC 4316A	35.6	64.5	**$(Au_{.64}Ag_{.36})$**
Silver	AMC 4316A	81.6	18.4	**$(Au_{.18}Ag_{.82})$**
Electrum	AMC 4316A	65.1	34.9	**$(Au_{.35}Ag_{.65})$**
Electrum	AMC 4316A	38.2	61.8	**$(Au_{.62}Ag_{.38})$**
Electrum	AMC 4316A	72.4	27.6	**$(Au_{.28}Ag_{.72})$**
Electrum	AMC 5060	41.1	58.9	**$(Au_{.59}Ag_{.41})$**
Electrum	AMC 5060	44.2	55.8	**$(Au_{.56}Ag_{.44})$**
Electrum	AMC 5060	56.9	43.1	**$(Au_{.43}Ag_{.57})$**
Electrum	MA-13	39.6	60.4	**$(Au_{.60}Ag_{.40})$**
Electrum	MA-13	59.7	40.3	**$(Au_{.40}Ag_{.60})$**
Electrum	MA-13	46.3	53.7	**$(Au_{.54}Ag_{.46})$**
Electrum	MA-13	54.4	45.6	**$(Au_{.46}Ag_{.54})$**
Electrum	MA-13	40.8	59.2	**$(Au_{.59}Ag_{.41})$**
Electrum	MA-13	43.7	56.3	**$(Au_{.56}Ag_{.44})$**
Electrum	MA-13	61.7	38.4	**$(Au_{.38}Ag_{.62})$**
Electrum	MA-13	44.4	55.6	**$(Au_{.56}Ag_{.44})$**
Electrum	MA-13	52.7	47.4	**$(Au_{.47}Ag_{.53})$**
Electrum	MA-13	38.2	61.8	**$(Au_{.62}Ag_{.38})$**
Electrum	MA-13	44.3	55.7	**$(Au_{.56}Ag_{.44})$**
Electrum	MA-13	43.3	56.8	**$(Au_{.57}Ag_{.43})$**
Electrum	MA-13	46.4	42.2	**$(Au_{.48}Ag_{.52})$**
Electrum	MA-30	73.8	26.3	**$(Au_{.26}Ag_{.74})$**
Silver	MA-30	90.0	10.0	**$(Au_{.10}Ag_{.90})$**
Silver	MA-30	93.6	6.5	**$(Au_{.06}Ag_{.94})$**
Electrum	MA-30	56.0	44.0	**$(Au_{.44}Ag_{.56})$**
Electrum	MA-30	50.4	49.6	**$(Au_{.50}Ag_{.50})$**
Electrum	AMC-4316	37.0	63.0	**$(Au_{.63}Ag_{.37})$**
Electrum	AMC-4316	77.0	23.0	**$(Au_{.23}Ag_{.77})$**
Electrum	AMC-4316	77.2	22.8	**$(Au_{.23}Ag_{.77})$**
Electrum	AMC-4316	66.4	33.6	**$(Au_{.34}Ag_{.66})$**
Electrum	AMC-4316	38.6	61.4	**$(Au_{.61}Ag_{.39})$**
Electrum	AMC-4316	76.3	23.8	**$(Au_{.24}Ag_{.76})$**
Electrum	AMC-4316	78.4	21.6	**$(Au_{.22}Ag_{.78})$**
Electrum	AMC-4316	44.0	56.0	**$(Au_{.56}Ag_{.44})$**
Electrum	88-10*	47.3	52.7	**$(Au_{.53}Ag_{.47})$**
Electrum	MA-8	53.7	46.3	**$(Au_{.46}Ag_{.54})$**
Electrum	MA-8	52.9	44.3	**$(Au_{.46}Ag_{.54})$**

*DMA 88-10, 171 ft.

3.1.1.2. Tetrahedrite/Tennantite

The tetrahedrite and tennantite were only found in samples with a high concentration of the common sulfide minerals, such as pyrite, galena, chalcopyrite, and sphalerite as seen in Figure 25 and 26. According to Mindat (accessed 2021), the ideal formula for tetrahedrite can be written as follows: $(Cu,Ag)_6Cu_4(Fe,Zn)_2(Sb,As)_4S_{13}$. The difference between tetrahedrite and tennantite depends on whether Sb or As, respectively, is dominant on an atomic % basis. The relationships between element pairs (in parentheses) in the tetrahedrite formula should be inversely related and have a slope of -1 (Figure 27). In addition, there is a positive relationship between Ag and Sb. The compositions of 20 grains of tetrahedrite-tennantite analyzed in this study by SEM-EDS are presented in Table 5 and show an average Ag content is 12.15 weight %. Although all the tetrahedrites contain a significant amount of silver, none have high enough to qualify as the mineral freibergite (a related species that has Ag > Cu in the "A" cation site, Mindat, 2022).

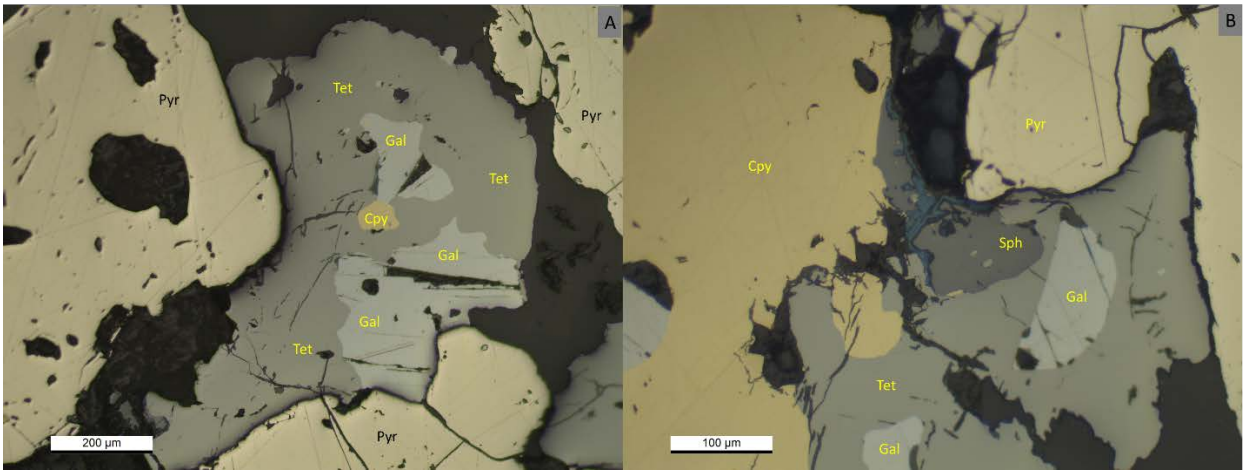

Figure 24: A) Example of tetrahedrite (Tet) from sample MA4-2016, with massive sulfide assemblage minerals galena (Gal), chalcopyrite (Cpy), and pyrite (Pyr). B) Another example of tetrahedrite from the same sample in massive sulfide assemblage.

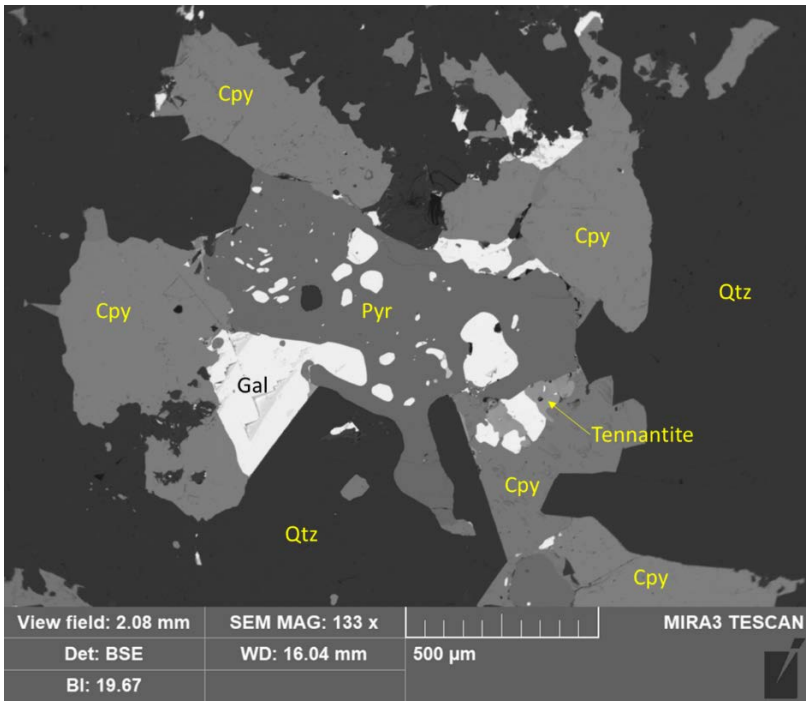

Figure 25: Tennantite from sample MA13 in massive sulfide assemblage.

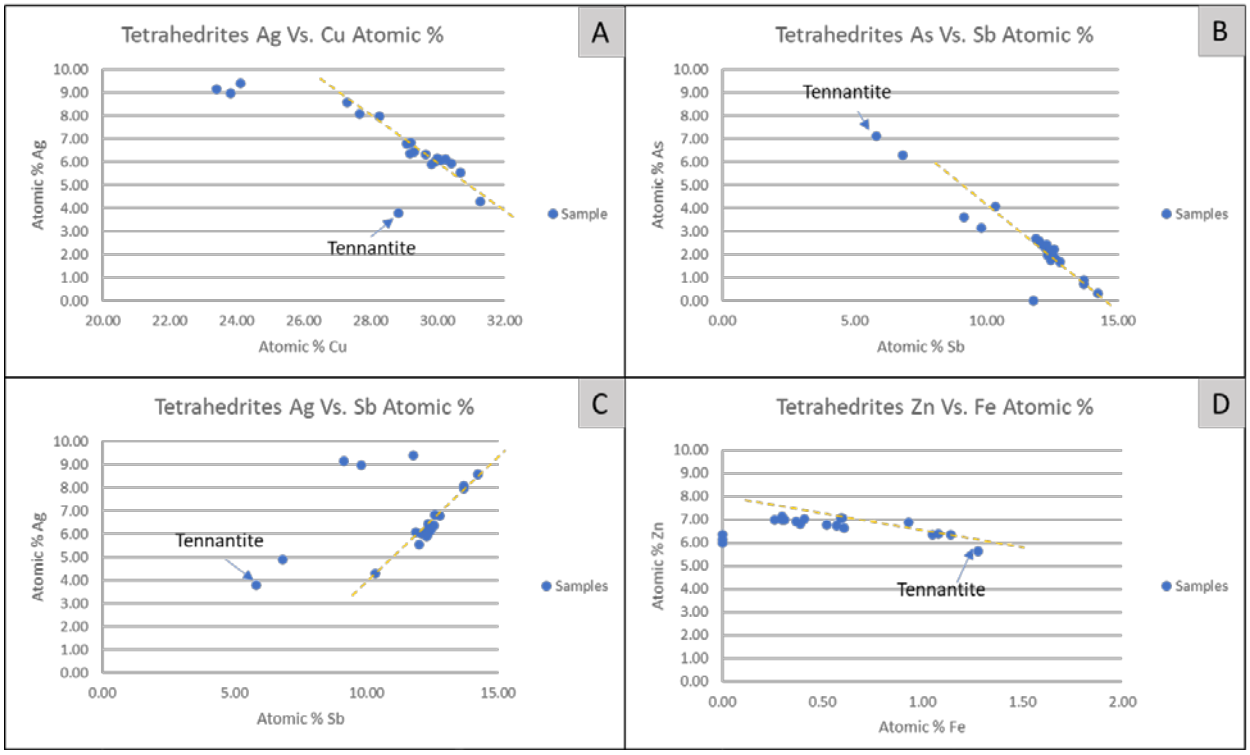

Figure 26:A) The inverse relationship between silver and copper. B) The inverse relationship between arsenic and antimony. C) The positive relationship between silver and antimony. D) The inverse relationship between zinc and iron.

Table 5: Atomic Percentages and Calculated Formulas from SEM-EDS Analysis of Tetrahedrite and Tennantite

		Atomic %							
Mineral	Sample #	Cu	Ag	Zn	Fe	Sb	As	S	Chemical Formula
Tetrahedrite	Old MA-4	30.0	6.2	7.0	0.4	12.4	1.8	42.2	$(Cu_{.72}Ag_{.28})_6(Cu)_4(Zn_{.94}Fe_{.06})_2(Sb_{.88}As_{.12})_4S_{13}$
Tetrahedrite	Old MA-4	29.9	6.0	6.7	0.6	12.1	2.5	42.2	$(Cu_{.72}Ag_{.28})_6(Cu)_4(Zn_{.92}Fe_{.08})_2(Sb_{.83}As_{.17})_4S_{13}$
Tetrahedrite	Old MA-4	29.1	6.8	7.0	0.3	12.8	1.7	42.4	$(Cu_{.68}Ag_{.32})_6(Cu)_4(Zn_{.96}Fe_{.04})_2(Sb_{.88}As_{.12})_4S_{13}$
Tetrahedrite	Old MA-4	29.2	6.4	6.4	1.1	12.6	2.2	42.1	$(Cu_{.70}Ag_{.30})_6(Cu)_4(Zn_{.86}Fe_{.14})_2(Sb_{.84}As_{.15})_4S_{13}$
Tetrahedrite	Old MA-4	28.3	8.0	7.1	0.3	13.7	0.7	41.9	$(Cu_{.63}Ag_{.37})_6(Cu)_4(Zn_{.96}Fe_{.04})_2(Sb_{.95}As_{.05})_4S_{13}$
Tetrahedrite	Old MA-4	30.7	5.6	7.1	0.6	12.0	2.6	41.5	$(Cu_{.74}Ag_{.26})_6(Cu)_4(Zn_{.92}Fe_{.08})_2(Sb_{.82}As_{.18})_4S_{13}$
Tetrahedrite	Old MA-4	29.3	6.4	6.3	1.1	12.4	2.2	42.2	$(Cu_{.70}Ag_{.30})_6(Cu)_4(Zn_{.85}Fe_{.15})_2(Sb_{.85}As_{.15})_4S_{13}$
Tetrahedrite	Old MA-4	29.2	6.8	6.8	0.4	12.6	1.9	42.3	$(Cu_{.68}Ag_{.32})_6(Cu)_4(Zn_{.95}Fe_{.05})_2(Sb_{.87}As_{.13})_4S_{13}$
Tetrahedrite	Old MA-4	29.8	5.9	7.0	0.3	12.3	2.4	42.3	$(Cu_{.72}Ag_{.28})_6(Cu)_4(Zn_{.96}Fe_{.04})_2(Sb_{.83}As_{.17})_4S_{13}$
Tetrahedrite	Old MA-4	30.2	6.1	7.0	0.3	12.2	2.3	41.8	$(Cu_{.72}Ag_{.28})_6(Cu)_4(Zn_{.96}Fe_{.04})_2(Sb_{.84}As_{.16})_4S_{13}$
Tetrahedrite	Old MA-4	30.4	5.9	7.1	0.6	12.3	2.0	41.7	$(Cu_{.73}Ag_{.27})_6(Cu)_4(Zn_{.92}Fe_{.08})_2(Sb_{.86}As_{.14})_4S_{13}$
Tetrahedrite	Old MA-4	30.1	6.1	6.9	0.9	11.9	2.7	41.4	$(Cu_{.72}Ag_{.28})_6(Cu)_4(Zn_{.88}Fe_{.12})_2(Sb_{.82}As_{.18})_4S_{13}$
Tetrahedrite	Old MA-4	29.7	6.3	6.8	0.5	12.4	2.1	42.3	$(Cu_{.71}Ag_{.29})_6(Cu)_4(Zn_{.93}Fe_{.07})_2(Sb_{.86}As_{.14})_4S_{13}$
Tetrahedrite	Old MA-4	27.7	8.1	6.9	0.4	13.7	0.9	42.4	$(Cu_{.62}Ag_{.38})_6(Cu)_4(Zn_{.95}Fe_{.05})_2(Sb_{.94}As_{.06})_4S_{13}$
Tetrahedrite	Old MA-4	31.3	4.3	6.4	1.1	10.4	4.1	42.6	$(Cu_{.80}Ag_{.20})_6(Cu)_4(Zn_{.86}Fe_{.14})_2(Sb_{.72}As_{.28})_4S_{13}$
Tetrahedrite	Old MA-4	27.3	8.6	6.6	0.6	14.2	0.4	42.3	$(Cu_{.60}Ag_{.40})_6(Cu)_4(Zn_{.92}Fe_{.08})_2(Sb_{.98}As_{.02})_4S_{13}$
Tetrahedrite	MA-15	23.8	9.0	6.1	0.0	9.8	3.2	48.1	$(Cu_{.54}Ag_{.46})_6(Cu)_4(Zn)_2(Sb_{.76}As_{.24})_4S_{13}$
Tetrahedrite	MA-15	24.1	9.4	6.3	0.0	11.8	0.0	48.3	$(Cu_{.53}Ag_{.47})_6(Cu)_4(Zn)_2(Sb)_4S_{13}$
Tetrahedrite	MA-15	23.4	9.2	6.0	0.0	9.2	3.6	48.7	$(Cu_{.53}Ag_{.47})_6(Cu)_4(Zn)_2(Sb_{.72}As_{.28})_4S_{13}$
Tennantite	MA-26B	28.9	3.8	5.7	1.3	5.8	7.1	47.4	$(Cu_{.81}Ag_{.19})_6(Cu)_4(Zn_{.82}Fe_{.18})_2(Sb_{.45}As_{.55})_4S_{13}$

3.1.1.3. Pearceite/Polybasite

Pearceite and polybasite are sulfosalts with the formula $(Ag,Cu)_6(As,Sb)_2S_7(Ag_9CuS_4)$, or $A_6B_2S_7(Ag_9CuS_4)$where pearceite has As > Sb and polybasite has Sb > As in the B site on an atomic % basis (Table 6). While proustite and pyrargyrite were listed as other sulfosalts in Win (1955), no samples were found that had mineral compositions consistent with these minerals in this study. Additionally, polybasite is much less common than pearceite in the samples examined (Figure 28 and 29). Pearceite-polybasite was often found associated with electrum and other Ag-rich sulfide minerals. Some of the samples as listed in Table 6 are slightly richer in copper than in silver in the A site and are therefore referred to as cupropearceite.

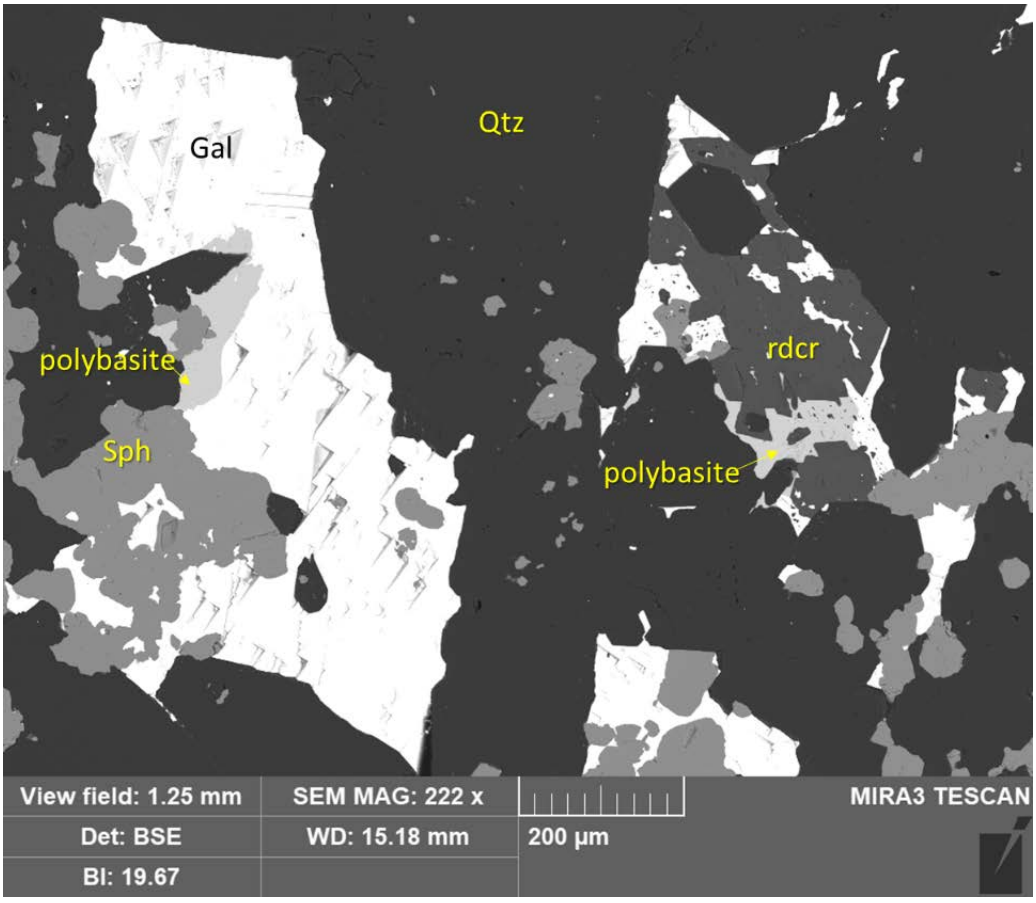

Figure 27: SEM-EDS photo of polybasite intergrown with galena (Gal) and sphalerite (Sph) from sample MA-19. Gangue is quartz (Qtz).

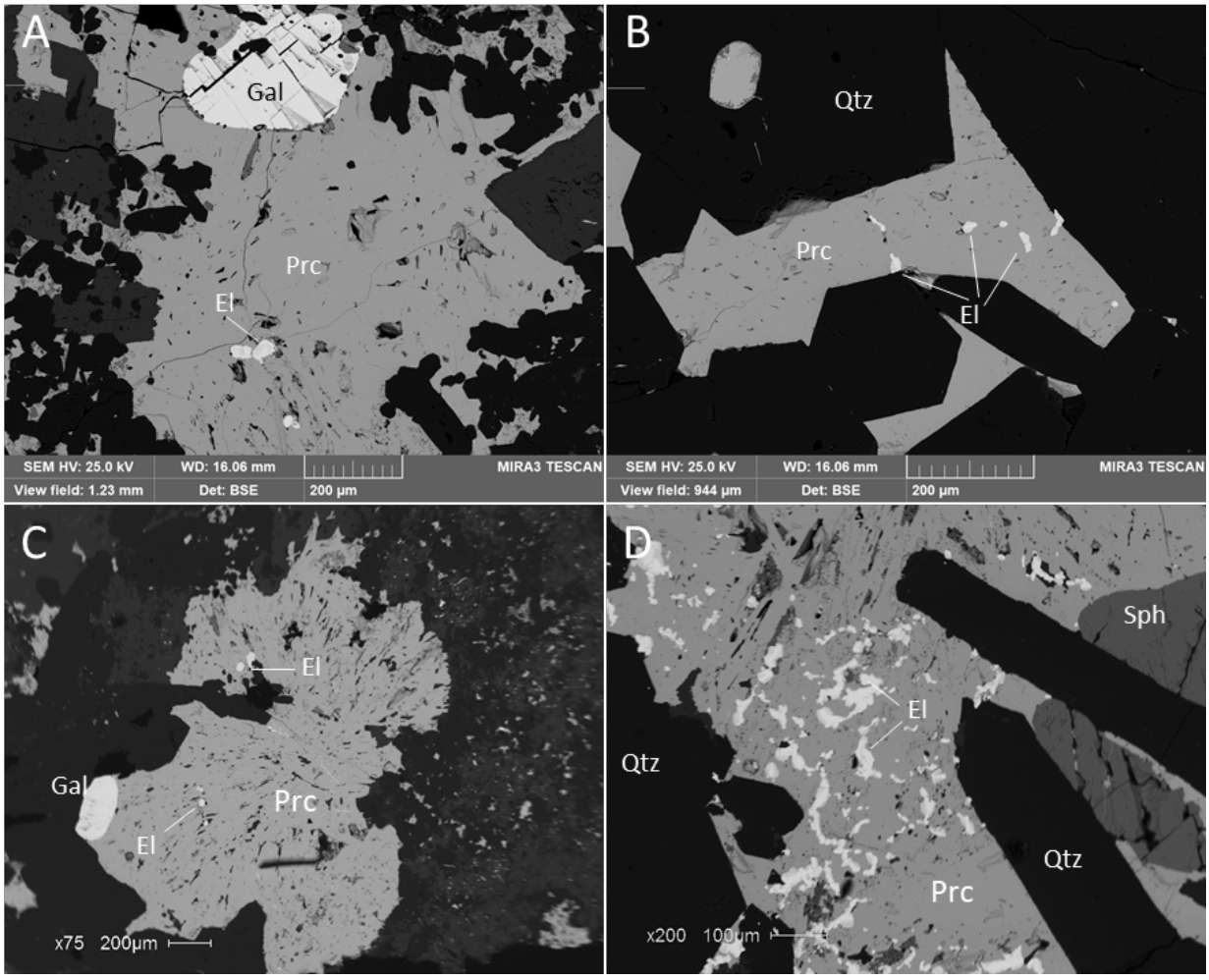

Figure 28: SEM-BSE photos of pearceite (Prc) intergrown with electrum (El) from sample AMC 4316, in a gangue of rhodochrosite and quartz.

Table 6: Atomic Percentages and Calculated Formulas from SEM-EDS Analysis of Pearceite and Polybasite

		Atomic %					
Mineral	Sample #	As	Cu	Ag	S	Sb	Chemical Formula
Pearceite	AMC 4316B	7.5	9.7	47.1	35.8	0.0	$[(Ag_{.69}Cu_{.31})_6As_2S_7][Ag_9CuS_4]$
Pearceite	AMC 4316B	6.7	9.7	47.5	34.4	0.0	$[(Ag_{.73}Cu_{.27})_6As_2S_7][Ag_9CuS_4]$
Pearceite	AMC 4316B	6.7	9.7	47.3	35.6	0.0	$[(Ag_{.73}Cu_{.27})_6As_2S_7][Ag_9CuS_4]$
Pearceite	AMC 4316B	5.6	8.2	51.5	34.7	0.0	$[(Ag_{.83}Cu_{.17})_6As_2S_7][Ag_9CuS_4]$
Pearceite	AMC 4316B	7.1	10.3	46.8	35.9	0.0	$[(Ag_{.31}Cu_{.69})_6As_2S_7][Ag_9CuS_4]$
Pearceite	AMC 4316A	6.9	9.3	47.4	36.4	0.0	$[(Ag_{.74}Cu_{.26})_6As_2S_7][Ag_9CuS_4]$
Pearceite	AMC 4316A	5.1	9.0	50.4	35.5	0.0	$[(Ag_{.81}Cu_{.19})_6As_2S_7][Ag_9CuS_4]$
Pearceite	AMC 4316A	6.8	8.0	50.8	34.4	0.0	$[(Ag_{.81}Cu_{.19})_6As_2S_7][Ag_9CuS_4]$
Pearceite	AMC 4316A	5.7	8.6	51.3	34.5	0.0	$[(Ag_{.82}Cu_{.18})_6As_2S_7][Ag_9CuS_4]$
Pearceite	AMC 4316A	6.3	8.2	49.3	36.2	0.0	$[(Ag_{.81}Cu_{.19})_6As_2S_7][Ag_9CuS_4]$
Pearceite	MA-19	3.8	4.0	50.6	38.7	3.0	$[(Ag_{.97}Cu_{.03})_{6(}As_{.56}Sb_{.44})_2S_7][Ag_9CuS_4]$
Polybasite	MA-19	0.0	3.7	50.3	41.1	4.9	$[(Ag_{.96}Cu_{.04})_6Sb_2S_7][Ag_9CuS_4]$
Pearceite	MA-30	6.0	12.9	39.0	42.1	0.0	$[(Ag_{.55}Cu_{.45})_6As_2S_7][Ag_9CuS_4]$
Pearceite	MA-30	6.8	12.5	38.9	41.9	0.0	$[(Ag_{.48}Cu_{.52})_6As_2S_7][Ag_9CuS_4]$
Polybasite	MA-15	0.0	4.0	50.1	40.3	5.6	$[(Ag_{.96}Cu_{.04})_6Sb_2S_7][Ag_9CuS_4]$
Pearceite	MA-30	6.0	12.9	39.0	42.1	0.0	$[(Ag_{.55}Cu_{.45})_6As_2S_7][Ag_9CuS_4]$
CuproPearceite	MA-30	6.8	12.5	38.9	41.9	0.0	$[(Ag_{.48}Cu_{.52})_6As_2S_7][Ag_9CuS_4]$
Pearceite	MA-19	3.8	4.0	50.6	38.7	3.0	$[(Ag_{.96}Cu_{.04})_6(As_{.56}Sb_{.44})S_7][Ag_9CuS_4]$
Polybasite	MA-19	0.0	3.7	50.3	41.1	4.9	$[(Ag_{.96}Cu_{.04})_6Sb_2S_7][Ag_9CuS_4]$
Polybasite	MA-19	0.0	3.7	50.0	41.4	5.0	$[(Ag_{.96}Cu_{.04})_6Sb_2S_7][Ag_9CuS_4]$
Polybasite	MA-19	0.0	3.5	51.5	39.6	5.0	$[(Ag_{.97}Cu_{.03})_6Sb_2S_7][Ag_9CuS_4]$
Polybasite	MA-19	0.0	3.6	51.4	39.9	5.2	$[(Ag_{.97}Cu_{.03})_6Sb_2S_7][Ag_9CuS_4]$
Pearceite	AMC-4316	6.3	8.1	45.9	40.0	0.0	$[(Ag_{.78}Cu_{.22})_6As_2S_7][Ag_9CuS_4]$
Pearceite	AMC-4316	5.0	6.6	55.4	33.0	0.0	$[(Ag_{.89}Cu_{.11})_6As_2S_7][Ag_9CuS_4]$
Pearceite	AMC-4316	6.2	8.0	45.5	40.3	0.0	$[(Ag_{.78}Cu_{.22})_6As_2S_7][Ag_9CuS_4]$
Pearceite	AMC-4316	6.0	7.9	46.3	39.8	0.0	$[(Ag_{.8}Cu_{.2})_6As_2S_7][Ag_9CuS_4]$
Pearceite	AMC-4316	6.0	8.7	44.4	40.9	0.0	$[(Ag_{.75}Cu_{.25})_6As_2S_7][Ag_9CuS_4]$
Pearceite	MA 88-10	6.0	12.1	40.0	41.8	0.0	$[(Ag_{.59}Cu_{.41})_6As_2S_7][Ag_9CuS_4]$
Pearceite	MA 88-10	4.4	10.7	51.1	33.8	0.0	$[(Ag_{.79}Cu_{.21})_6As_2S_7][Ag_9CuS_4]$
Pearceite	MA 88-10	4.8	10.6	52.8	31.9	0.0	$[(Ag_{.79}Cu_{.21})_6As_2S_7][Ag_9CuS_4]$
Pearceite	MA 88-10	5.2	11.6	48.7	34.5	0.0	$[(Ag_{.74}Cu_{.26})_6As_2S_7][Ag_9CuS_4]$
Pearceite	MA 88-10	4.3	9.5	53.3	33.0	0.0	$[(Ag_{.82}Cu_{.18})_6As_2S_7][Ag_9CuS_4]$
Pearceite	MA 88-10	4.2	9.2	54.2	32.5	0.0	$[(Ag_{.83}Cu_{.17})_6As_2S_7][Ag_9CuS_4]$
Pearceite	MA 88-10	6.2	13.2	39.4	41.2	0.0	$[(Ag_{.53}Cu_{.47})_6As_2S_7][Ag_9CuS_4]$
Pearceite	MA 88-10	5.2	10.7	49.6	34.5	0.0	$[(Ag_{.77}Cu_{.23})_6As_2S_7][Ag_9CuS_4]$
Pearceite	MA 88-10	4.7	10.1	52.1	33.1	0.0	$[(Ag_{.80}Cu_{.20})_6As_2S_7][Ag_9CuS_4]$
Pearceite	MA 88-10	5.3	11.3	36.4	37.0	0.0	$[(Ag_{.59}Cu_{.41})_6As_2S_7][Ag_9CuS_4]$

3.1.1.4. Jalpaite

Jalpaite (pronounced hal-pite) is a copper-bearing silver sulfide that is a tetragonal sulfosalt with the formula Ag_3CuS_2 (complex mineral composition with the general formula of $A_mB_nX_p$ where (m+n):p = 2:1) (Mindat, 2022). Ideal jalpaite has a silver to copper ratio of 3:1. The average ratio for all the samples analyzed in this study is 3.11 (Table 7). None of the analyses show a low enough ratio for mckinstryite ($Ag_5Cu_3S_4$), which has an Ag/Cu atomic ratio of 1.67. Jalpaite in some samples occurs as individual grains, while in others it occurs as intergrowths with acanthite and pearceite (Figure 30). It is possible that the acanthite-jalpaite intergrowths represent exsolution from a higher temperature Ag-Cu-S phase (Figure 31). As discussed in Barton and Skinner (1979), high-temperature solid solutions in the Ag-Cu-S system cannot be quenched to low temperatures, and instead separate into different minerals. Assuming that the intergrowths formed by exsolution, this means that the original body-centered cubic (bcc) solid phase had to have formed at a temperature above 106°C, and therefore did not form by weathering and supergene processes.

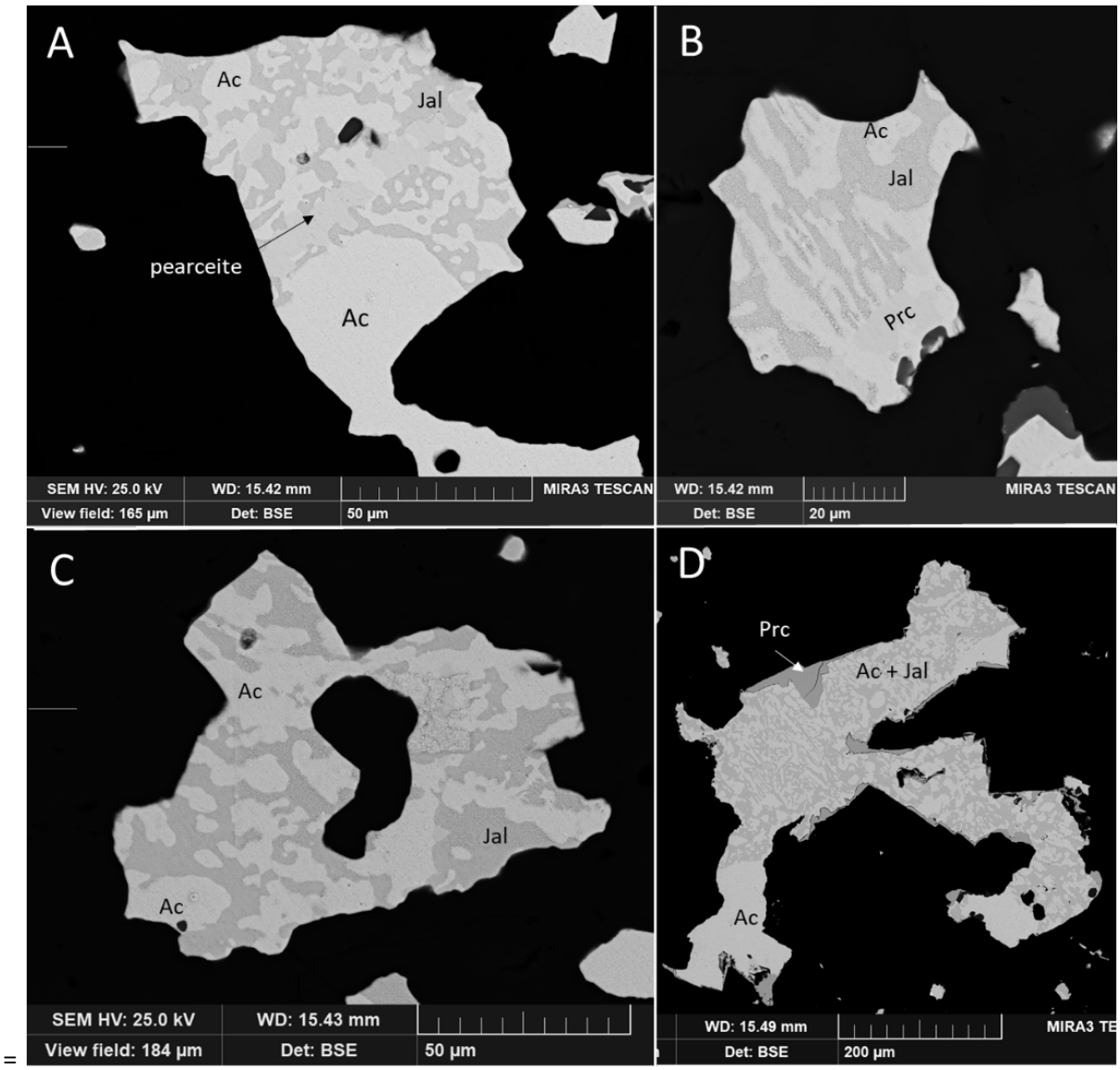

=

Figure 29: SEM-BSE images of "symplectic" intergrowths of acanthite (Ac) and jalpaite (Jal), with minor pearceite (Prc) from sample AMC 4316.

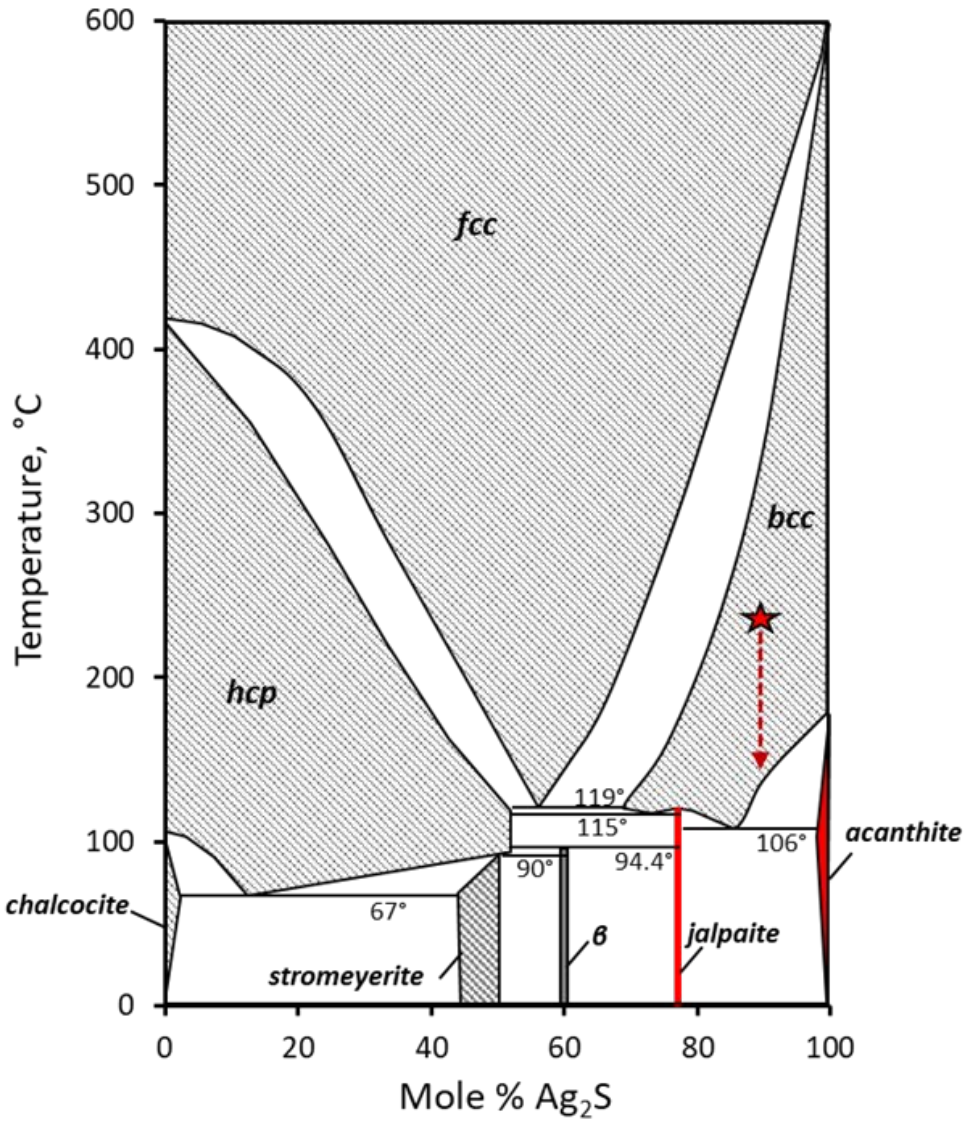

Figure 30: Phase diagram for the Cu-Ag-S system, redrawn from (Skinner, 1966). A higher temperature phase with composition shown by the star will exsolve into a mix of jalpaite + acanthite after cooling below 106°C. The β "phase" is now recognized as the mineral mckinstryite.

Table 7: Atomic Percentages and Calculated Formulas from SEM-EDS Analysis of Jalpaite.

		Atomic %			
Mineral	Sample #	S	Ag	Cu	Ag:Cu Ratio
Jalpaite	MA-7B	29.7	52.0	18.2	2.85
Jalpaite	MA-7B	25.7	59.3	15.1	3.94
Jalpaite	MA-7B	26.0	57.4	16.6	3.45
Jalpaite	MA-7B	25.9	59.2	15.0	3.96
Jalpaite	AMC 5060	31.7	52.4	15.9	3.28
Jalpaite	AMC 5060	32.9	49.6	17.5	2.84
Jalpaite	AMC 5060	31.0	55.2	14.2	3.90
Jalpaite	MA-13	38.0	45.1	16.9	2.67
Jalpaite	MA-13	38.8	43.4	17.8	2.44
Jalpaite	MA-13	37.9	47.0	15.2	3.09
Jalpaite	MA-13	38.2	45.3	16.5	2.74
Jalpaite	MA-13	36.7	48.0	15.3	3.14
Jalpaite	MA-13	36.6	47.4	16.0	2.96
Jalpaite	MA-13	38.0	43.8	18.2	2.40
Jalpaite	MA-13	38.0	44.3	17.6	2.52
Jalpaite	MA-13	38.5	42.9	18.6	2.31
Jalpaite	MA-13	38.5	43.1	18.4	2.34
Jalpaite	MA-13	37.6	49.4	13.0	3.81
Jalpaite	MA-13	38.9	41.5	19.7	2.11
Jalpaite	MA-13	38.9	43.4	17.8	2.44
Jalpaite	MA-13	36.5	48.4	15.1	3.21
Jalpaite	MA-13	35.8	45.3	15.6	2.90
Jalpaite	MA-13	39.2	43.2	17.6	2.46
Jalpaite	MA-30	31.9	56.2	12.0	4.68
Jalpaite	MA-30	37.3	44.2	18.6	2.38
Jalpaite	MA-30	36.6	43.4	15.0	2.89
Jalpaite	MA-30	36.8	47.6	15.6	3.05
Jalpaite	MA-30	34.9	51.3	13.7	3.75
Jalpaite	MA 88-10	36.3	48.5	15.2	3.19
Jalpaite	MA 88-10	37.0	47.6	15.3	3.11
Jalpaite	MA 88-10	37.7	51.4	10.8	4.74
Jalpaite	MA 88-10	38.3	47.2	14.6	3.24
Jalpaite	MA 88-10	37.2	47.6	15.2	3.13
Jalpaite	MA 88-10	35.0	50.2	14.9	3.37
Jalpaite	MA 88-10	36.0	49.1	14.9	3.29
Jalpaite	MA 88-10	37.9	45.3	16.8	2.69
Jalpaite	MA 88-10	33.7	53.4	12.9	4.14
Jalpaite	MA 88-10	34.8	50.5	14.7	3.45
Jalpaite	MA 88-10	39.0	43.4	17.6	2.46

3.1.1.5. Acanthite

Acanthite is a pseudomorph of argentite and forms at lower temperatures. At room temperature the mineral is acanthite, when heated to above 177°C at atmospheric pressure then the stable mineral is argentite (Mindat, 2022). Acanthite is the most common sulfide mineral of silver found in this study. The chemical formula for acanthite is Ag_2S where Ag can be substituted with minor Cu or Au. Results of SEM-EDS analysis of acanthite in this study are given in Appendix Table 15. Figure 32 shows acanthite (Ac) intergrown with pearceite (Prc), native silver, and chalcopyrite. Some of the pearceite and native silver could have formed by weathering of the acanthite since they are concentrated around the edge.

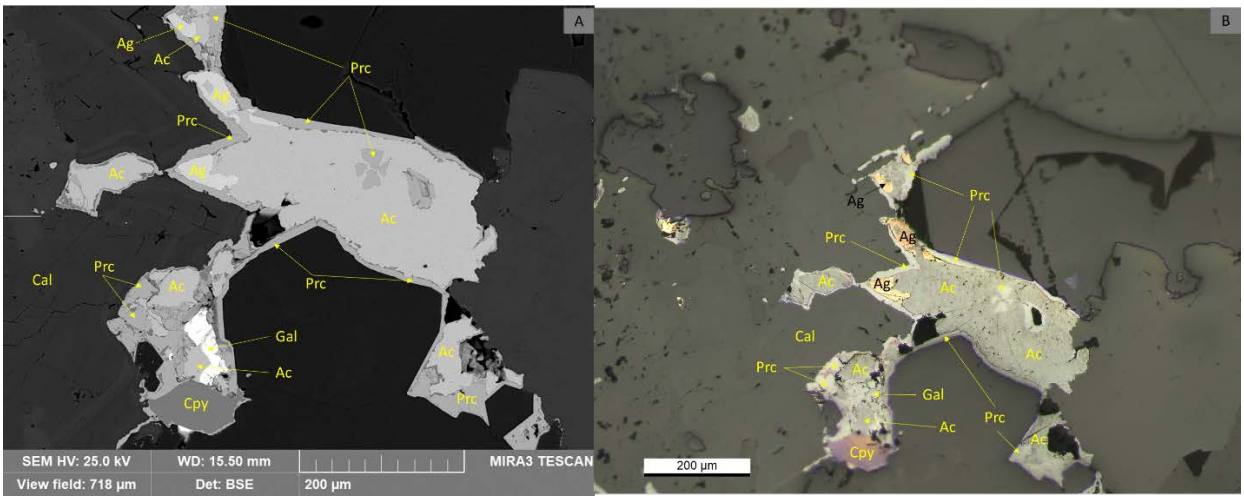

Figure 31. A) SEM-BSE image of sample MA88-10 181 ft. showing elemental (native) silver (Ag), acanthite (Ac), pearceite (Prc), calcite (Cal), chalcopyrite (Cpy), and galena (Gal). B) Same view under reflected light, showing pearceite and silver rimming the acanthite.

3.1.1.6. Sphalerite

Sphalerite (ZnS) is a common mineral and found in abundance in the Marget Ann mine, mostly along with the silver sulfides and in massive sulfide assemblages. The minerals in the massive sulfide assemblages include chalcopyrite, pyrite, tennantite, tetrahedrite, galena, some quartz gangue, and sphalerite(Figure 33). Sphalerite has a 1:1 ratio between zinc and sulphur, but many other metals can substitute for zinc, including iron (Fe), manganese (Mn), and cadmium (Cd). Most sphalerite grains examined in this study had < 0.1 atomic % Fe (the approximate detection limit for the SEM-EDS), although a few grains had measurable Fe up to a maximum of 4 atomic % (Table 8). The majority of the sphalerites had detectable Mn, and 5 analyses had detectable Cd. Many of the sphalerite samples were observed to have small inclusions of chalcopyrite, sometimes referred to as “chalcopyrite disease” (Figure 34). Chalcopyrite disease can form by reaction of Cu-rich fluids with Fe-bearing sphalerite (Barton and Bethke, 1987). If so, then the original Fe-content of the sphalerites would have been higher. However, the texture can also form by co-precipitation of chalcopyrite and sphalerite during sphalerite growth (Bortnikov et al., 1991).

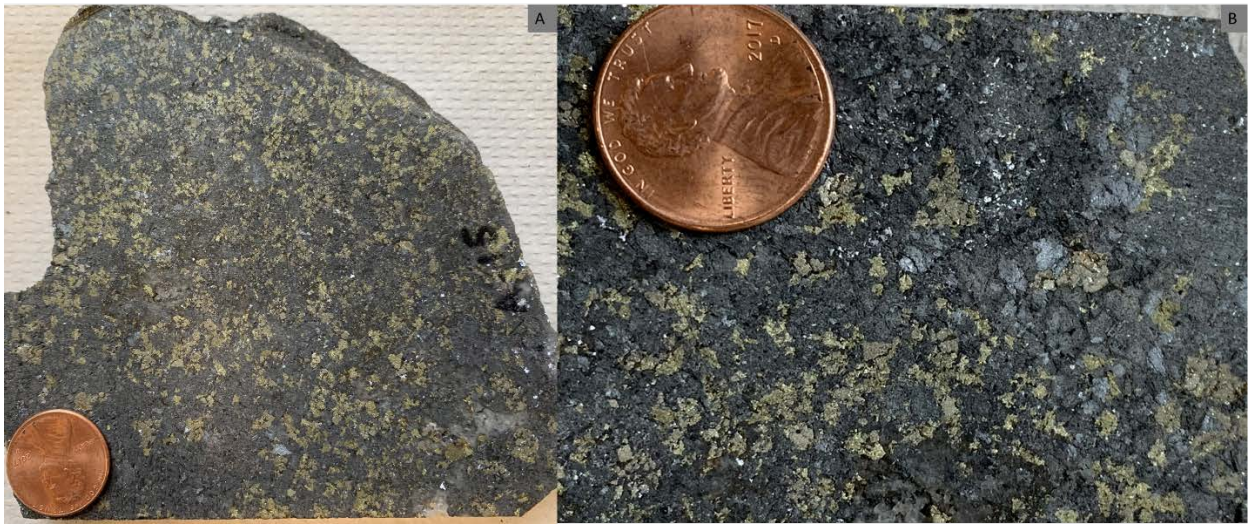

Figure 32: A) Massive sulfides from Marget Ann sample MA-15. B) Closer image of sample in photo A, dark gray is a mix of sphalerite and galena, and the yellow/gold is pyrite and chalcopyrite.

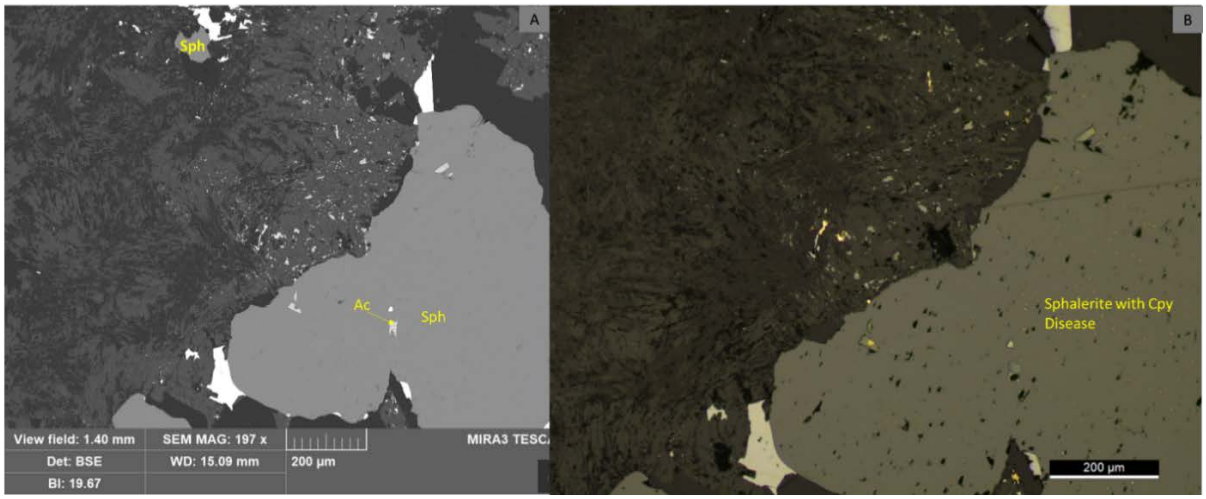

Figure 33: A) SEM image of sphalerite (Sph) from sample MA-13 with small sample of acanthite (Ac). B) Same view under reflected light showing sphalerite with chalcopyrite disease (these are all the small yellow dots).

Table 8: Atomic Percentages and Calculated Formulas from SEM-EDS Analysis of Sphalerite.

		Atomic %					
Mineral	Sample #	Zn	Fe	Cd	Mn	S	Chemical Formula
Sphalerite	Old MA-4	50.75	0.15	0.29	0.84	47.97	$(Zn_{.98}Cd_{.01}Mn_{.02})S$
Sphalerite	Old MA-4	50.37	0.37	0.34	0.92	84.01	$(Zn_{.98}Fe_{.01}Cd_{.01}Mn_{.02})S$
Sphalerite	Old MA-4	51.27	0.16	0.30	0.92	48.01	$(Zn_{.98}Cd_{.01}Mn_{.02})S$
Sphalerite	Old MA-4	50.50	0.43	0.39	0.80	47.88	$(Zn_{.98}Fe_{.01}Cd_{.01}Mn_{.02})S$
Sphalerite	Old MA-4	51.00	0.46	0.43	0.92	47.13	$(Zn_{.98}Fe_{.01}Cd_{.01}Mn_{.02})S$
Sphalerite	AMC 4316A	49.34	0.20	0.00	0.96	49.50	$(Zn_{.98}Mn_{.02})S$
Sphalerite	AMC 4316A	49.56	0.89	0.00	0.89	49.28	$(Zn_{.96}Fe_{.02}Mn_{.02})S$
Sphalerite	AMC 4316A	51.18	0.00	0.00	0.92	47.91	$(Zn_{.98}Mn_{.02})S$
Sphalerite	MA-15	47.17	0.00	0.00	0.77	52.06	$(Zn_{.98}Mn_{.02})S$
Sphalerite	MA-15	47.53	0.00	0.00	0.00	50.79	**ZnS**
Sphalerite	MA-15	47.70	0.00	0.00	0.98	51.45	$(Zn_{.98}Mn_{.02})S$
Sphalerite	MA-13	64.62	0.00	0.00	0.73	51.76	$(Zn_{.99}Mn_{.01})S$
Sphalerite	MA-13	50.52	0.00	0.00	1.18	45.88	$(Zn_{.98}Mn_{.02})S$
Sphalerite	MA-13	51.09	0.00	0.00	0.95	47.96	$(Zn_{.98}Mn_{.02})S$
Sphalerite	MA-30	47.56	0.00	0.00	0.85	51.58	$(Zn_{.98}Mn_{.02})S$
Sphalerite	MA-30	46.07	0.00	0.00	1.30	51.83	$(Zn_{.97}Mn_{.03})S$
Sphalerite	MA-30	46.90	0.00	0.00	1.30	51.81	$(Zn_{.97}Mn_{.03})S$
Sphalerite	MA-30	46.59	0.00	0.00	2.25	51.16	$(Zn_{.95}Mn_{.05})S$
Sphalerite	MA-30B	47.06	0.00	0.00	1.03	51.91	$(Zn_{.98}Mn_{.02})S$
Sphalerite	MA-30B	46.44	0.00	0.00	2.15	51.41	$(Zn_{.96}Mn_{.04})S$
Sphalerite	MA-26B	46.92	0.00	0.00	0.93	52.16	$(Zn_{.98}Mn_{.02})S$
Sphalerite	MA-19	47.33	0.00	0.00	0.00	52.67	**ZnS**
Sphalerite	MA-19	47.29	0.00	0.00	0.00	52.71	**ZnS**
Sphalerite	MA-19	47.01	0.00	0.00	0.91	52.08	$(Zn_{.98}Mn_{.02})S$
Sphalerite	MA-19	47.88	0.00	0.00	0.00	52.12	**ZnS**
Sphalerite	MA-23	45.92	2.00	0.00	0.00	52.08	$(Zn_{.96}Fe_{.04})S$
Sphalerite	MA-23	47.74	0.00	0.00	0.75	51.52	$(Zn_{.98}Mn_{.02})S$
Sphalerite	MA-14C	47.11	0.43	0.00	1.07	51.39	$(Zn_{.97}Fe_{.01}Mn_{.02})S$
Sphalerite	AMC-4316	46.98	0.00	0.00	0.83	52.19	$(Zn_{.98}Mn_{.02})S$

3.1.1.7. Ag-Au Sulfides and Native Silver

One of the most interesting discoveries in this thesis is the presence of copper-rich uytenbogaardtite (Figure 35) in three samples (AMC 4316, MA-8, and MA-13). This mineral has the ideal formula Ag_3AuS_2, and often has some Cu. The general formula can be written as $A_mB_nX_p$ were (m+n):p =2:1 (Mindat, 2022). The analyses presented in Table 9 have (Ag+Au)/S ratios near 2, conforming to uytenbogaardtite. All of the grains have significant Cu as well. Makotoite, an extremely rare mineral with formula $Ag_{12}(Cu_3Au)S_8$, has an overall chemistry similar to uytenbogaardtite, but with a Cu:Au atomic ratio that is exactly 3:1. Since none of the grains examined by SEM-EDS in this thesis fit the stoichiometry of makotoite, the grains are more likely Cu-rich uytenbogaardtite.

Figure 35 (below) shows two occurrences of Cu-rich uytenbogaardtite. In sample MA-13, the uytenbogaardtite forms discrete grains about 20 microns in size that are perched on either side of an electrum grain, in close contact with jalpaite and acanthite. In reflected light, uytenbogaardtite is darker with a slight brown tint next to acanthite (Fig. 35 B), whereas under SEM-BSE, it is almost impossible to tell the two minerals apart (Fig. 35 A). The uytenbogaardtite in Figure 35 C and D forms a narrow reaction rim between electrum and jalpaite. This rim does not form between the pearceite and electrum, only the jalpaite and electrum.

As stated above, it was common to see acanthite and jalpaite intergrown with odd geometric patterns, suggesting exsolution from a higher temperature, mixed phase. In some cases, intergrowths of jalpaite + acanthite + electrum were observed in a consistent volume ratio of roughly 8:4:1, respectively (Figure 36). This suggests that the high-temperature phase that exsolved to form the textures observed under the microscope contained a mixture of Ag, Cu and Au.

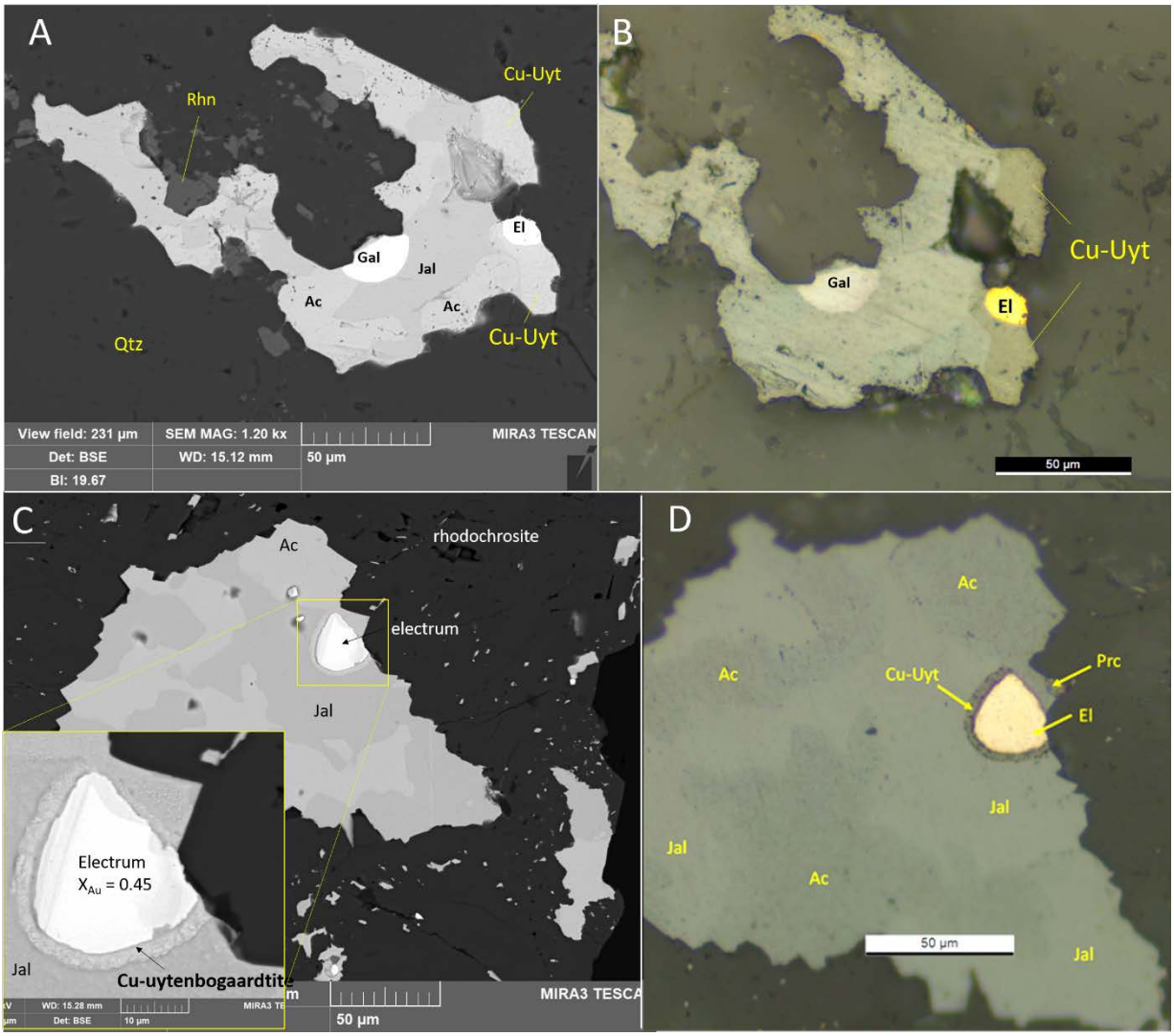

Figure 34: Photos of high-grade samples containing Cu-rich uytenbogaardtite (Cu-Uyt). Left panels are SEM-BSE, right panels are reflected light. A, B = Sample MA-13; C,D = AMC 4316.

Table 9: Atomic Percentages and Calculated Formulas from SEM-EDS Analysis of Cu-rich Utenbogarrdtite (Ag_3AuS_2)

		Atomic %				Ratios	
Mineral	Sample #	S	Ag	Cu	Au	Ag/(Au+Cu)	(Ag+Au)/S
Cu-Rich Uytenbogaardtite	MA-13	31.1	60.0	7.27	4.67	5.02	2.1
Cu-Rich Uytenbogaardtite	MA-13	29.8	56.5	9.08	4.56	4.14	2.0
Cu-Rich Uytenbogaardtite	MA-13	31.9	53.8	6.98	7.35	3.76	1.9
Cu-Rich Uytenbogaardtite	MA-8	32.2	53.9	7.98	5.95	3.87	1.9
Cu-Rich Uytenbogaardtite	MA-8	26.2	59.6	8.68	5.50	4.20	2.5
Cu-Rich Uytenbogaardtite	MA-8	31.5	56.8	5.58	6.05	4.89	2.0
Cu-Rich Uytenbogaardtite	MA-8	30.2	58.5	5.87	5.39	5.20	2.1
Cu-Rich Uytenbogaardtite	MA-8	28.1	55.2	5.90	10.79	3.31	2.3

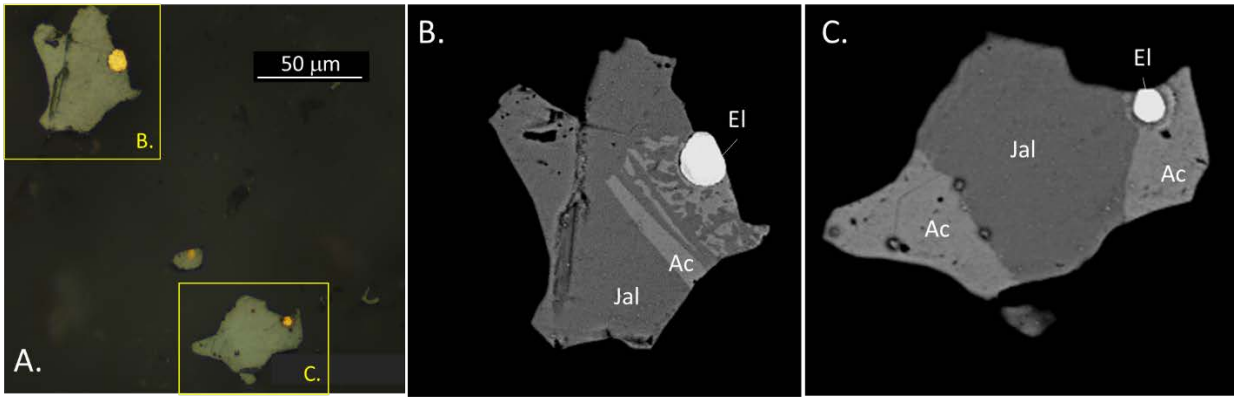

Figure 35: Intergrowths from sample MA-13 of jalpaite, acanthite, and electrum. A) Reflected light photo showing three mineral intergrowths with similar ratios; B) and C) are closeups of two of the intergrowths under SEM-BSE.

The first record of native silver at Marget Ann was noted by Sahinen (1953). He stated that the silver was in wire form and increased with depth. In this study, the SEM did pick up a few grains that were 100 % atomic weight silver (Figure 32). However, not enough native silver samples were found to determine its exact position in the overall paragenesis. Based on observations from the Butte district as a whole (Gammons, Szarkowski, & Stevenson, 2016), it is likely that most of the native silver from Marget Ann is supergene, or formed by weathering of pre-existing silver minerals, such as acanthite or tetrahedrite. Stromeyerite (AgCuS) was identified in one sample (MA-13), the atomic ratio between Ag, Cu, and S being close to the ideal 1:1:1. However, stromeyerite is not a common phase at Marget Ann. Some other metallic minerals found in this study include covellite (CuS) and wulfenite ($PbMoO_4$), both of which are thought to be supergene, and not important ore minerals.

3.1.1.8. Gangue Minerals

Gangue minerals of importance in the Marget Ann veins include quartz, calcite, dolomite, potassium feldspar (adularia), muscovite (sericite), rhodonite, and rhodochrosite. In addition, oxidized veins have abundant red-brown Fe-oxides (hematite, goethite) and brown-black Mn-oxides. Example hand-sample photos are given in figure 37 and Appendix E. Less important gangue minerals include fluorapatite (only 1 grain found) and various clay minerals, some of which may have formed during weathering. The quartz in the Marget Ann is both milky/opaque and vitreous/transparent. Colloform or parallel-symmetric banding is common, as are vein breccias cemented by quartz and other gangue and sulfide minerals. Voids are common, and multiple generations of veining can be seen in some samples. Overall, the samples have the appearance of shallow, epithermal-style veins.

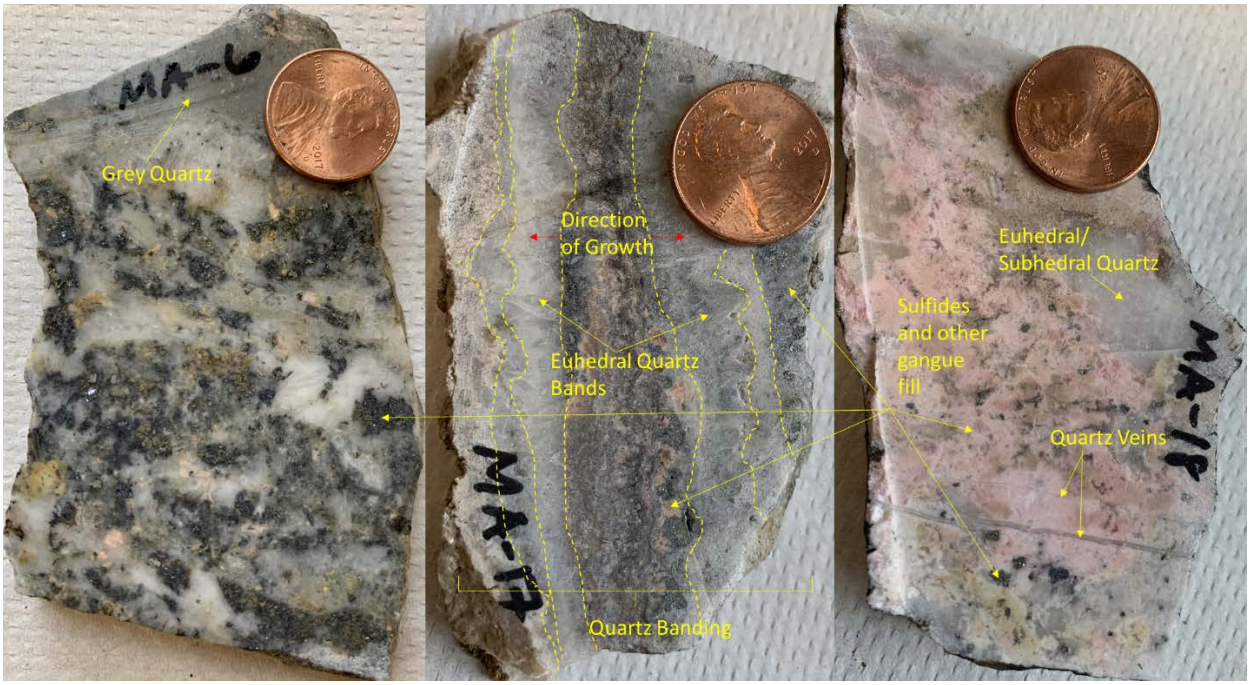

Figure 36: Different samples with examples of quartz coloring (grey and colorless), coliform banding with large blades, small blades and interwoven with calcite and dolomite, and infilling of sulfides and other gangue minerals.

Figure 38 shows some interesting mineral textures under SEM-BSE from sample MA-30. This sample is very high-grade in silver and gold, and also has a rich gangue mineral assemblage. The gangue is a mix of rhodonite + rhodochrosite + quartz, with numerous euhedral grains of K-feldspar (adularia). Figure 38 D shows that some of the K-feldspar has been altered to an unidentified Mg-Si rich clay mineral (possibly vermiculite or chlorite). The type of fine-grained, intergrown gangue textures shown in Figure 38 A, with its constellation of finely disseminated Ag-Au particles, is best explained by rapid deposition in open space, possibly due to boiling. Boiling would also help to explain the associated K-feldspar, since adularia often precipitates from boiling geothermal waters due to increases in pH and solute concentration (Simmons, White, & John, 2005).

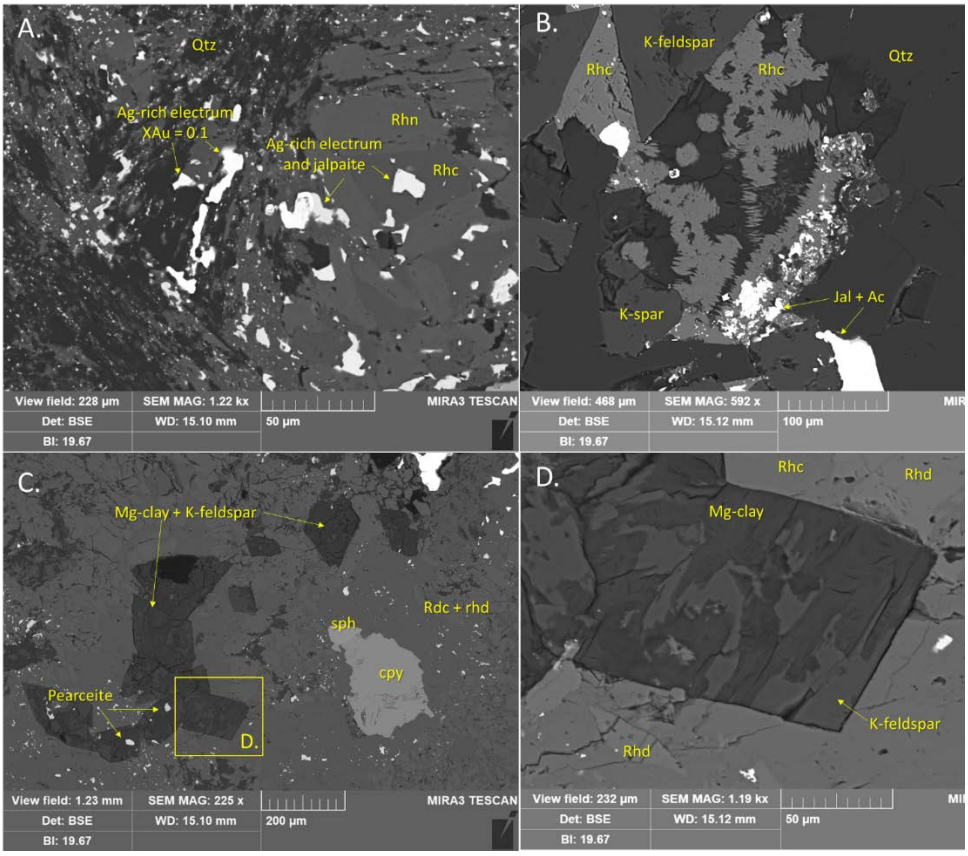

Figure 37: SEM-BSE photos showing interesting gangue and ore mineral textures from sample MA-30. Abbreviations: Qtz = quartz; Rhn = rhodonite; Rhc = rhodochrosite; K-spar = K-feldspar; Jal = jalpaite; Ac = acanthite; Sph = sphalerite; Cpy = chalcopyrite.

3.2. Fluid Inclusions

The Marget Ann has abundant fluid inclusions in coarse, comb-like quartz that range in size from less than 1 μm to over 100 μm (Figure 39). Most of the fluid inclusions are roughly 20% bubble by volume (B20), and are simple two-phase inclusions (Figure 39, B) (Rusk, Reed, & Dilles, 2008a). Some of the fluid inclusions contain feathery, anisotropic daughter minerals that may be dawsonite, $NaAlCO_3(OH)_2$ (Figure 40) (Coveney & Kelley, 1971). Dawsonite can be colorless like quartz, is orthorhombic, and grows in a radial pattern (Mindat, 2022). The radial hair like pattern can be seen in Figure 41 D and E. These crystals do not dissolve upon heating to the temperature of vapor bubble disappearance (T_h). Very few vapor-rich inclusions were found, no 3-phase carbon dioxide (CO_2) rich inclusions were found, and no CO_2 clathrates were seen, indicating low CO_2 content and that boiling was not happening at the same time that the coarse-grained quartz was forming/growing.

Whenever possible, both the temperature of homogenization (T_h) and the temperature of ice melting (T_m) were recorded for the same fluid inclusion. However, in practice, Th data are easier to measure and therefore this study has more T_h vs. T_m readings (see Appendix B). The homogenization temperatures show a bell-shaped curve recording temperatures between 220°C and 310°C with some lower temperature outliers (Figure 42A). The average T_h for all measurements (n = 131) is 251°C. Temperature of ice melting is used to calculate the salinity of the samples. These salinities ranged from 0.5 to 7 wt% $NaCl_{eq}$, with an average of 2.2 wt% $NaCl_{eq}$ (n = 77) (Figure 42B). The plot of salinity versus temperature shows a possible mixing trend of three solutions (Figure 42C). Fluid 1 is interpreted to be magmatic water (high temperature, high salinity), Fluid 2 is heated meteoric water (high temperature, low salinity), and Fluid 3 is the tail to lower temperatures for meteoric water (low temperature, low salinity).

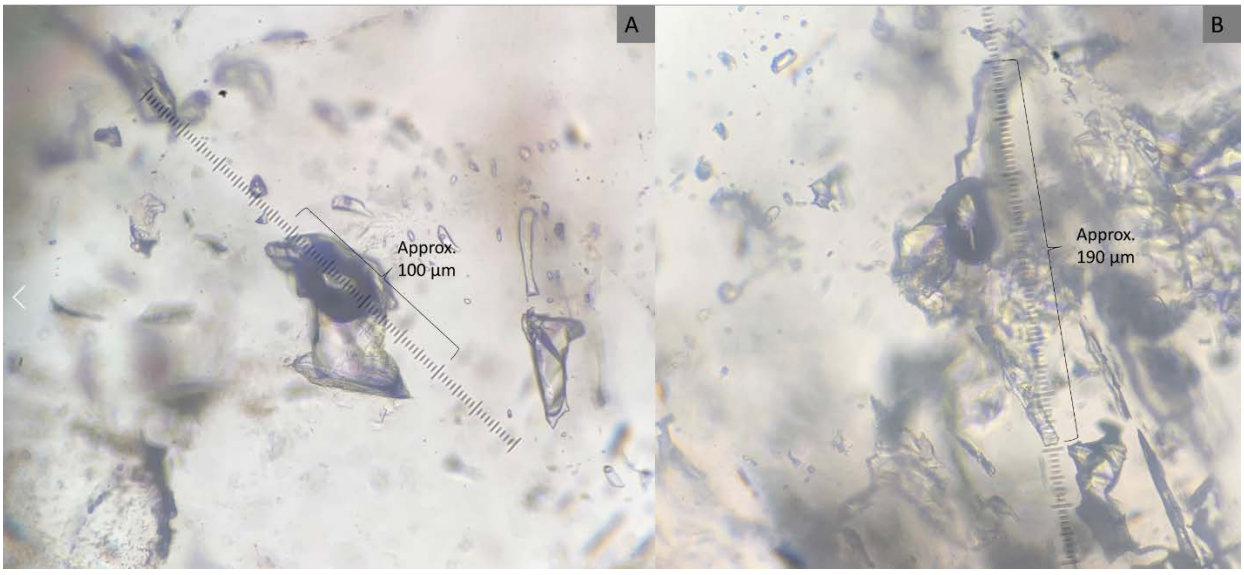

Figure 38: A) Large fluid inclusion with greater than 20% bubble volume. B) Extremely large fluid inclusion that does have roughly 20% bubble volume.

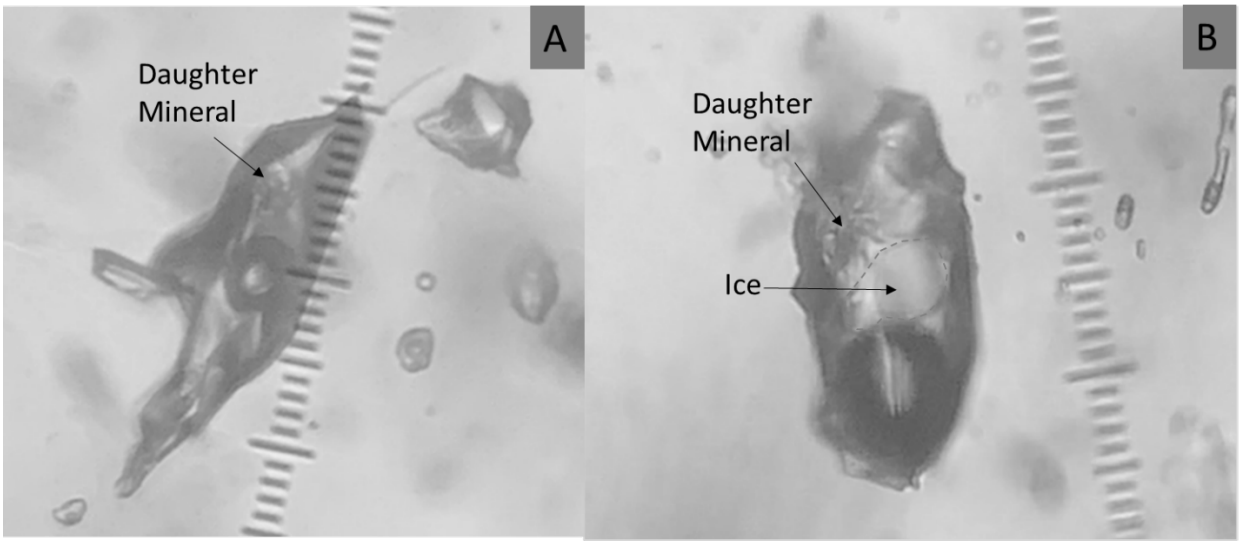

Figure 39: A) Daughter mineral in B20 inclusion. B) Daughter mineral during freezing run with ice and enlarged bubble.

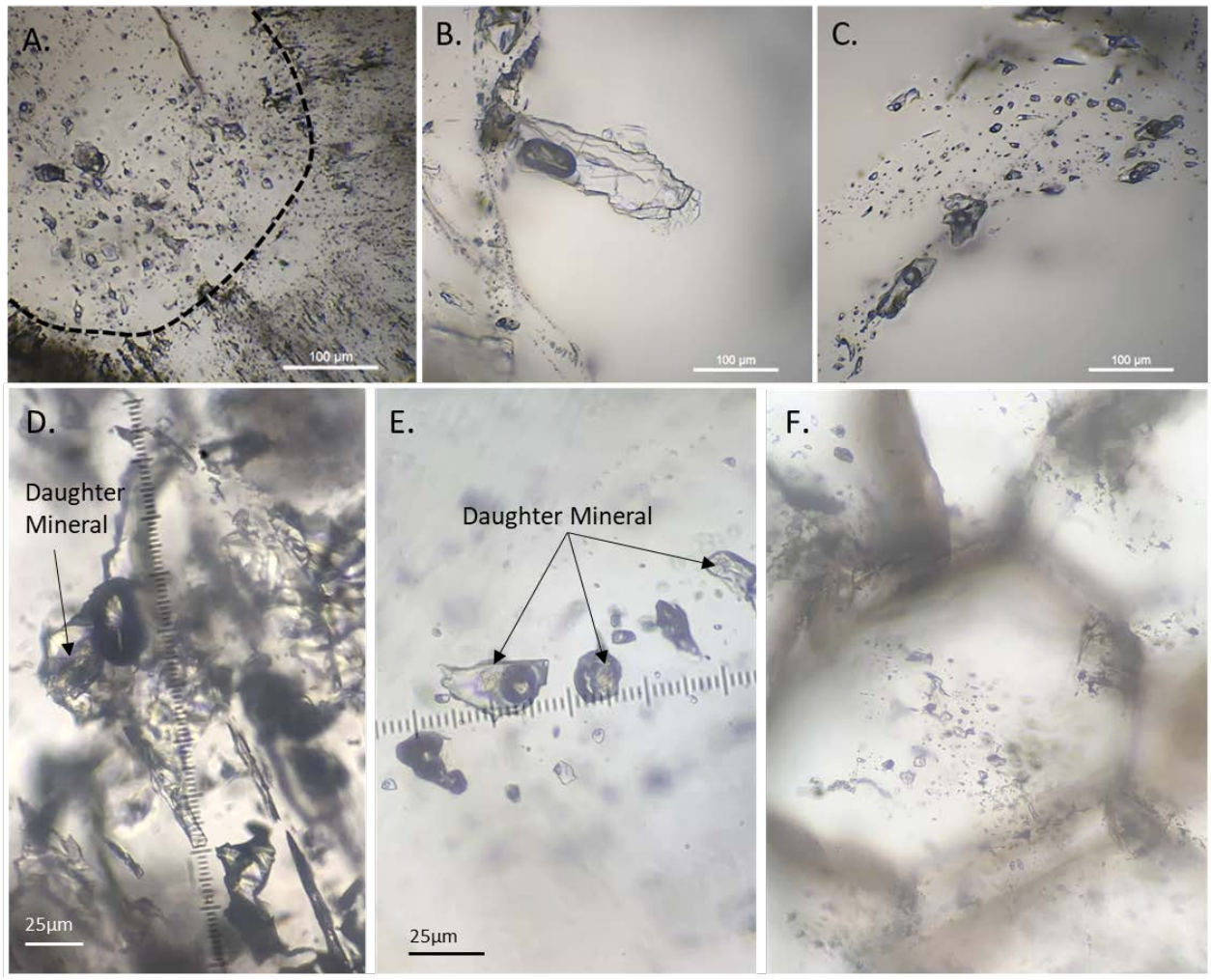

Figure 40. Fluid inclusions in quartz from Marget Ann. A) Cluster of primary fluid inclusions 5 to 30 µm in diameter in the core of a zoned quartz crystal; B) and C) Very large, B20 fluid inclusions in quartz; D) Very large B20 fluid inclusion with daughter mineral (dawsonite?); E) Group of fluid inclusions with unknown daughter minerals; F) Cluster of primary fluid inclusions in core of a quartz grain.

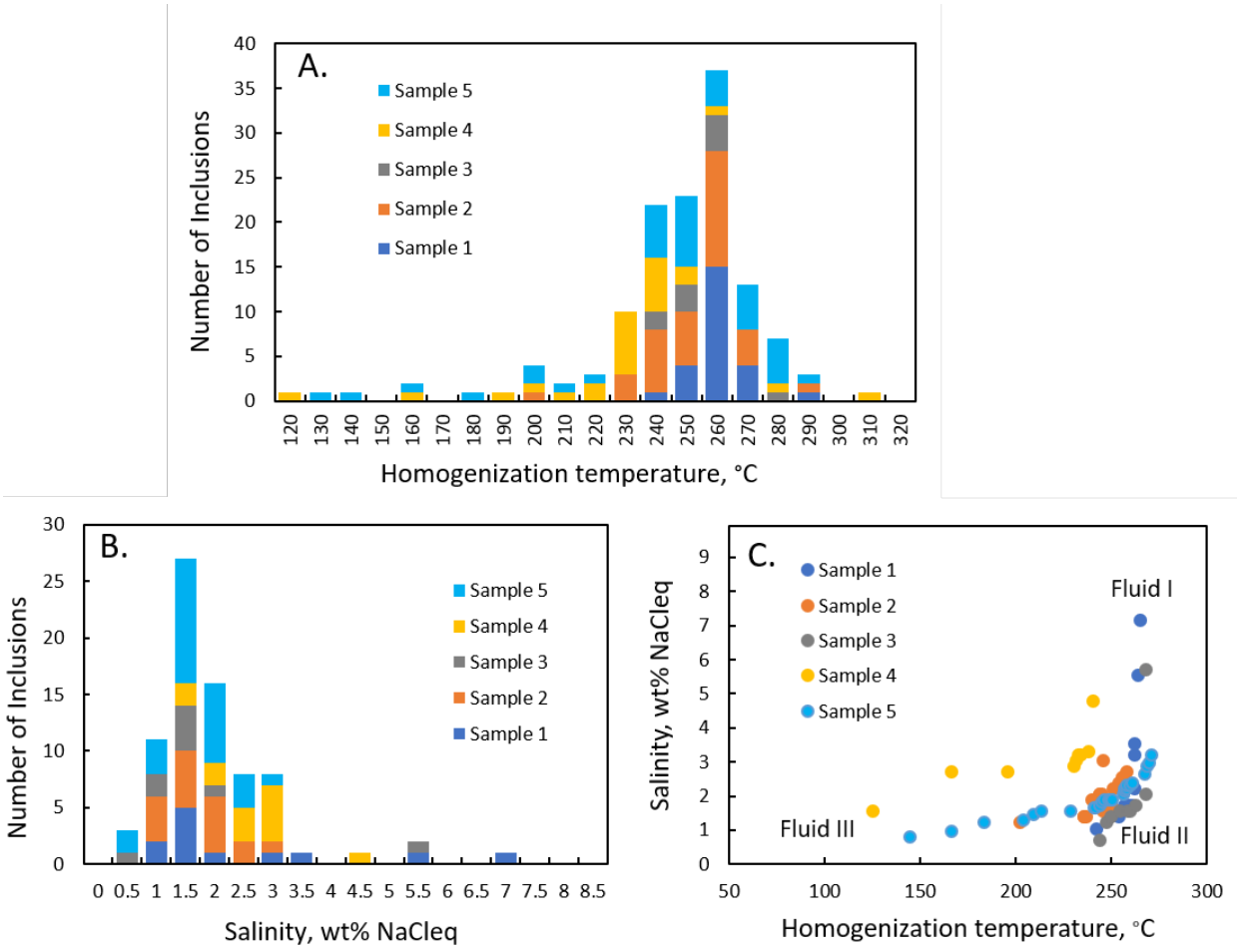

Figure 41. Fluid inclusion data from Marget Ann. A) Histogram of homogenization temperatures; B) Histogram of salinity values; C) Salinity vs. T_h cross plot.

4. Discussion

4.1. Comparison with Previous Work

4.1.1. Mineralogy

Many minerals were found at the Marget Ann. Sahinen was only able to visually identify native silver, quartz, pyrite, chalcopyrite, galena, rhodonite, and rhodochrosite. Sahinen had trouble identifying minerals because the plugs would not polish properly (Sahinen, 1953). Win was able to identify many more minerals, including several silver minerals (Table 10). The most notable difference is that Win stated seeing pyrargyrite and proustite, while the present study did not find these minerals. Win did not have a scanning electron microscope, and may have mis-identified proustite-pyrargyrite as pearceite-polybasite, which are also ruby silver minerals and have similar compositions and optical properties. It's also possible that proustite-pyrargyrite exists at Marget Ann but was not found in the current work.

The study of Gammons, Szarkowski, and Stevenson (2016) examined the mineralogy of silver across the Butte district, and included some specimens from Marget Ann. They reported many of the same minerals as in this study (e.g., pearceite, electrum, jalpaite), but had fewer SEM-EDS analyses. Some other rare Ag-minerals reported by Gammons et al. (2016), such as larosite and furutobeite, were found in Main Stage veins closer to the center of the district, while andorite and stephanite were found in the far west mine dumps (e.g., Bluebird Mine). Native silver was found in the Marget Ann, Orphan Boy, and Orphan Girl mines above the pre-mining water tables, and Gammons et al. (2016) assumed that the elemental silver is supergene. Native silver was found in the current study, but native gold was not. The "gold" in previous studies (e.g., Win, Sahinen) may have been confused with electrum.

Although ankerite was reported from the Marget Ann Mine by Win (1955), she was not able to perform chemical analyses to determine the mineral composition. According to Mindat

(2022), most examples of “ankerite” from the older literature are actually Fe-bearing dolomite. Dolomite that contains Fe will weather out to a rusty color, which led early workers to use the term ankerite. However, by modern conventions, in order to be classified as ankerite, a carbonate mineral needs to have more Fe than Mg by atomic% in the 2nd cation site, i.e., $Ca(Fe,Mg)(CO_3)_2$, which is relatively uncommon (Mindat, 2022). It is likely that the ankerite reported by Win (1955) was actually dolomite.

The most interesting mineral found in this study and not before recorded in Butte, Montana is uytenbogaardtite. This gold-silver sulfide mineral is a low temperature hydrothermal mineral that is commonly associated with acanthite and electrum (Barton, Kieft, Burke, & Oen, 1978). The formation of exsolution textures involving jalpaite and acanthite (Figure 30) prove that these minerals did not form by supergene enrichment, but rather from decomposition of a higher temperature Ag-Cu-S solid solution with body-centered cubic (BCC) symmetry (Figure 31). Also, the regular proportions of electrum, jalpaite and acanthite in some samples (Figure 35) suggests the possible pre-existence of a Ag-Au-Cu-S solid solution. However, no experimental studies have been done on this four-element system to compare with the textures reported here.

Adularia (hydrothermal K-feldspar) was also found for the first time at Marget Ann in this study. If the adularia could be separated from the other gangue minerals, it could be used in $^{40}Ar/^{39}Ar$ radiometric dating of the veins.

Table 10: Minerals found in this study compared to previous works.

Mineral	Formula	Sahinen W.M., (1953)	Win M.S., (1955)	Current Study (2020-2021)
Quartz	SiO_2	✓	✓	✓
Pyrite	FeS_2	✓	✓	✓
Chalcopyrite	$CuFeS_2$	✓	✓	✓
Galena	PbS	✓	✓	✓
Sphalerite	ZnS	✓	✓	✓
Rhodonite	$MnSiO_3$	✓	✓	✓
Rhodochrosite	$MnCO_3$	✓	✓	✓
Tetrahedrite	$(Cu, Fe)_{12}Sb_4S_{13}$		✓	✓
Calcite	$CaCO_3$		✓	✓
Ankerite	$Ca(Mg, Fe^{2+}, Mn)(CO_3)_2$		✓	
Silver	Ag	✓		✓
Gold	Au		✓	
Pyrargyrite	Ag_3SbS_3		✓	
Proustite	Ag_3AsS_3		✓	
Argentite/Acanthite	Ag_2S		✓	✓
Jalpaite	Ag_3CuS_2			✓
Electrum	Au(Ag)			✓
Uytenbogaardtite	Ag_3AuS_2			✓
Polybasite	$[(Ag,Cu)_6(Sb,As)_2S_7][Ag_9CuS_4]$			✓
Pearceite	$[(Ag,Cu)_6(As,Sb)_2S_7][Ag_9CuS_4]$			✓
Adularia	$KAlSi_3O_8$			✓

4.1.2. Fluid Inclusions

Rusk and others (2008a) published an important study of fluid inclusions from the pre-Main Stage, porphyry Cu-Mo mineralization at Butte. A follow-up paper by Rusk and others (2008b) presented some data on fluid inclusions from several Main Stage Veins. Figure 43 shows the salinity vs. T_h data obtained by Rusk and others (2008b) along with data from this study overlain. The Marget Ann data overlaps with the data collected by Rusk and others, with the exception that few fluid inclusions with $T_h > 275°C$ were found in the present study. This difference could be explained by the location of the Marget Ann mine at the extreme north end of the district, further from the porphyry Cu center.

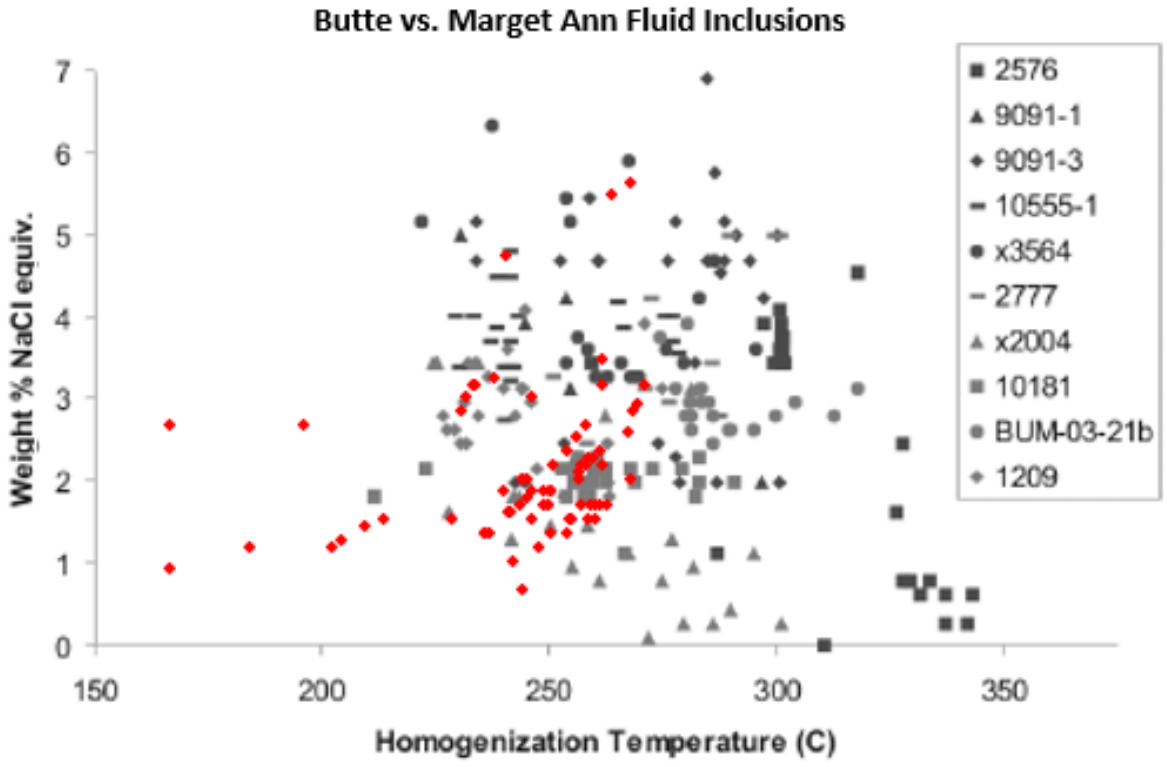

Figure 42: Comparison of the fluid inclusion data from Rusk, Miller, and Reed 2008b for Butte Main Stage Veins, overlain by the Marget Ann fluid inclusion data from this study (in red). The sample identifiers are as follows: 2576 & 9091 – Leonard, 10555 – Berkeley Pit, 2777 – Belmont, 10181 – Continental Pit, 1209 – Emma, X2004 – Elm Orlu, BUM-03-21b Lexington, and X3564 – Mt. Con.

4.2. Conditions of Ore Formation

The Marget Ann mineral assemblages of electrum + acanthite and sphalerite + pyrite can be used to estimate the sulfide gas ($S_2(g)$) activity during ore formation. The estimation of $S_2(g)$ is important because polymetallic lode deposits are often referred to as having low (LS), intermediate (IS), or high (HS) sulfidation states (Einaudi, Hedenquist, & Inan, 2003). Figure 44 summarizes the $S_2(g)$ activity versus temperature conditions for the Marget Ann mine drawn using thermodynamic data for the common sulfide minerals taken from Barton & Skinner (1979) and electrum from White, Orr, & Hultgren (1957). In Figure 44 the equations for iron (Fe) content of sphalerite were taken from two sources: 1) (Barton & Toulmin, 1964) and 2) (Scott & Barnes, 1971). Two equations from (Barton & Skinner, 1979) used are as follows:

$$\log X_{FeS} = 7.16 - \frac{7730}{T} - \frac{1}{2} Log f_{S_2} \quad (1)$$

$$\log X_{FeS} = 6.65 - \frac{7340}{T} - \frac{1}{2} Log f_{S_2} \quad (2)$$

X_{FeS} is the mole ratio average from Table 8. Temperature (T) is in Kelvin. The Marget Ann sphalerite is low in Fe, with a maximum value of $X_{FeS} = 0.05$. The X_{Au} used is from Table 4 and has a composition between 0.4 to 0.6. None of the veins contained bornite, which is predicted from Figure 44, while the Marget Ann has abundant coexisting electrum + Ag_2S (acanthite/argentite). In Figure 44 the yellow area represents the boundaries for ore formation in the Marget Ann. In comparison, the tan area is the estimated conditions for the formation of the Central Zone of Butte, which is rich in both bornite and Fe-poor sphalerite (Ortelli, Kouzmanov, Dilles, & Rusk, 2013). The central Main Stage veins most likely formed at higher temperatures and higher S_2 activities (HS style) than the veins of Marget Ann (IS style). Figure 44 also shows

how the Marget Ann fluid inclusion temperatures agree with the temperature range indicated from the mineral compositions.

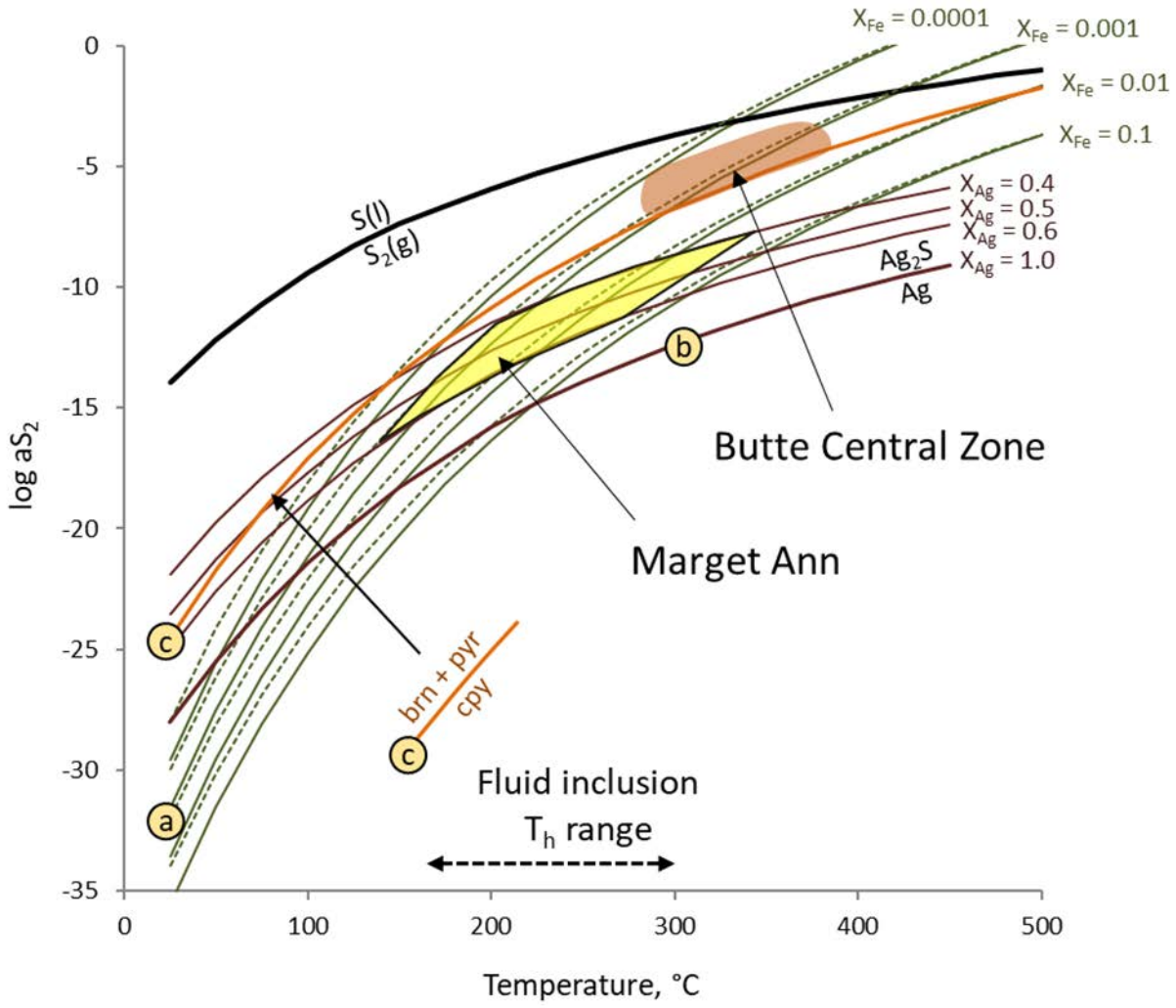

Figure 43: aS_2 Temperature diagram showing the conditions of formation of hypogene mineralization in the Marget Ann veins. A) Atomic percent of Iron (Fe) in sphalerite. B) Atomic percent of silver in electrum. C) Is the mineral formation line between bornite (brn) and pyrite (pyr) above and chalcopyrite (cpy) below.

4.3. Age of Mineralization

There is currently a controversy over the timing of Main Stage mineralization at Butte with respect to the emplacement of the ~ 76 Ma Butte Pluton and the ~ 65 Ma quartz-porphyry dikes. Brimhall (1979, 1980) advanced a theory that the deep but low-grade porphyry-style mineralization in Butte, which presumably formed at ~ 65 Ma, was the "protore" for remobilization of metals into the high-grade Main Stage veins by later hydrothermal fluids. Later thermodynamic modeling led Reed, Rusk, & Palandri (2013) to argue that all of the mineral-deposit types of Butte (porphyry Cu-Mo and zoned Main Stage veins) formed at essentially the same time from essentially the same starting fluid, a moderate-salinity magmatic fluid genetically related to the 65 Ma porphyry dikes. More recently, Lund et al. (2018) presented new $^{40}Ar/^{39}Ar$ dates of hydrothermal muscovite that show that some of the Main Stage veins, in particular the Ag-Pb-Zn veins of the Peripheral Zone, are much closer in age to the Butte Granite than to the quartz porphyry dikes. Lund et al. (2018) published dates for several Ag-rich veins in the northern part of the district, as follows: East Glengarry (72.9 Ma); Pollock (76 Ma); Boston (73.5 Ma); North Wabash (66.9 Ma), and Blackstone (66.7 Ma). The authors argued that the dates between 72.9 to 76 Ma represent a district-wide, lode-type mineralization of Ag-Pb-Zn that predated the emplacement of the porphyry Cu-Mo mineralization by at least 6 million years. Their conclusion was that the Cu-rich Butte porphyry intruded into a set of pre-existing Ag-Pb-Zn lodes.

This thesis has no new dates that could be used to weigh in on the "Two-event" model of Lund et al. (2018) vs. the "One fluid explains all" model of Reed et al. (2013). However, since the Marget Ann Mine is situated on an adjacent claim block with the East Glengarry Mine (Figure 3), it is likely that at least some of the mineralization at Marget Ann dates to ~ 72.9 Ma,

the age of hydrothermal sericite at East Glengarry. Further work is needed to show if the younger 65 Ma event in Butte brought more metals into the Marget Ann veins.

4.4. Ore Deposit Model

The ore in the Marget Ann is controlled by fissures created by localized faulting, and the filling of those fissures with base and precious metals (Win, 1955). The ore in the veins formed at temperatures between 200°C and 300°C from a mix of meteoric and magmatic waters. The Butte ore bodies are schematically shown in a classic diagram from Hedenquist and Lowenstern (1994) (Figure 45). Figure 45 shows the current level of erosion in Butte as a dashed yellow line. The stars represent an estimate as to where the current and past mines sit within this system. The Marget Ann is noted with a white arrow (next to the Lexington mine) with its Main Stage veins in red that dip to the north. The Marget Ann is also at a higher elevation than the other mines including the Lexington Mine. Although the top of the Lexington sits at about 6220 ft., most production came from the lower levels, below 1000' from surface. The Marget Ann shaft sits at about 6320 ft. with a shaft that extends at most 600 ft. deep.

Overall, the position of the Marget Ann mine at the outskirts of the Butte system, at a higher elevation, and with veins that dip north, away from the porphyry center of the district, are all consistent with the idea that this mine would have been more influenced by meteoric water as opposed to magmatic water. This may also help to explain the higher gold content of the Marget Ann veins. However, it needs to be stressed that the model shown in Figure 45 assumes that all of the porphyry and lode mineralization is happening at the same time. This may not be the case for Butte (Lund et al., 2015).

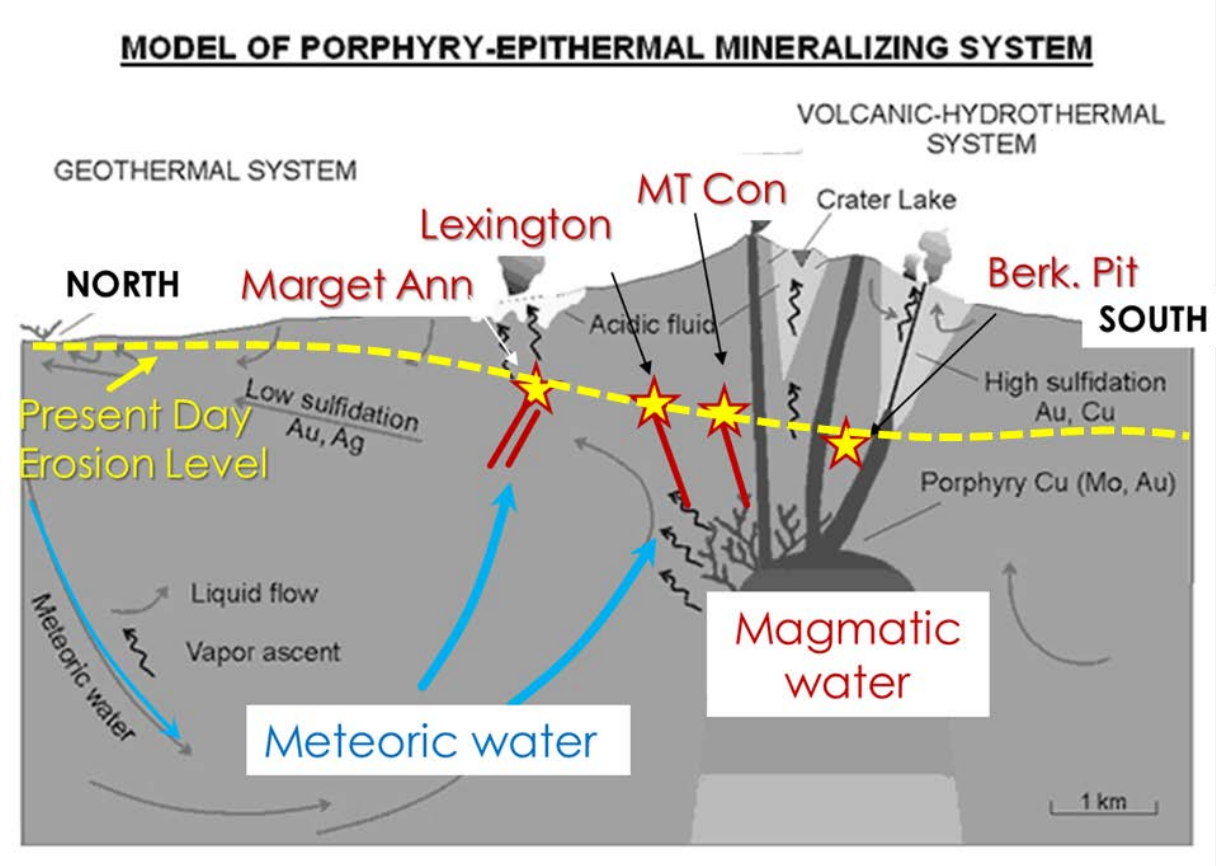

Figure 44: Redrawn image from (Hedenquist & Lowenstern, 1994) for a generic porphyry-epithermal system. The yellow line represents the present-day erosion level in Butte, the red lines represent the Butte Main Stage veins, and the blue lines represent the meteoric waters circulating around the periphery which mix with magmatic water coming from the porphyry intrusions.

5. Conclusions

5.1. Major Findings

- The ore in the Marget Ann is the richest when associated with rhodonite and rhodochrosite. These minerals fill void space between coarse, comb-textured quartz.
- Two of the more abundant silver ore minerals in the Marget Ann include acanthite and tetrahedrite. These minerals are common to other Butte veins, especially in the Peripheral zone. However, the Marget Ann also contains locally high amounts of jalpaite and pearceite, with trace polybasite and tennantite. The rarer silver ore minerals include stromeyerite, native silver, and uytenbogaardtite.
- Electrum is frequently found in delicate intergrowths that include acanthite and jalpaite in a consistent volume ratio of roughly 8:4:1. All of these phases were probably mixed together in a high-temperature solid solution which exsolved upon cooling to room temperature.
- Veins in the Marget Ann mine formed at temperatures between 150°C and 300°C based on fluid inclusion thermometry. Based on fluid inclusion studies, the average temperature is 251°C and average salinity is 2.2 weight % $NaCl_{eq}$. There is a range in both parameters, however, which suggests possible mixing between higher salinity magmatic fluids and lower salinity meteoric fluids.
- The fluid inclusions suggest relatively low CO_2, and no vapor-rich inclusions were seen, indicating that boiling did not occur when the coarse-grained early quartz grew.

- Thermodynamic calculations of equilibrium mineral assemblages indicate a range of temperature of formation between 150°C-350°C. These temperatures agree with the fluid inclusion temperatures, as well as estimates from previous workers for the temperature of formation of the Peripheral zone of Butte.
- Uytenbogaardtite (copper rich) was found in a mineral assemblage including electrum, acanthite, and jalpaite. This is the first time this mineral has been reported to occur in Butte.
- Hydrothermal potassium feldspar (adularia) exists as a gangue mineral in some of the veins of the Marget Ann. This mineral is important because it can allow for future ore body dating by the Ar-Ar method.

5.2. Recommendation for Further Work

- Stable isotopes should be completed on samples from the Marget Ann, especially sulfur (S) of sulfides, oxygen (O) of quartz, and carbon/oxygen (C,O) of the carbonates.
- Dating mines located in the peripheral zone of the Butte Cu-Mo porphyry with methods such as Ar-Ar of sericite or adularia, Re-Os of sulfide minerals, may help sort out if the Marget Ann mine fits into the “One Fluid Explains All” model of Mark Reed or the “Two Event Mineralization” model of Karen Lund.
- Mines in the north part of Butte should be re-evaluated for the possibility of a gold resource, including the Glengarry mine which is directly northwest of the Marget Ann mine.
- Uytenbogaardtite needs to be sent off for electron probe microanalysis to confirm the presence of this mineral.
- Dawsonite needs to be confirmed as it could be another identifier for gold veins and could help determine the type of ore forming brine the gold was transported in.

6. References

Barton, M. D., Kieft, C., Burke, E., & Oen, I. S. (1978). Uytenbogaardtite, a new silver-gold sulfide. *Canadian Mineralogist, 16*, p. 651-657.

Barton, P. B., & Bethke, P. M. (1987). Chalcopyrite disease in sphalerite; pathology and epidemiology. *American Mineralogist, 72*(5-6), p. 451-467.

Barton, P. B., & Skinner, B. J. (1979). Sulfide mineral stabilities. Ch. 7 in Barnes, H.L. In *Geochemistry of Hydrothermal Ore Deposits* (2nd ed.). New York: J. Wiley.

Barton, P. B., & Toulmin, P. (1964). The electrum-tarnish method for the determination of the fugacity of sulfur in laboratory sulfide systems. *Geochimica et Cosmochimica Acta, 28*(5), p. 619-640.

Bortnikov, N. S., Genkin, A. D., Dobrovol'Skaya, M. G., Muravitskaya, G. N., & Filimonova, A. A. (1991). The nature of chalcopyrite inclusions in sphalerite, exosolution, coprecipitation, or "disease"? *Economic Geology, 85*(5), p. 1070-1082.

Brimhall, G. H. (1979). Lithologic determination of mass transfer mechanisms of muliple-stage porphyry copper mineralization at Butte, Montana; vein formation by hypogene leaching and enrichment of potassium-silicate protore. *Economic Geology, 73*(3), p. 556-589.

Brimhall, G. H. (1980). Deep hypogene oxidation of prophyry copper potassium-silicate protore at Butte, Montana; a theoretical evalution of the copper remobilzation hypothesis. *Economic Geology, 75*(3), p. 384-409.

Coveney, R. M., & Kelley, W. C. (1971). Dawsonite as a daughter mineral in hydrothermal fluid inclusions. *Contributions to Mineralogy and Petrology, 32*, p. 334-342.

Czehura, S. J. (2006). Butte, a world class ore deposit. *Mining Engineering, 58*, p. 14-19.

du Bray, E. A., Aleinikoff, J. N., & Lund, K. (2012). Synthesis of petrographic, geochemical, and isotopic data for the Boulder Batholith, southwest Montana: U.S. Geological Survey Professional Paper 1793. p. 39.

Dudás, F., Ispolatov, V., Harlan, S., & Snee, L. (2010). 40Ar/39Ar geochronology and geochemical reconnaissance of the Eocene Lowland Creek Volcanic Field, west central Montana. *Journal of Geology, 118*(3), p. 295-304.

Einaudi, M. T., Hedenquist, J. W., & Inan, E. E. (2003). Sulfidation state of fluids in active and extinct hydrothermal systems: transitions from porphyry to epithermal environments. *Giggenbach Volume, Society of Economic Geologists and Geochemical Society, Special Publication*(10), p. 51.

Elliot, J. E., Loen, J. S., Wise, K. K., & Blaskowski, M. J. (1992). Maps showing locations of mines and prospects in the Butte 1x2 quadrangle, western Montana. U.S. Geological Survey Miscellaneous Investigations Series Map I-2050-C.

Gammons, C. H., Szarkowski, J., & Stevenson, R. (2016). New investigations of the mineralogy of silver in the world-class porphyry-lode deposits of Butte, MT. *Mining Engineering*, pp. 1-8.

Hedenquist, J., & Lowenstern, J. B. (1994). The role of magmas in the formation of hydrothermal ore deposits. *Nature, 370*, pp. 519-527.

Houston, R. A., & Dilles, J. H. (2013). Structural geologic evolution of the Butte District, Montana. *Economic Geology, 108*, p. 1397-1424.

Lund, K., Aleinikoff, J. N., Kunk, M. J., Unruh, D. M., Zeihen, G. D., Hodges, W. C., . . . O'Neill, J. M. (2002). SHRIMP U-Pb and 40Ar/39Ar age constraints for relating

plutonism and mineralization in the boulder batholith region, Montana. *Economic Geology 2002, 97*(2), p. 241-267.

Lund, K., McAleer, R. J., Aleinikoff, J. N., Cosca, M. A., & Kunk, M. J. (2018). Two-event lode-ore depostion at Butte, USA: 40Ar/39Ar and U-Pb documentation of Ag-Au-polymetallic lodes overprinted by younger stockwork Cu-Mo ores and penecontemporaneous Cu lodes. *Ore Geology Reviews, 102*, p. 666-700.

Meyer, C., Shea, E., Goddard, C., & and staff. (1968). Ore deposits at Butte, Montana, in Ridge, J.D., ed., Ore deposits of the United States 1933-1967. *The Graton Sales Volume: New York, American Institute of Mining, Metallurigcal, and Petroleum Engineers, 2*, pp. 1363-1416.

Mindat. (2022, March 16). *Acanthite: Mineral information, data and localities.* Retrieved from Mindat: https://www.mindat.org/min-10.html

Mindat. (2022, March 27). *Dawsonite: Mineral information, data and localities*. Retrieved from Mindat: https://www.mindat.org/min-1240.html

Mindat. (2022, March 15). *Jalpaite: Mineral information, data and localities*. Retrieved from Mindat: https://www.mindat.org/min-2069.html

Mindat. (2022, March 20). *Uytenbogaardtite: Mineral information, data and localities*. Retrieved from Mindat: https://www.mindat.org/min-4127.html

Noranda Exploration, Inc. & Others. (1974, June 3rd). Marget Ann Mine - Composite Plan showing 200, 300, 400, and 550 levels. Butte, Montana.

Ortelli, M., Kouzmanov, K., Dilles, J. H., & Rusk, B. G. (2013). District-scale fluid evolution in the Main Stage veins at Butte, Montana. In: Proceedings 12th Society for Geology Applied to MIneral Deposits (SGA) Biennial Meeting. p. 849-852.

Reed, M., & Dilles, J. (in press). Ore Deposits at Butte, Montana. *Montana Bureau of Mines and Geology Special Publication 122, Geology of Montana, 2*.

Rusk, B. G., Miller, B. J., & Reed, M. H. (2008b). Fluid-inclusion evidence for the formation of Main Stage polymetallic base-metal veins. *Arizona Geological Society Digest 22*, p. 573-581.

Rusk, B. G., Reed, M. H., & Dilles, J. H. (2008a). Fluid inclusion evidence for magmatic-hydrothermal fluid evolution in the porphyry copper-molybdenum deposit at Butte, Montana. *Economic Geology, 103*, p. 307-334.

Sahinen, W. M. (1953). Geology of the Marget Ann Mine, Butte District, Montana. *B.S. thesis, 407*, pp. 1928-1970. Montana Tech, Butte, MT.

Scott, S. D., & Barnes, H. L. (1971). Sphalerite geothermometry and geobarometry. *Economic Geology, 66*, p. 653-669.

Simmons, S. F., White, N. C., & John, D. A. (2005). Geological characteristics of epithermal precious and base metal deposits. *Economic Geology, 100th Anniversary Volume*, p. 485-522.

Skinner, B. (1966). The System Cu-Ag-S. *Econ. Geol.*(61), p. 1-26.

White, J. L., Orr, R. L., & Hultgren, R. (1957). The thermodynamic properties of silver-gold alloys. *Atca Metallurgica, 5*, p. 747-760.

Win, M. S. (1955). Geology and Ore Deposits of the Marget Ann Mine Silver Bow County, Montana, M.S. Thesis. Montana Tech, Butte, MT.

7. Appendix A: SEM-EDS Atomic Percentages and Calculated Formulas

Table 11: Atomic Percentages and Calculated Formulas from SEM-EDS Analysis of Rhodonite

		Atomic %				
Mineral	Sample #	O	Si	Ca	Mn	Chemical Formula
Rhodonite	Old MA5060	42.5	30.4	4.5	22.7	$(Mn_{.83}Ca_{.17})SiO_3$
Rhodonite	Old MA5060	41.7	30.4	3.8	24.1	$(Mn_{.86}Ca_{.14})SiO_3$
Rhodonite	MA-13	59.5	20.2	3.7	16.6	$(Mn_{.82}Ca_{.18})SiO_3$
Rhodonite	MA-13	59.2	20.1	2.4	18.3	$(Mn_{.88}Ca_{.12})SiO_3$
Rhodonite	MA-13	62.4	15.5	3.2	19.0	$(Mn_{.86}Ca_{.14})SiO_3$
Rhodonite	MA-13	59.2	20.0	2.8	18.0	$(Mn_{.87}Ca_{.13})SiO_3$
Rhodonite	MA-13	59.1	19.9	4.1	16.9	$(Mn_{.81}Ca_{.19})SiO_3$
Rhodonite	MA-13	59.6	19.8	3.9	16.7	$(Mn_{.81}Ca_{.19})SiO_3$
Rhodonite	MA-30	59.1	20.5	4.1	16.3	$(Mn_{.80}Ca_{.20})SiO_3$
Rhodonite	MA-30	59.3	20.0	4.0	16.8	$(Mn_{.81}Ca_{.19})SiO_3$
Rhodonite	MA-30	59.3	20.1	2.5	18.1	$(Mn_{.88}Ca_{.12})SiO_3$
Rhodonite	MA-30	58.8	20.0	3.6	17.7	$(Mn_{.83}Ca_{.17})SiO_3$
Rhodonite	MA-30	59.2	20.0	3.7	17.2	$(Mn_{.82}Ca_{.18})SiO_3$
Rhodonite	AMC-4316	64.0	15.4	3.6	17.0	$(Mn_{.82}Ca_{.18})SiO_3$
Rhodonite	MA-16 2016	59.2	20.5	3.1	15.9	$(Mn_{.84}Ca_{.16})SiO_3$
Rhodonite	MA-16 2016	61.3	20.8	2.9	13.7	$(Mn_{.83}Ca_{.17})SiO_3$
Rhodonite	MA-16 2016	58.6	21.2	3.0	15.2	$(Mn_{.83}Ca_{.17})SiO_3$
Rhodonite	MA-16 2016	60.3	21.0	2.8	15.9	$(Mn_{.85}Ca_{.15})SiO_3$
Rhodonite	MA-16 2016	57.8	21.0	3.0	18.3	$(Mn_{.86}Ca_{.14})SiO_3$
Rhodonite	MA-13 2016	57.7	21.1	2.3	18.9	$(Mn_{.89}Ca_{.11})SiO_3$

Table 12: Atomic Percentages and Calculated Formulas from SEM-EDS Analysis of Feldspar and Muscovite

		Atomic %					
Mineral	Sample #	O	Al	Si	K	Mg	Chemical Formula
Feldspar	MA-30	60.3	8.7	23.1	7.9	0.0	**$K(AlSi_3O_8)$**
Feldspar	MA-30	59.9	8.7	23.4	8.0	0.0	**$K(AlSi_3O_8)$**
Feldspar	MA-30	59.9	8.7	23.4	8.0	0.0	**$K(AlSi_3O_8)$**
Feldspar	MA-30	59.9	8.7	23.4	8.1	0.0	**$K(AlSi_3O_8)$**
Feldspar	MA-14C	60.1	9.2	23.1	7.7	0.0	**$K(AlSi_3O_8)$**
Feldspar	MA-14C	59.7	9.0	23.4	7.9	0.0	**$K(AlSi_3O_8)$**
Feldspar	MA-14C	64.1	3.3	30.4	2.3	0.0	**$K(AlSi_3O_8)$**
Muscovite	MA-14C	60.3	15.0	19.0	4.7	1.0	**$KAl_2(AlSi_3O_{10})(F, OH)_2$**
Muscovite	MA-14C	61.2	14.0	18.5	4.7	1.7	**$KAl_2(AlSi_3O_{10})(F, OH)_2$**
Feldspar	MA-16 2016	59.3	8.7	24.2	7.9	0.0	**$K(AlSi_3O_8)$**
Feldspar	MA-13 2016	58.9	8.9	24.0	8.2	0.0	**$K(AlSi_3O_8)$**

Table 13: Atomic Percentages and Calculated Formulas from SEM-EDS Analysis of Calcite

		Atomic %					
Mineral	Sample #	C	O	Ca	Mn	Si	Chemical Formula
Calcite	Old MA-4	15.8	54.0	25.9	4.3	0.0	**$(Ca_{.86}Mn_{.14})CO_3$**
Calcite	Old MA-4	15.7	53.1	25.9	5.3	0.0	**$(Ca_{.83}Mn_{.17})CO_3$**
Calcite	AMC 5060	17.1	51.9	22.5	6.9	1.6	**$(Ca_{.76}Mn_{.24})CO_3$**
Calcite	MA 88-10	13.7	62.1	21.9	2.3	0.0	**$(Ca_{.90}Mn_{.10})CO_3$**
Calcite	MA 88-10	13.1	60.8	22.9	3.3	0.0	**$(Ca_{.87}Mn_{.13})CO_3$**

Table 14: Atomic Percentages and Calculated Formulas from SEM-EDS Analysis of Rhodochrosite

		Atomic %						
Mineral	Sample #	O	Mg	Ca	Mn	Zn	C	Chemical Formula
Rhodochrosite	AMC 4316B	56.4	0.0	5.0	38.6	0.0	0.0	$(Mn_{.89}Ca_{.11})\ CO_3$
Rhodochrosite	AMC 4316B	54.9	0.0	3.0	42.0	0.0	0.0	$(Mn_{.93}Ca_{.07})\ CO_3$
Rhodochrosite	AMC 4316A	52.2	0.0	1.5	45.8	0.4	0.0	$(Mn_{.96}Ca_{.03}Zn_{.01})\ CO_3$
Rhodochrosite	AMC 4316A	61.2	0.5	4.9	33.2	0.0	0.0	$(Mn_{.86}Ca_{.13}Mg_{.01})\ CO_3$
Rhodochrosite	AMC 4316A	62.4	0.0	2.5	35.2	0.0	0.0	$(Mn_{.93}Ca_{.07})\ CO_3$
Rhodochrosite	AMC 5060	54.1	0.0	2.2	43.7	0.0	0.0	$(Mn_{.95}Ca_{.05})\ CO_3$
Rhodochrosite	AMC 5060	53.7	0.0	2.7	43.6	0.0	0.0	$(Mn_{.94}Ca_{.06})\ CO_3$
Rhodochrosite	AMC 5060	49.1	0.0	1.8	31.3	0.0	0.0	$(Mn_{.94}Ca_{.06})\ CO_3$
Rhodochrosite	MA-15	60.8	1.2	2.6	18.1	0.0	17.3	$(Mn_{.83}Ca_{.12}Mg_{.05})\ CO_3$
Rhodochrosite	MA-13	71.6	0.0	2.0	26.4	0.0	0.0	$(Mn_{.93}Ca_{.07})\ CO_3$
Rhodochrosite	MA-13	69.0	0.0	2.0	29.0	0.0	0.0	$(Mn_{.94}Ca_{.06})\ CO_3$
Rhodochrosite	MA-13	68.7	2.3	2.7	26.3	0.0	0.0	$(Mn_{.84}Ca_{.08}Zn_{.07})\ CO_3$
Rhodochrosite	MA-13	70.6	0.0	1.2	27.4	0.0	0.0	$(Mn_{.96}Ca_{.04})\ CO_3$
Rhodochrosite	MA-13	67.0	0.0	1.6	31.3	0.0	0.0	$(Mn_{.95}Ca_{.05})\ CO_3$
Rhodochrosite	MA-13	67.7	0.0	1.8	30.5	0.0	0.0	$(Mn_{.94}Ca_{.06})\ CO_3$
Rhodochrosite	MA-13	69.0	0.0	2.2	28.8	0.0	0.0	$(Mn_{.93}Ca_{.07})\ CO_3$
Rhodochrosite	MA-13	39.6	0.0	3.8	27.7	0.0	0.0	$(Mn_{.88}Ca_{.12})\ CO_3$
Rhodochrosite	MA-13	68.5	0.0	1.4	30.1	0.0	0.0	$(Mn_{.96}Ca_{.04})\ CO_3$
Rhodochrosite	MA-13	68.3	0.0	0.7	31.0	0.0	0.0	$(Mn_{.98}Ca_{.02})\ CO_3$
Rhodochrosite	MA-13	69.5	0.0	2.8	27.7	0.0	0.0	$(Mn_{.91}Ca_{.09})\ CO_3$
Rhodochrosite	MA-30	69.4	0.0	4.1	26.5	0.0	0.0	$(Mn_{.87}Ca_{.13})\ CO_3$
Rhodochrosite	MA-30	68.4	0.0	1.9	29.7	0.0	0.0	$(Mn_{.94}Ca_{.06})\ CO_3$
Rhodochrosite	MA-30	70.8	0.0	5.2	24.0	0.0	0.0	$(Mn_{.82}Ca_{.18})\ CO_3$
Rhodochrosite	MA-30	61.7	0.0	3.3	19.5	0.0	15.5	$(Mn_{.85}Ca_{.15})\ CO_3$
Rhodochrosite	MA-30	70.8	0.0	4.3	25.0	0.0	0.0	$(Mn_{.85}Ca_{.15})\ CO_3$
Rhodochrosite	MA-30	69.1	0.0	2.7	28.2	0.0	0.0	$(Mn_{.91}Ca_{.09})\ CO_3$
Rhodochrosite	MA-30	69.5	0.0	3.3	27.2	0.0	0.0	$(Mn_{.89}Ca_{.11})\ CO_3$
Rhodochrosite	MA-30B	69.4	0.0	3.6	27.0	0.0	0.0	$(Mn_{.88}Ca_{.12})\ CO_3$
Rhodochrosite	MA-30B	69.9	0.0	3.6	26.5	0.0	0.0	$(Mn_{.88}Ca_{.12})\ CO_3$
Rhodochrosite	MA-30B	70.0	0.0	4.3	25.8	0.0	0.0	$(Mn_{.86}Ca_{.14})\ CO_3$
Rhodochrosite	MA-19	69.3	0.0	2.4	28.4	0.0	0.0	$(Mn_{.92}Ca_{.08})\ CO_3$
Rhodochrosite	MA-19	69.4	0.0	2.8	27.8	0.0	0.0	$(Mn_{.91}Ca_{.09})\ CO_3$
Rhodochrosite	MA-14C	70.6	0.0	6.8	22.6	0.0	0.0	$(Mn_{.77}Ca_{.23})\ CO_3$
Rhodochrosite	AMC- 4316	63.6	1.1	5.6	15.3	0.0	14.4	$(Mn_{.70}Ca_{.25})\ CO_3$
Rhodochrosite	MA-13 2016	60.2	0.0	3.9	17.4	0.0	18.5	$(Mn_{.82}Ca_{.18})\ CO_3$
Rhodochrosite	MA-13 2016	59.6	0.0	1.9	20.5	0.0	18.7	$(Mn_{.92}Ca_{.08})\ CO_3$
Rhodochrosite	MA 88-10	72.7	0.0	7.2	20.1	0.0	0.0	$(Mn_{.74}Ca_{.26})\ CO_3$
Rhodochrosite	MA-8	63.2	0.0	2.1	20.7	0.0	14.0	$(Mn_{.91}Ca_{.09})\ CO_3$
Rhodochrosite	MA-8	62.6	0.0	3.6	16.7	0.0	15.5	$(Mn_{.82}Ca_{.18})\ CO_3$
Rhodochrosite	MA-8	66.9	0.0	3.9	29.2	0.0	0.0	$(Mn_{.88}Ca_{.12})\ CO_3$
Rhodochrosite	MA-8	62.7	0.0	2.8	20.2	0.0	14.3	$(Mn_{.88}Ca_{.12})\ CO_3$

Table 15: Atomic Percentages and Calculated Formulas from SEM-EDS Analysis of Acanthite

		Atomic %			
Mineral	Sample #	S	Ag	Cu	Chemical Formula
Acanthite	Old MA-7B	39.0	59.3	1.7	$Ag_{1.94}Cu_{.06}S$
Acanthite	Old MA-7B	31.0	67.4	1.6	$Ag_{1.95}Cu_{.05}S$
Acanthite	Old MA-7B	26.8	71.9	1.3	$Ag_{1.96}Cu_{.04}S$
Acanthite	AMC 4316A	39.0	59.3	0.0	Ag_2S
Acanthite	AMC 5060	39.7	55.0	5.4	$Ag_{1.82}Cu_{.18}S$
Acanthite	AMC 5060	35.3	56.5	8.1	$Ag_{1.75}Cu_{.25}S$
Acanthite	AMC 5060	36.3	55.8	7.9	$Ag_{1.75}Cu_{.25}S$
Acanthite	MA-13	35.9	62.3	1.8	$Ag_{1.94}Cu_{.06}S$
Acanthite	MA-13	34.4	65.6	0.0	Ag_2S
Acanthite	MA-13	32.2	67.8	0.0	Ag_2S
Acanthite	MA-13	39.5	60.5	0.0	Ag_2S
Acanthite	MA-13	31.8	66.4	1.9	$Ag_{1.95}Cu_{.05}S$
Acanthite	MA-13	46.1	53.9	0.0	Ag_2S
Acanthite	MA-13	32.5	67.6	0.0	Ag_2S
Acanthite	MA-13	33.7	66.3	0.0	Ag_2S
Acanthite	MA-13	40.0	60.0	0.0	Ag_2S
Acanthite	MA-13	34.8	65.2	0.0	Ag_2S
Acanthite	MA-13	31.8	66.4	1.9	$Ag_{1.95}Cu_{.05}S$
Acanthite	MA-13	33.4	66.6	0.0	Ag_2S
Acanthite	MA-13	29.1	70.9	0.0	Ag_2S
Acanthite	MA-13	33.8	66.2	0.0	Ag_2S
Acanthite	MA-13	27.9	72.1	0.0	Ag_2S
Acanthite	MA-13	37.8	62.2	0.0	Ag_2S
Acanthite	MA-30	28.9	71.1	0.0	Ag_2S
Acanthite	MA-30	29.3	70.7	0.0	Ag_2S
Acanthite	MA-30	25.4	74.6	0.0	Ag_2S
Acanthite	MA-30	27.4	72.6	0.0	Ag_2S
Acanthite	MA-30	27.4	72.6	0.0	Ag_2S
Acanthite	MA-30	40.1	59.9	0.0	Ag_2S
Acanthite	MA-30	26.9	73.1	0.0	Ag_2S
Acanthite	MA-30	23.5	76.5	0.0	Ag_2S
Acanthite	MA-30B	44.6	55.4	0.0	Ag_2S
Acanthite	MA-30B	47.1	52.9	0.0	Ag_2S
Acanthite	AMC-4316	25.9	70.1	0.0	Ag_2S
Acanthite	MA-16 2016	29.6	66.9	0.0	Ag_2S
Acanthite	MA-13 2016	38.0	62.0	0.0	Ag_2S
Acanthite	MA- 88-10	32.8	67.2	0.0	Ag_2S
Acanthite	MA- 88-10	30.2	69.8	0.0	Ag_2S
Acanthite	MA- 88-10	33.3	66.7	0.0	Ag_2S
Acanthite	MA- 88-10	31.9	68.1	0.0	Ag_2S
Acanthite	MA- 88-10	33.1	66.9	0.0	Ag_2S
Acanthite	MA- 88-10	27.1	64.1	0.0	Ag_2S
Acanthite	MA- 88-10	30.0	69.7	0.0	Ag_2S
Acanthite	MA- 88-10	30.4	69.6	0.0	Ag_2S
Acanthite	MA- 88-10	31.4	68.6	0.0	Ag_2S
Acanthite	MA-8	33.0	67.0	0.0	Ag_2S
Acanthite	MA-8	27.7	72.3	0.0	Ag_2S
Acanthite	MA-8	38.9	61.1	0.0	Ag_2S
Acanthite	MA-8	35.5	64.5	0.0	Ag_2S
Acanthite	MA-8	35.5	64.5	0.0	Ag_2S

8. Appendix B: Fluid Inclusion Data

Table 16: Flinc Sample 1 Data Set

Flinc sample 1 from Marget Ann mine					
Heating runs done on 3/12 and 3/19/21. Freezing runs on 3/19/21.					
			Salinity		
Flinc	Diameter [µm]	T_m, Ice [°C]	wt% NaCl	T_h, [°C]	Notes
1	100	-1	1.73	274	Pix, dawsonite sprays, repeated
2	50	-4.5	7.15	255	Dawsonite
3	15	-1	1.73	267	Negative crystal shape
4	15			265	
5	25	-0.8	1.39	262	
6	20	-1	1.73	267	
7	50			268	
8	15			260	
9	20			264	
10	20			266	
11	30			268	
12	37.5			242	
13	25	-1.3	2.23		
14	30	-1	1.73	261	Hard to get Tm, ice. Used average value
15	25	-1.9	3.21	262	
16	25			268	
17	35			254	
18	37.5	-2.1	3.53	257	
19	35	-0.9	1.56	262	
20	25	-0.6	1.05		
21	30	-3.4	5.55		beautiful flinc, but bubble never came back
22	12			277	
23	12			293	
24				259	
25				270	
26				265	
27				268	
28				271	
29				273	
30				264	
31	17.5	-1	1.73	264	
32	5	-1.05	1.81	244	
33	12.5	-1.6	2.72	244	
34	5			248	
35	5	-0.85	1.47	279	Difficult to see
36		-1	1.73	270	
37				250	
38	17.5			254	
39	55			202	Difficult to see
40	25			259	
41	12.5			273	
42	7.5			196	
43	12.5			278	
44	25			282	
45	12.5			268	

Table 17: Flinc Sample 2 Data Set

Flinc sample 2 from Marget Ann mine					
Analyzed on 4/4/21, Old sample made by CHG					
			Salinity		
Flinc	Diameter [µm]	T_m, Ice [°C]	wt% NaCl	T_h [°C]	Notes
1	15	-1.8	3.05	256	
2	22	-0.8	1.39	266	
3	35			272	
4	15			262	
5	22			267	
6	12			264	
7	25	-0.8	1.39	264	
8	25	-1.2	2.06		
9	50				
10	25			265	
11	25			254	
12	20			264	
13	20			267	
14	20				
15	20			277	
16	15	-1.2	2.06	262	
17	20	-0.8	1.39	270	
18	20	-0.7	1.22	250	
19	20			265	
20	15	-1.1	1.90	245	
21	12				
22	20			278	
23	30	-1.2	2.06	240	
24	20			264	
25	20			294	

Table 18: Flinc Sample 3 Data Set

Flinc sample 3 from Marget Ann mine					
Heating runs done on 5/28/21. Freezing runs on 5/28/21.					
			Salinity		
Flinc	Diameter [µm]	T_m, Ice [°C]	wt% NaCl	T_h [°C]	Notes
1		-0.7	1.22		
2	50				
3		-0.8	1.39		
4	15				
5	15				
6	22				
7	22				
8	12	-0.9	1.56		
9	175	-0.4	0.70		Huge flinc - burned up for heating run
10	50	-1	1.73		Burned up attempting to get heating value
11	25	-0.9	1.56	260	
12	12.5			250	
13	10			255	
14	30	-1.2	2.06	248	hard to get Tm, ice
15		-3.5	5.70		Burst in heating run
16	17.5			268	Extremely clear and easy to see
17	25			281	Couldn't see melting during freezing run
18	25	-0.9	1.56	259	
19				244	very small
20	25			263	Couldn't see bubble after second run
21	25			268	

Table 19: Flinc Sample 4.1 and 4.4 Data Set

Flinc sample 4 from Marget Ann Mine					
Heating runs done on 8/20/21. Freezing runs on 9/1/21.					
4.1			Salinity		
Flinc	Diameter [µm]	T_m, Ice [°C]	wt% NaCl	T_h [°C]	Notes
1	20	-1.95	3.29	196	oddly shaped
2	17.5			246	Large bubble, possible daughter mineral, burnt up prior to freezing run
3	15	-1.6	2.72	233	
4				166	Upper Bubble, Two bubbles in one inclusion - separated by small bridge in center - burnt up prior to freezing run
5				126	Bottom Bubble, Two bubbles in one inclusion - separated by small bridge in center - burnt up prior to freezing run
6	17.5	-1.9	3.21	232	
7	20	-1.6	2.72	231	
8	7.5	-1.9	3.21	249	
9	25	-1.8	3.05	238	Possible daughter mineral
10		-2.9	4.79		Possible daughter mineral, very large inclusion, dark bubble, seemed to expand while doing other freezing runs - hard to see
11	27.5	-1.7	2.89	318	
12	7.5	-0.9	1.56	234	Follows along a plane
13	3.75			240	Follows along a plane
14	12.5			247	Follows along a plane
15				245	Follows along a plane - very clear
16	27.5			251	
17	37.5			251	
Heating runs done on 9/20/21. Freezing runs on 9/16/21.					
4.4			Salinity		
Flinc	Diameter [µm]	T_m, Ice [°C]	wt% NaCl	T_h [°C]	Notes
1	15	-1.45	2.48	229	Hard to see bubble go away completely
2	12.5			206	Attempted two freezing runs
3		-1	1.73	213	
4	10	-1.9	3.21	245	Possible Daughter Mineral
5	25			233	
6	20	-1.25	2.15	223	
7	12.5			261	Hard to see for freezing runs
8				237	Extremely dark
9	37.5			285	Extremely dark, could see the bubble deform during freezing but could not see ice melt

Table 20: Flinc Sample 5.2 Data Set

Flinc sample 5 from Marget Ann Mine					
Heating runs done on 10/4/2021. Freezing runs on 9/28/2021.					
5.2			Salinity		
Flinc	Diameter [µm]	T_m, Ice [°C]	wt% NaCl	T_h [°C]	Notes
1	32.5	-1.1	1.90	250	
2	10			258	
3	12.5			270	
4	25	-0.85	1.47		
5	17.5	-1.1	1.90		
6	12.5			250	
7	12.5			246	
8	32.5			258	
9	15			267	
10	17.5			289	
11	7.5			279	
12	17.5			273	
13	7.5			271	
14	62.5	-0.75	1.30		
15	17.5	-0.7	1.22	287	
16	35	-0.9	1.56	280	
17	35	-0.95	1.64	291	
18	17.5			288	
19	20			287	
20	62.5	-1.2	2.06		
21	57.5	-1	1.73		
22	37.5	0.5	-0.90	275	
23	45			209	

Table 21: Flinc Sample 5.3 Data Set

Flinc sample 5 from Marget Ann Mine					
Heating runs done on 10/19/2021. Freezing runs on 10/18/2021.					
5.3			Salinity		
Flinc	Diameter [µm]	T_m, Ice [°C]	wt% NaCl	T_h [°C]	Notes
1	18.75	-1.3	2.23	145	
2	7.5	-1.2			Could have daughter mineral
3	2.5	-0.95	1.64	204	
4	80	-0.75		166	Bubble measured 15µm
5	20	-0.2			
6	10			137	
7	7.5			214	
8	22.5			184	

Table 22: Flinc sample 5.4 Data Set

Flinc sample 5 from Marget Ann Mine					
Heating runs done on 9/27/2021. Freezing runs on 9/27/2021.					
5.4			Salinity		
Flinc	Diameter [µm]	T_m, Ice [°C]	wt% NaCl	T_h, [°C]	Notes
1	190	-1.05	1.81		Huge inclusion, bubble measured 37.5. Possible yellow daughter mineral. Heating could not be done on this inclusion because of size
2	87.5	-0.55	0.96		Possible Daughter Mineral
3	75	-0.45	0.79		Dark inclusion with large bubble
4	62.5	-1.9	3.21	269	Possible Daughter Mineral
5	55	-1.55	2.64	229	This was the best example of daughter mineral - the mineral moved during heating and was caught on camera
6	25	-0.9	1.56	250	Has daughter mineral
7		-1.35	2.31	249	Has daughter mineral
8		-1.4	2.40	242	Has daughter mineral
9	70	-1.1	1.90		Extremely dark, could see the bubble deform during freezing but could not see ice melt
10	37.5	-1.1	1.90	245	
11	35			244	
12	20	-1.25	2.15		
13	37.5	-1.75	2.97	260	Has daughter mineral
14		-1.3	2.23	241	
15	30	-1.7	2.89	257	
16	35	-1.35	2.31	261	
17	112.5	-1.1	1.90		Bubble was large and measured at 42.5
18	162.5			257	
19	20			256	

9. Appendix C: Extra Fluid Inclusion Photos

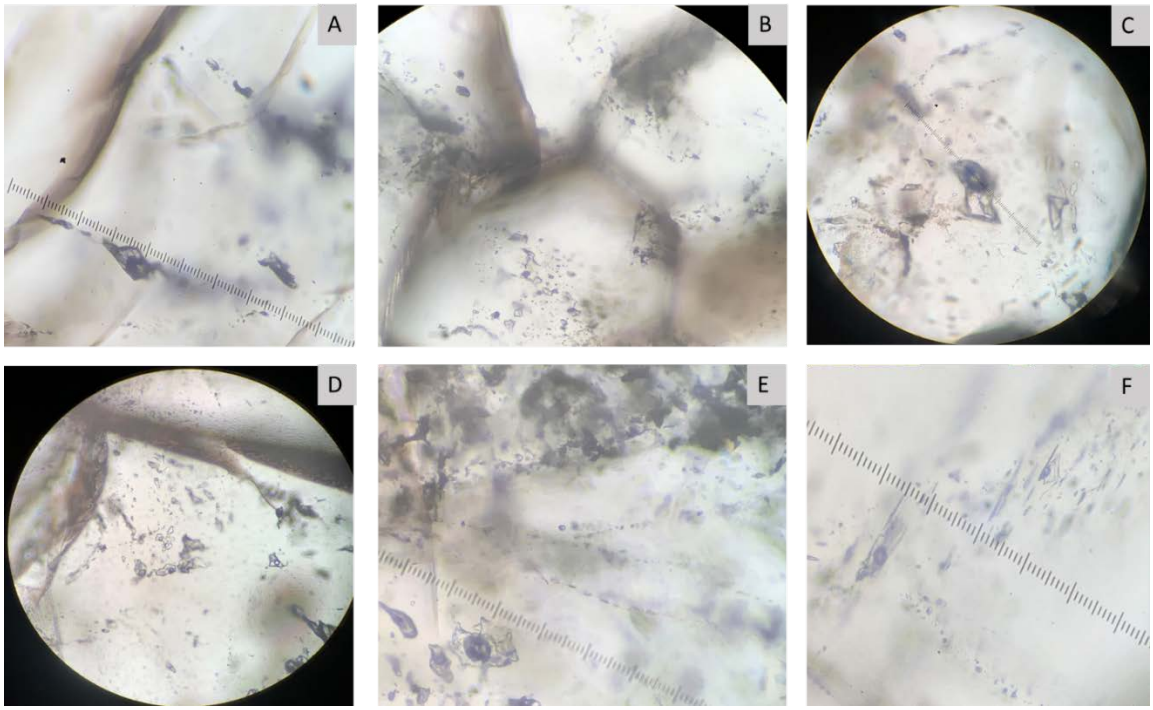

Figure 45: A) Image of large fluid inclusion. B) Euhedral quartz with primary inclusions. C)Large inclusion approximately 50 µm. D) Cluster of inclusions, one inclusion with two bubbles that after heating formed one bubble. E) Large inclusion with larger bubble. F) Series of inclusions.

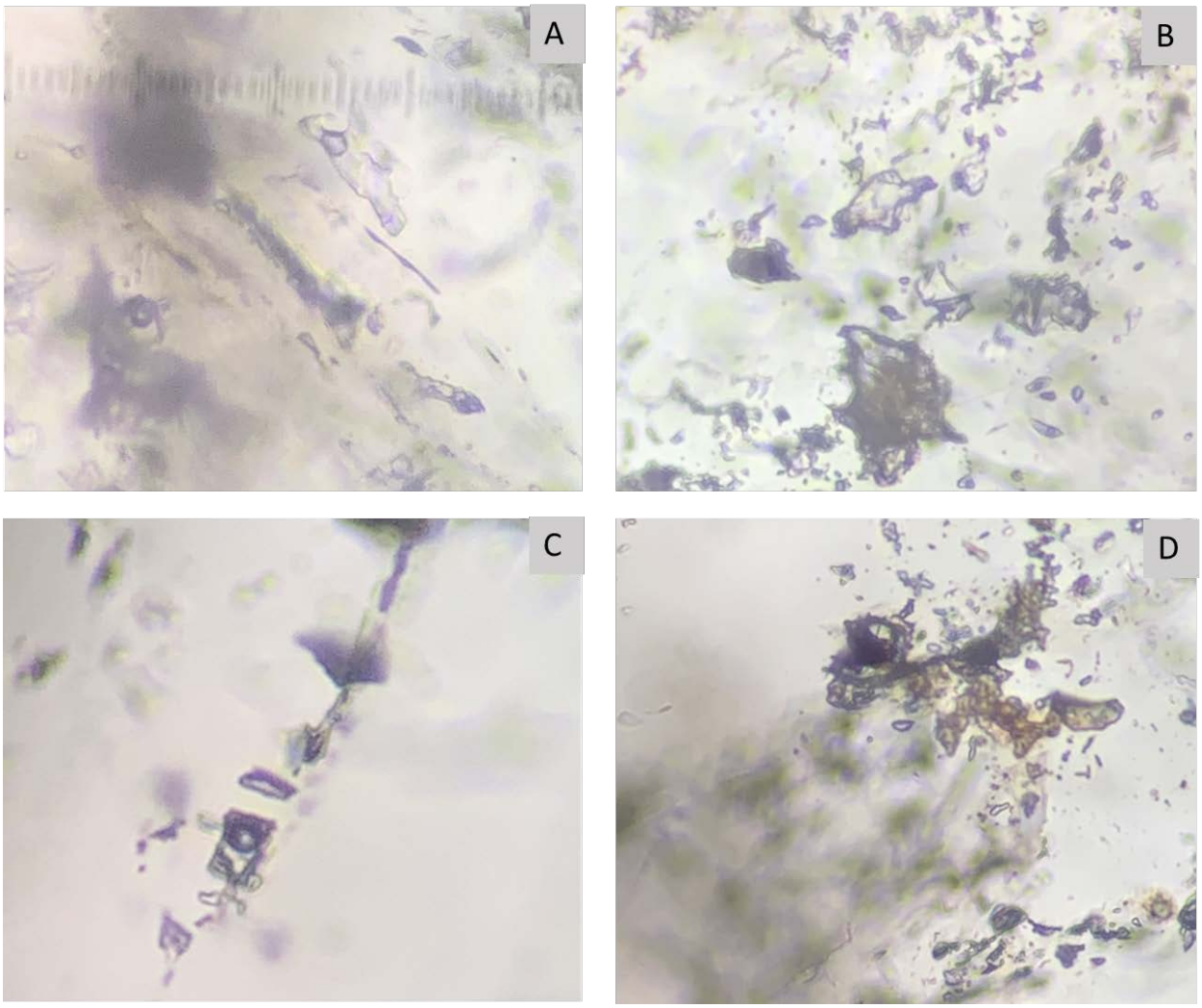

Figure 46: A) Small inclusions. B) Cluster of hard to see dark inclusions. C) Line of fluid inclusions. D) Dark bubbles in hard to see cluster of inclusion.

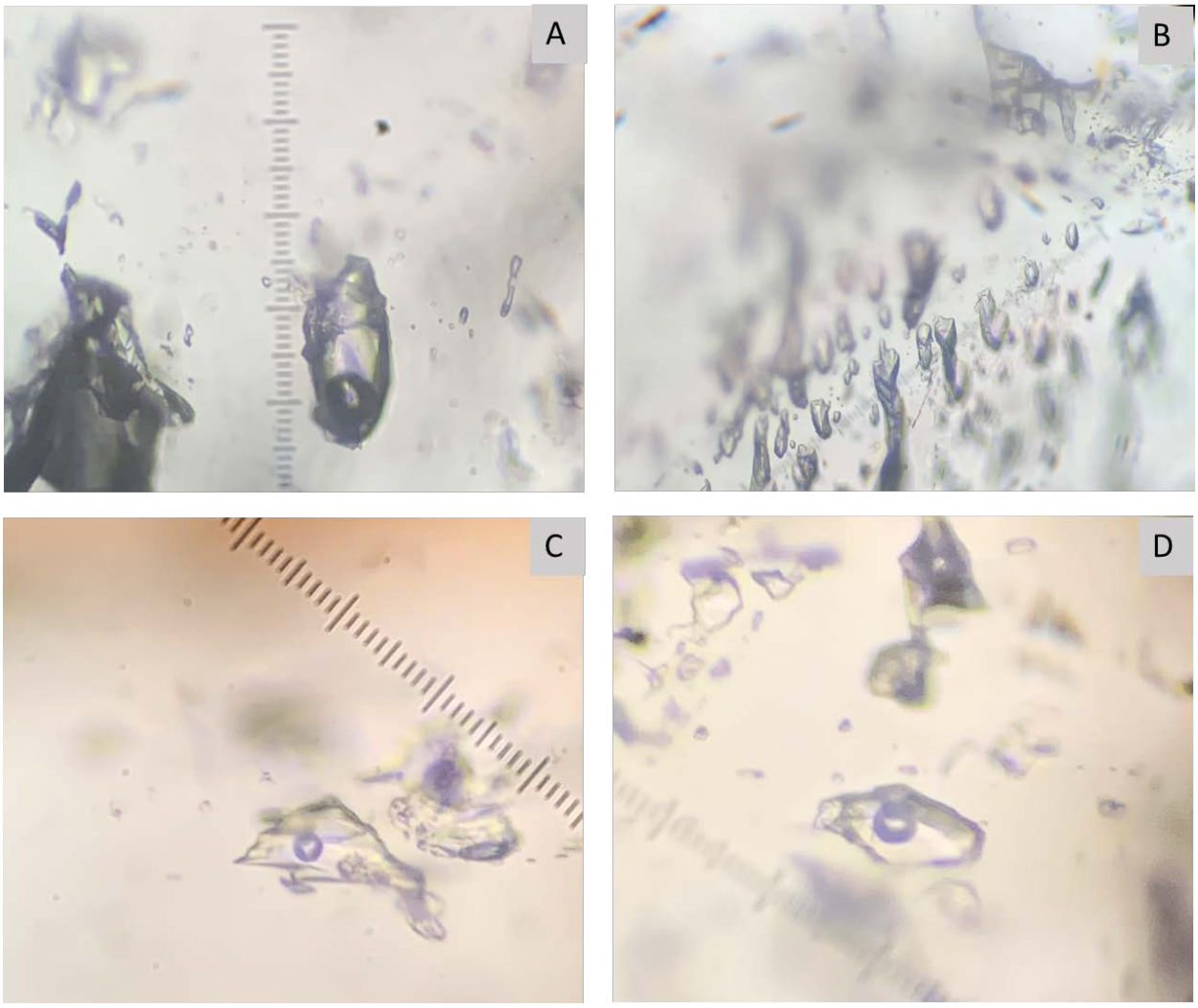

Figure 47: A) Fluid inclusion with daughter mineral. B) Cluster of secondary inclusions with no visible bubble. D) B20 inclusion with daughter mineral. F) Clear inclusion.

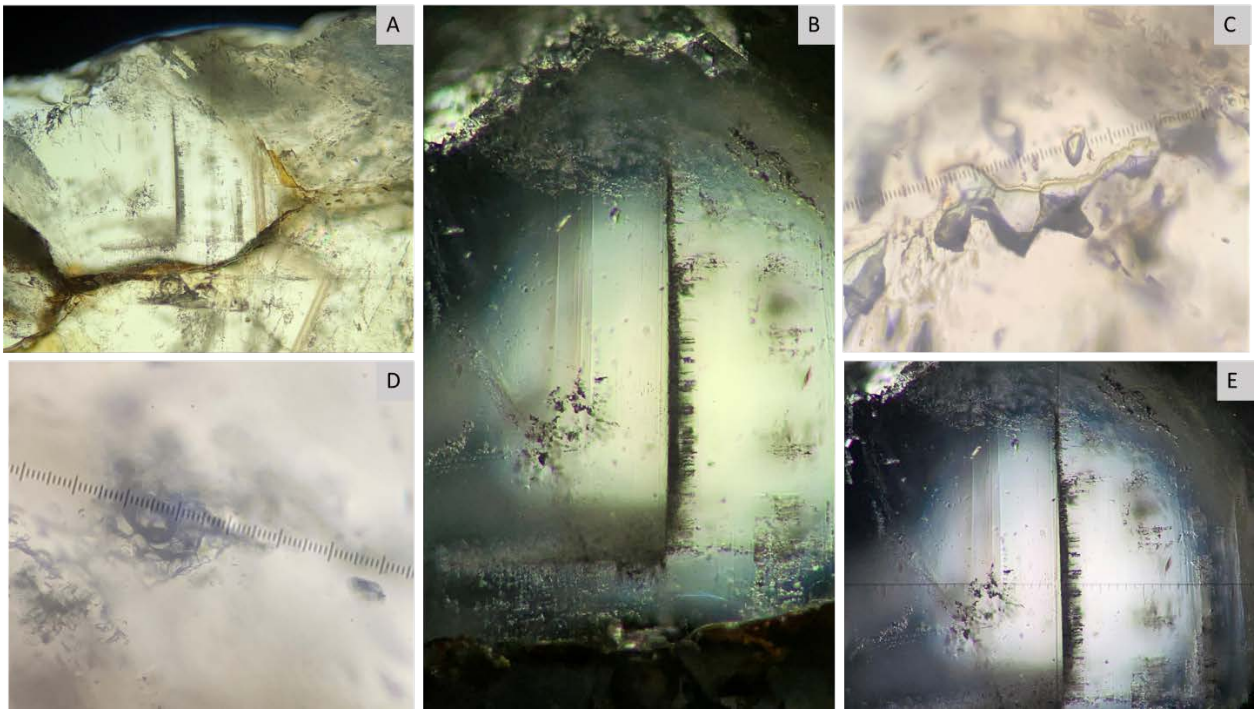

Figure 48: A) Zoomed out image of fluid inclusion location. B) Location of primary and secondary inclusion in growth zone. C) Image of fluid escaping inclusions during heating. D) Large bubble in comparison to inclusion. E) Image of B but with brighter light.

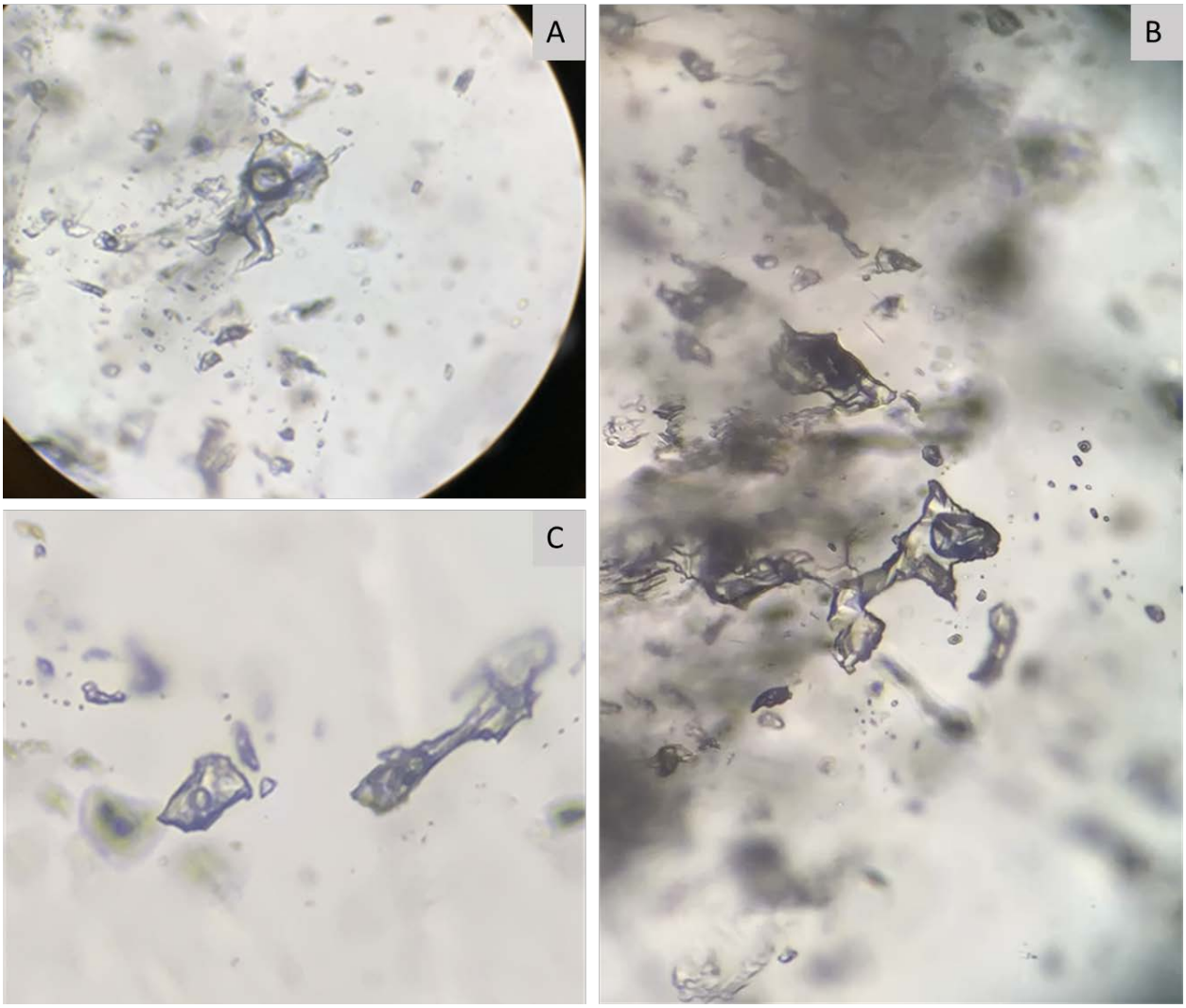

Figure 49: A) Typical Marget Ann inclusion within cluster of much smaller inclusions. B) B20 Inclusion. C) Inclusions with possible daughter mineral.

10. Appendix D: Core Photos

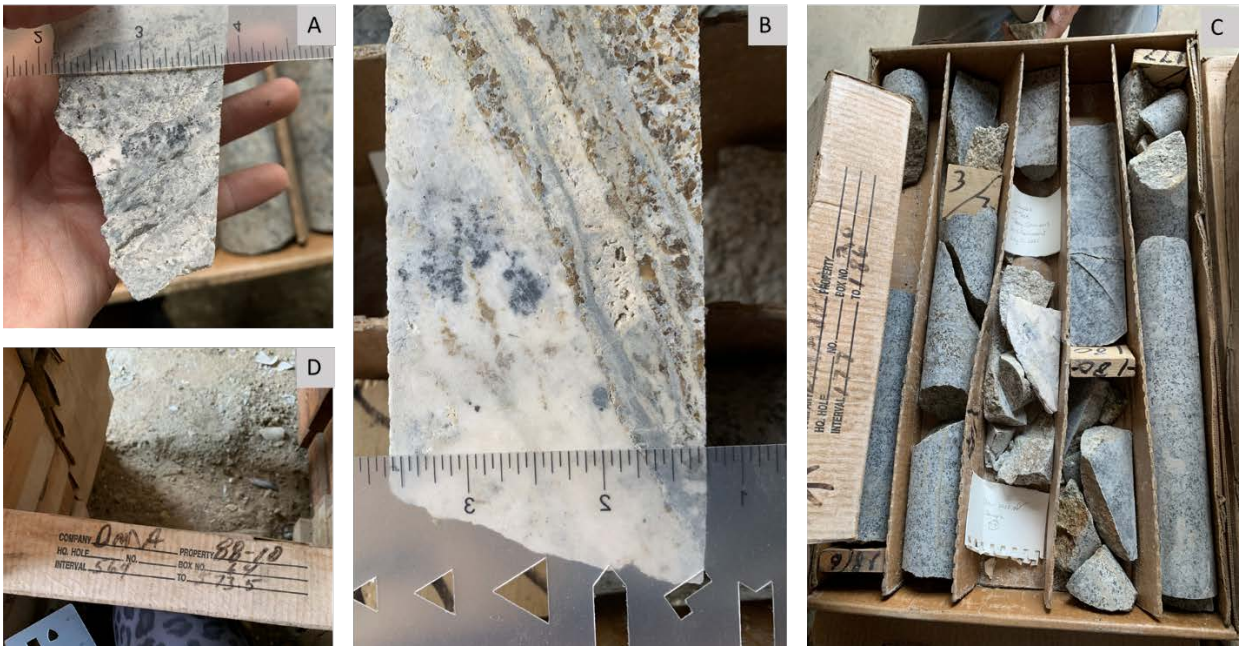

Figure 50: A) 1 ½ Core sample from DMA 88-10. B) Close up of core sample with sulfides inside matrix of carbonates. C) Image of entire core box. D) Image of lid label.

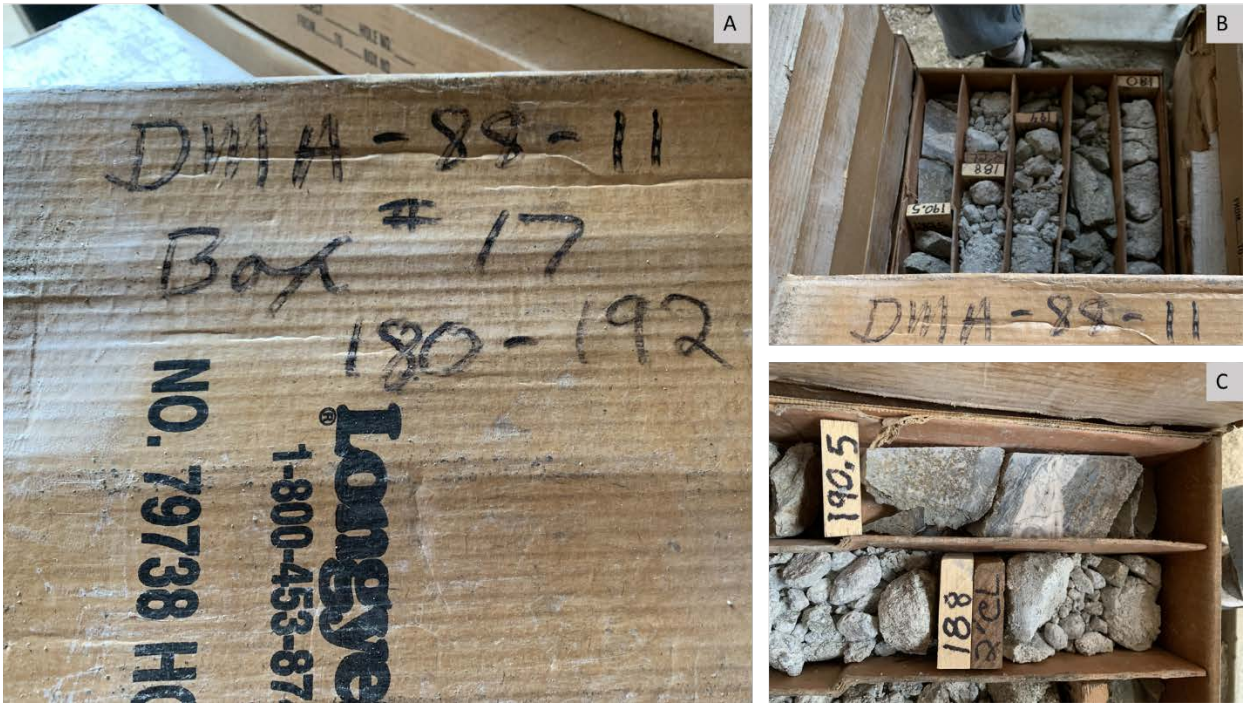

Figure 51: A) DMA 88-11 Box#17 lid. B) Image of core inside core box. C) Image of possible sulfides in the 190.5 ft. section.

Figure 52: A) Core box for DMA 88-11, box 19. B) Image of Veinlet with weathering. C) Box lid for DMA 88-11. D) Collecting XRF data from core sample.

Figure 53: A) Clay minerals on core sample from box DMA 88-11, box 25. B) Sample of core with sulfides. C) Box lid for DMA 88-11, box 25. D) Image of core in box 25. E) Core with 2 small sulfide veinlets.

11. Appendix E: Hand Samples

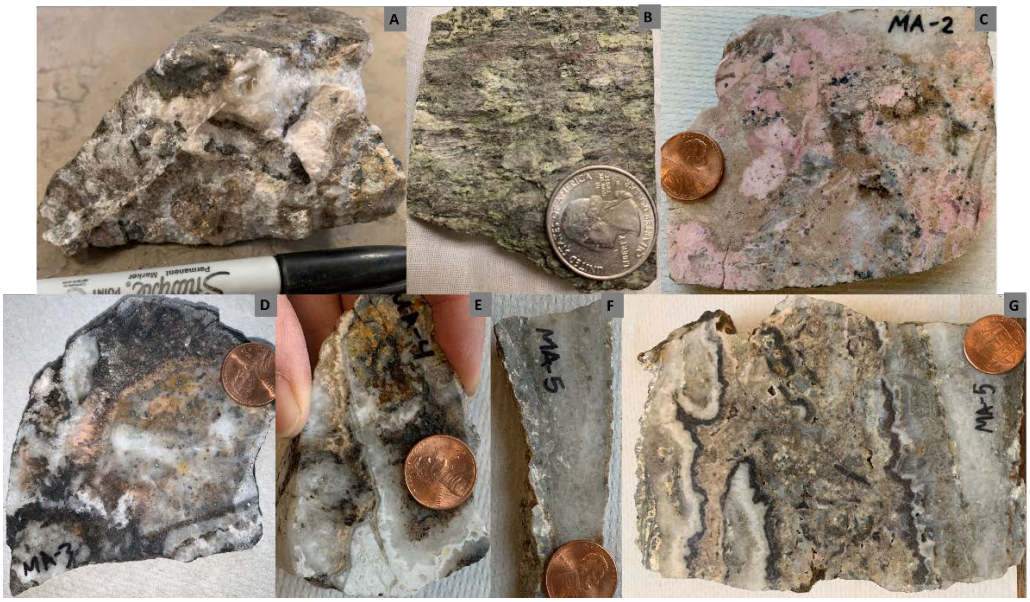

Figure 54: A) MA-105 (label on back of sample) B) Example of clay from Blackjack core, sample 88-7, box 33, 276.5-286 ft. deep.

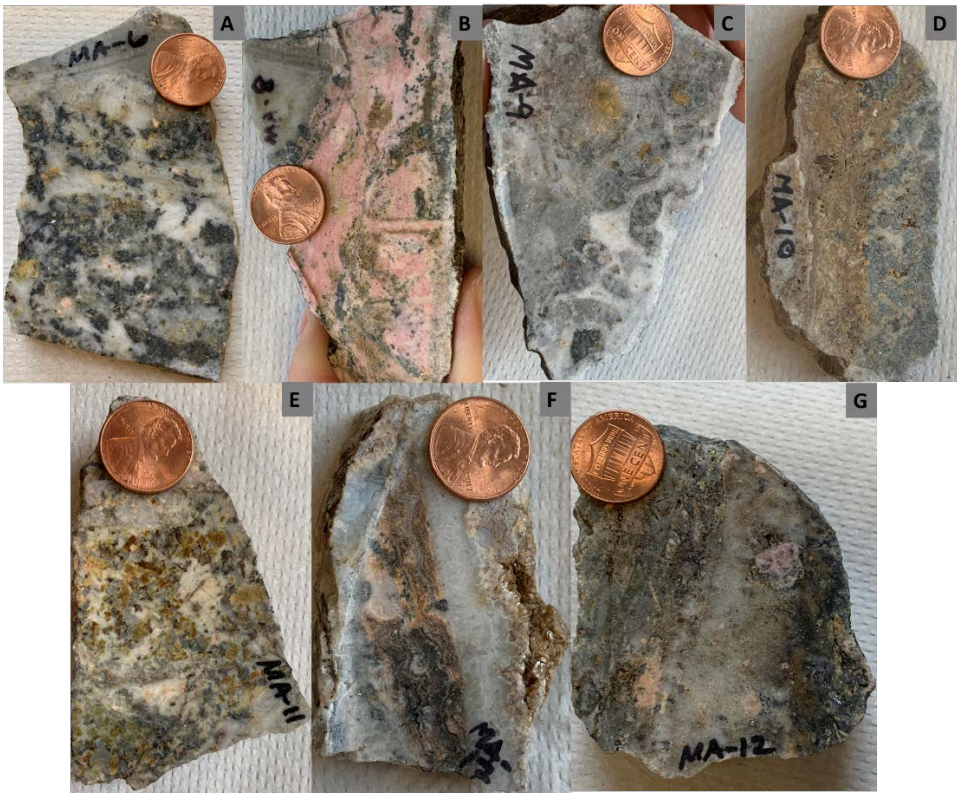

Figure 55: A) MA-6 B) MA-8 C) MA-9 D) MA-10 E) MA-11 F) MA-12 G) MA-12

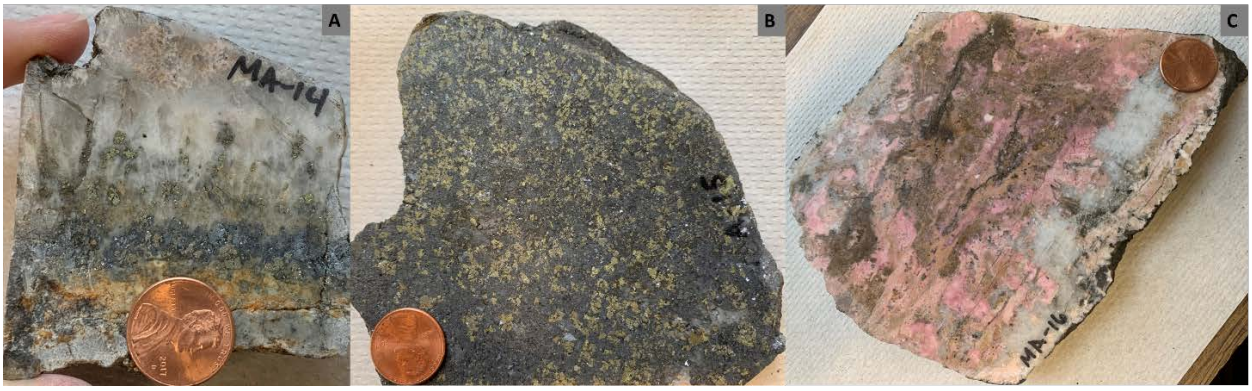

Figure 56: A) MA-14 B) MA-15 C) MA-16

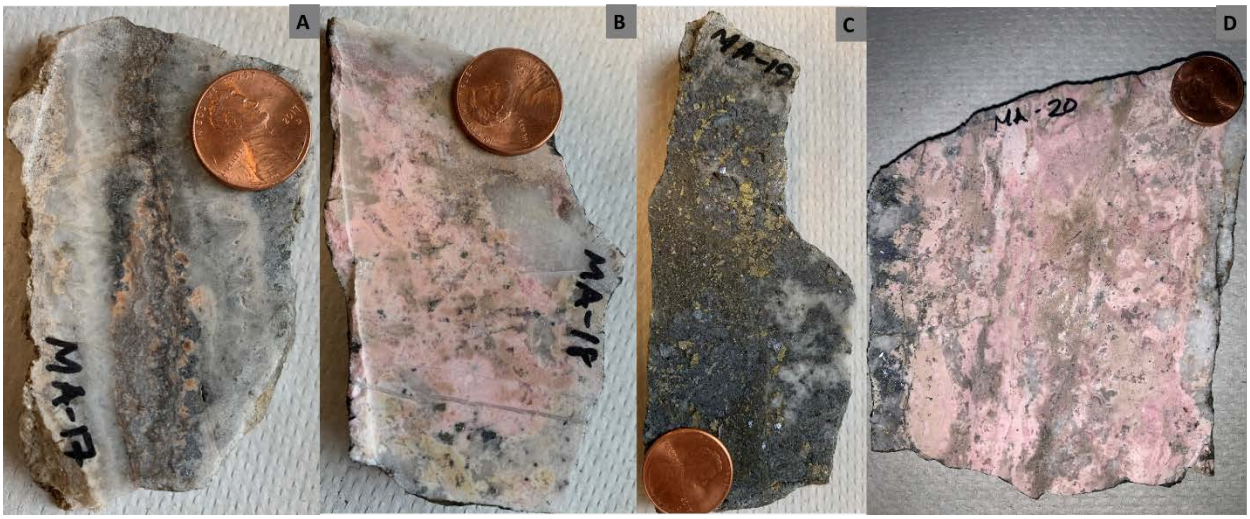

Figure 57: A) MA-17 B) MA-18 C) MA-19 D) MA-20

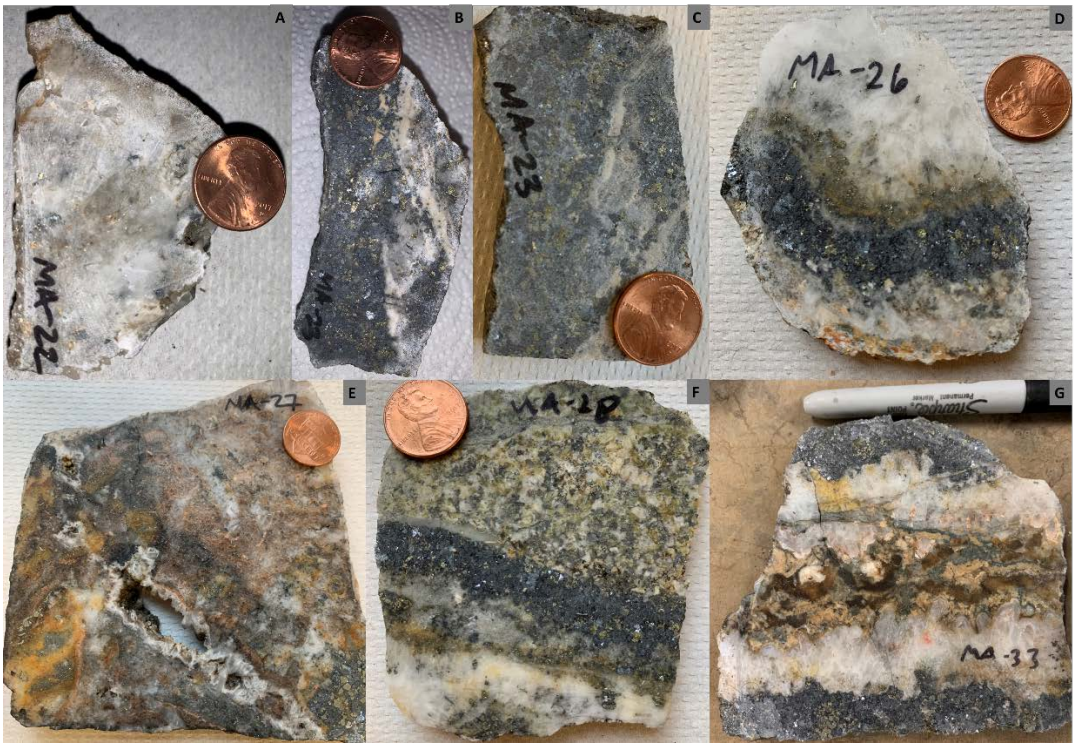

Figure 58: A) MA-22 B) and C) MA-23 D) MA-26 E) MA-27 F) MA-28 G) MA-33

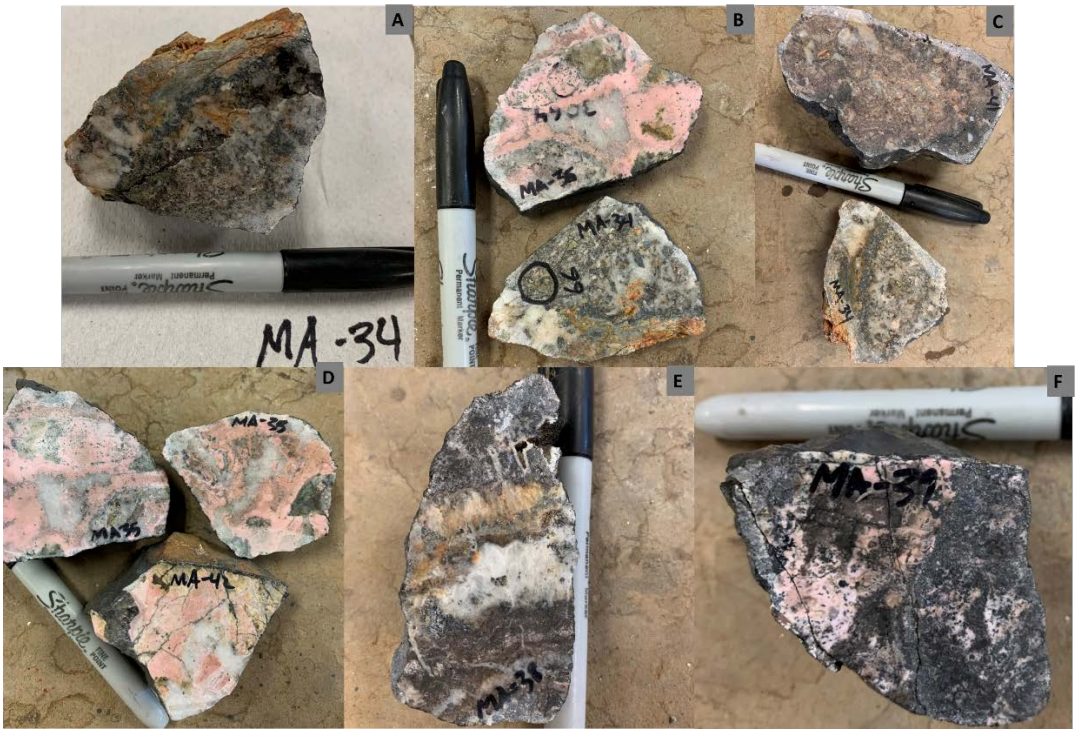

Figure 59: A) MA-34 B) MA-34 & MA-36 C) MA-34 & MA-41 D) MA-35 & MA-42 E) MA-38 F) MA-39

Figure 60: A) MA-40 B) MA-41 C) MA-42 D) MA-43 E) MA-44

Figure 61: A) MA-45 B) MA-50 C) MA-100 D) MA-101 E) MA-102 F) MA – 103

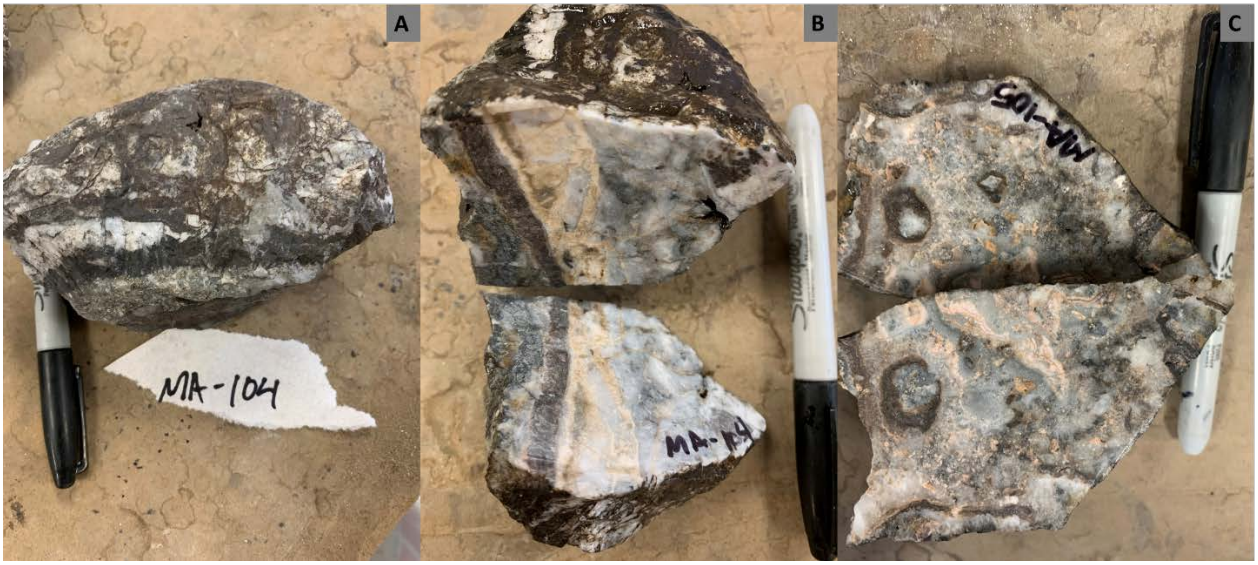

Figure 62: A) MA-104 B) MA-104 (sawn) C) MA-105

Figure 63: A) MA-106 B) MA-107 C) Granite sample with single pyrite or chalcopyrite in the middle.